SPECTRAL PROPERTIES AND POPULATION DYNAMICS OF THE HARMFUL DINOFLAGELLATE *Cochlodinium polykrikoides* (Margalef) IN SOUTHWESTERN PUERTO RICO

by

Deborah J. Cedeño Maldonado

A thesis submitted in partial fulfillment of the requirements for the degree of
DOCTOR OF PHILOSOPHY
in
MARINE SCIENCES
(Biological Oceanography)

UNIVERSITY OF PUERTO RICO
MAYAGÜEZ CAMPUS
2008

Approved by:

_____	_____
Jorge R. García Sais, PhD Member, Graduate Committee	Date
_____	_____
Fernando Gilbes Santaella, PhD Member, Graduate Committee	Date
_____	_____
Carmelo R. Tomas, PhD Member, Graduate Committee	Date
_____	_____
Roy A. Armstrong, PhD Chairperson, Graduate Committee	Date
_____	_____
José Cortés Figueroa, PhD Representative of Graduate Studies	Date
_____	_____
Nilda E. Aponte, PhD Chairperson of the Department	Date

Abstract

Recurrent blooms of the potentially ichthyotoxic dinoflagellate *Cochlodinium polykrikoides* were observed since 1958 at Bahía Fosforescente, a bioluminescent bay in southwestern Puerto Rico. Despite its potential deleterious effects, no previous efforts have been conducted to understand the population dynamics of this organism within this bay. This pioneer study assessed the role of climatological and physical-chemical parameters on the bloom dynamics of *C. polykrikoides* in Bahía Fosforescente. Monthly samplings took place at six stations from May 2002 to July 2003. Sea surface temperature, salinity, dissolved oxygen concentration and vertical attenuation coefficients of downwelling irradiance [K_d (PAR)] were determined at each station. Surface water samples were simultaneously collected for determinations of *C. polykrikoides* abundance, nutrients and chlorophyll *a* concentrations. *Cochlodinium polykrikoides* showed a strongly aggregational spatial distribution towards the northwest margin of the bay, where cell abundance ranged from 0 (undetectable) to 1.34 x 10^6 cells L^{-1}. The temporal distribution of *C. polykrikoides* blooms at this site followed a similar tendency to that observed for the rainfall regime. Statistical analyses showed that both the spatial and temporal distributions of *C. polykrikoides* blooms in these waters are associated with high concentrations of nutrients, particularly phosphates. A combination of factors including the semi-isolated nature of the area, prevailing southeast winds, low tidal amplitude, processes promoting enhanced nutrient availability (i.e. precipitation, nutrient cycling and turbulent mixing), as well as adaptative strategies and specific life-form characteristics of *C. polykrikoides*, contribute to the recurrence of blooms of this species in the northwestern margin of the bay.

Given the potential noxious effects of *Cochlodinium polykrikoides*, effective strategies to monitor the blooms of this species in Bahía Fosforescente are needed. The strong bio-optical signatures (striking brownish-red water discolorations) usually associated with these blooms make them suitable for optical detection. This work reports the first comprehensive characterization of the optical properties of *C. polykrikoides*, aimed to facilitate the accurate interpretation of the variations in ocean color observed during blooms of this species in natural waters. The feasibility of *in situ* hyperspectral remote sensing reflectance [R_{rs} (λ)] data to discriminate and quantify *C. polykrikoides* blooms in Bahía Fosforescente was also evaluated. The pigment composition, and the apparent (R_{rs}) and inherent (absorption, scattering, backscattering and attenuation) optical properties of *C. polykrikoides* were characterized based on pure cultures. Field data, including measurements for determinations of R_{rs} (λ) and inherent optical properties, as well as water samples for determinations of *C. polykrikoides* abundance, chlorophyll *a* concentration and other biogeochemical parameters, were collected in Bahía Fosforescente during May 2002 to July 2003, and/or during May 2007. *Cochlodinium polykrikoides* showed the typical pigment profile and absorption properties of most dinoflagellates with strong backscattering signals at 589 and 620 nm, accounting for the characteristic brownish-red discoloration of its blooms. Results suggested the potential application of *in situ* hyperspectral R_{rs} data to differentiate the blooms of *C. polykrikoides* from that of some other bloom-forming species present in Bahía Fosforescente. This data also proved suitable for quantitative estimations of *C. polykrikoides* abundance under bloom conditions, through the application of chlorophyll-based semi-empirical algorithms.

Resumen

Desde el año 1958 se han observado florecimientos recurrentes del dinoflagelado potencialmente ictiotóxico *Cochlodinium polykrikoides* en la Bahía Fosforescente, al suroeste de Puerto Rico. A pesar de sus posibles efectos nocivos, no se han realizado esfuerzos previos por entender la dinámica poblacional de este organismo en la bahía. Este estudio pionero evaluó el rol de parámetros climatológicos y físico-químicos en la dinámica de los florecimientos de *C. polykrikoides* en la Bahía Fosforescente. Se realizaron muestreos mensuales en seis estaciones desde mayo de 2002 a julio de 2003, incluyendo determinaciones de temperatura en la superficie del mar, salinidad, concentración de oxígeno disuelto y coeficientes de atenuación vertical de la irradianza descendente [K_d (PAR)]. Se tomaron muestras simultáneas en la superficie del agua para determinar la abundancia de *C. polykrikoides* y la concentración de nutrientes y clorofila *a*. *Cochlodinium polykrikoides* mostró una marcada distribución espacial de agregación hacia el margen noroeste de la bahía, donde la abundancia de células fluctuó desde 0 (no detectable) a 1.34×10^6 células L^{-1}. La distribución temporal de florecimientos de *C. polykrikoides* mostró una tendencia similar a la observada para el régimen de lluvia. Los análisis estadísticos mostraron que la distribución espacial y temporal de florecimientos de *C. polykrikoides* están asociadas a altas concentraciones de nutrientes, en particular fosfatos. Una combinación de factores como la naturaleza semi-aislada del área, vientos prevalecientes del sureste, amplitud baja de las mareas, procesos que promueven la disponibilidad de nutrientes (precipitación, reciclaje de nutrientes y mezcla turbulenta), así como adaptaciones estratégicas y características específicas de la forma de vida de *C. polykrikoides*, contribuyen a la recurrencia de florecimientos de esta especie en el margen noroeste de la bahía.

Dados los posibles efectos nocivos de *Cochlodinium polykrikoides*, es necesario establecer estrategias efectivas para detectar y monitorear los florecimientos de esta especie en la Bahía Fosforescente. Las características bio-ópticas llamativas usualmente asociadas a estos florecimientos (decoloraciones marrón-rojizas evidentes en el agua) hacen de la detección óptica un método apropiado para su estudio. Este trabajo presenta la primera caracterización comprensiva de las propiedades ópticas de *C. polykrikoides* dirigida a facilitar la interpretación precisa de las variaciones en el color del océano observadas durante florecimientos de esta especie en aguas naturales. También se evaluó la capacidad de utilizar datos hiperespectrales de reflectancia teledetectada [R_{rs} (λ)] colectados *in situ* para discriminar y cuantificar florecimientos de *C. polykrikoides* en la Bahía Fosforescente. La composición de pigmentos y las propiedades ópticas aparentes (R_{rs}) e inherentes (absorción, dispersión, retrodispersión y atenuación) de *C. polykrikoides* fueron caracterizadas mediante medidas obtenidas de cultivos puros de la especie. Se obtuvieron datos de campo mediante muestreos en varias estaciones en la Bahía Fosforescente durante el periodo de mayo de 2002 a julio de 2003, y en mayo de 2007. Estos datos incluyeron medidas para determinaciones de R_{rs} (λ) y propiedades ópticas inherentes, así como muestras de agua para determinar la abundancia de *C. polykrikoides*, concentración de clorofila *a* y otros parámetros biogeoquímicos. *Cochlodinium polykrikoides* mostró tener un perfil de pigmentos y propiedades de absorción típicos de la mayoría de los dinoflagelados, así como señales fuertes de retrodispersión en las longitudes de onda de 589 y 620 nm, lo cual explica la decoloración marrón-rojiza característica de sus florecimientos. Los resultados de este estudio sugieren el posible uso de datos de R_{rs} hiperespectral *in situ* para discriminar florecimientos de *C. polykrikoides* de aquellos producidos por algunas otras especies presentes en la Bahía Fosforescente. Estos datos también mostraron ser adecuados para estimar cuantitativamente la abundancia de *C. polykrikoides* en condiciones de florecimiento, mediante el uso de algoritmos semi-empíricos para clorofila.

Dedication

To my parents, José and Raquel, for being my inspiration.

To my brothers, Joe, Ricky and Arny, for sharing and believing in my dream.

To my husband Alexis, in deep gratitude for your patience, love and unconditional support.

I love you all very dearly!

Acknowledgements

I would like to express my gratitude to all the people who have supported me during my many years studying in the Department of Marine Sciences. Without their help the culmination of this work would not have been possible. First and foremost, I would like to thank Dr. Roy A. Armstrong, president of my graduate committee, for the opportunity to work in the Bio-Optical Oceanography Laboratory and for his guidance, infinite patience and support during this research. I am also very grateful to the rest of my graduate committee members, Dr. Jorge R. García Sais, Dr. Fernando Gilbes Santaella and Dr. Carmelo R. Tomas, for their encouragement and help throughout this research and for their careful review and valuable comments to this manuscript.

My sincere gratitude to Dr. Juan G. González Lagoa for introducing me to the world of marine sciences and for sharing with me his wisdom and passion for phytoplankton. Special thanks to Dr. Yasmín Detrés, who offered me not only her friendship, but also her generous and unselfish help during the samplings and many, many other tasks.

Thanks to Dr. Jorge García, Dr. Jorge Corredor, Dr. Thomas Tosteston, Dr. Govind Nadathur and Dr. David Ballantine, for letting me use their laboratory facilities and/or instrumentation. My appreciation to my fellow students Patrick Reyes, Marcos Rosado, Ramón López and Oswaldo Cárdenas, and to research technician Val Hensley, for kindly helping with the CDOM, absorption, pigment and nutrient analyses. I am also thankful to Dr. Mónica Alfaro and Dr. Aldo Croquer for their assistance with the statistical analyses.

My appreciation to the administrative staff of the Department of Marine Sciences, especially to Taty, Zulma and Lilivette, for keeping me updated with my paperwork and for providing emotional support during difficult times. I am also deeply grateful to Marcos Rosado

for his unconditional availability and help during the samplings, and to all the Maintenance and Small Boats personnel for their assistance and willingness to cooperate with my work. I am also indebted to Luis Lugo (Vitamina) for his generous help with the microalgal cultures and for his good wishes.

I would like to thank my lab mates and many other friends from the Marine Sciences family for their help, encouragement and unconditional support throughout this whole process. I am particularly grateful to my dear friend Áurea Rodríguez, who has been with me since the beginning of my graduate studies. Thanks Aury for sharing with me so many good times, but mostly for being enormously supportive during some very difficult ones.

Finally, I would like to thank my beloved husband Alexis for providing balance to my life outside the laboratory and for giving me the space needed to accomplish my goal. I must also thank my family, for their love, faith, motivation and encouragement throughout this amazing journey!

This research was funded by the NOAA Educational Partnership Program with Minority Serving Institutions (EPP/MSI) under cooperative agreements NA17AE1625 and NA17AE1623 and by the Tropical Center for Earth and Space Studies (NASA Grant NCC5-518).

Table of Contents

Abstract ii

Resumen iv

Dedication vi

Acknowledgements vii

Table List x

Figure List xi

Appendix List xiv

General Introduction 1

1 **Population dynamics of the harmful dinoflagellate *Cochlodinium polykrikoides* (Margalef) in Bahía Fosforescente, southwestern Puerto Rico** 6

1.1 Introduction 6

1.2 Materials and Methods 10

1.3 Results 17

1.4 Discussion 35

1.5 Conclusions 47

2 **Optical properties of the harmful dinoflagellate *Cochlodinium polykrikoides* (Margalef)** 49

2.1 Introduction 49

2.2 Materials and Methods 57

2.3 Results 73

2.4 Discussion 130

2.5 Conclusions 144

Literature Cited 146

Table List

Tables **Page**

Table 1. Physical-chemical data measured at Bahía Fosforescente during the sampling period. 20

Table 2. Summary of discriminant function analysis (DFA) of physical-chemical parameters that better discriminate *C. polykrikoides* bloom and non-bloom periods. 34

Table 3. Summary of cell abundances and chlorophyll *a* concentrations obtained during the nine-step dilution sequence of a pure culture of *C. polykrikoides* used to determine a linear regression equation for estimations of cell abundance based on chlorophyll *a* measurements. 78

Table 4. Summary of parameters measured during the five-step *C. polykrikoides* culture addition sequence for determinations of R_{rs} (λ). 80

Table 5. Wavelength positions (nm) of pigment absorption features identified in the second-derivative plots of R_{rs} (λ) spectra measured during the five-step addition sequence of *C. polykrikoides* cultures. 88

Table 6. *In vivo* absorption maxima for phytoplankton pigments as reported in the literature. .. 89

Table 7. Summary of wavelength positions (nm) of pigment absorption features identified in derivative plots by several authors. 90

Table 8. Summary of linear regression analyses of *C. polykrikoides* cell abundance/ chlorophyll *a* concentration versus second-derivative peak magnitudes of R_{rs} (λ) spectra based on pure cultures..... 93

Table 9. Summary of cell abundances and chlorophyll *a* concentrations obtained during the ten-step addition sequence of *C. polykrikoides* cultures for determinations of inherent optical properties [a (λ), b_b (λ), b(λ) and c (λ)]. 95

Table 10. Summary of bio-geochemical parameters measured at Bahía Fosforescente during the samplings of May 16 and 18, 2007. ..... .113

Table 11. A comparison of the relationships between various semi-empirical algorithms and *C. polykrikoides* cell abundance for the R_{rs} (λ) data set (n = 10) collected in Bahía Fosforescente during blooms of *C. polykrikoides* from July 2002 to May 2007. ……...128

Figure List

Figures **Page**

Figure 1. Bloom of *Cochlodinium polykrikoides* in the northwest inlet of Bahía Fosforescente.. 4

Figure 2. Two-celled chain of *Cochlodinium polykrikoides*..... 4

Figure 3. Map of Bahía Fosforescente illustrating the location of the sampling stations..... 11

Figure 4. Distribution of weekly precipitation in La Parguera throughout the sampling period. 18

Figure 5. Vectors indicating the wind speed and direction measured in La Parguera throughout the study period. 19

Figure 6. Principal component analysis (PCA) ordination plot of sampling stations based on physical-chemical parameters. 25

Figure 7. Vertical attenuation coefficients of downwelling PAR irradiance, K_d (PAR), measured at Bahía Fosforescente throughout the sampling period. 27

Figure 8. Chlorophyll *a* concentrations measured at Bahía Fosforescente throughout the sampling period..... 29

Figure 9. *Cochlodinium polykrikoides* abundances at the six sampling stations in Bahía Fosforescente during the study period. 30

Figure 10. Principal component analysis (PCA) ordination plot of *C. polykrikoides* bloom (B) and non-bloom (N) periods based on physical-chemical parameters. 32

Figure 11. Experimental set-up for $R_{rs}(\lambda)$ measurements of pure cultures of *C. polykrikoides*.. 61

Figure 12. Map of Bahía Fosforescente indicating the location of the stations sampled during May 16 and 18, 2007. 66

Figure 13. Representative HPLC chromatogram of pigment extracts obtained from *C. polykrikoides* cultures. 74

Figure 14. Mean absorption spectrum [$a_{ph}(\lambda)$] of *C. polykrikoides* cultures obtained from six culture samples collected during different dates..... 75

Figure 15. CDOM absorption spectra [$a_g(\lambda)$] corresponding to *C. polykrikoides* cultures and to the L1 culture medium..... 77

Figure 16. Comparison between measured and estimated downwelling irradiances, $E_d(0^+, \lambda)$, during the *C. polykrikoides* culture experiment for determinations of $R_{rs}(\lambda)$. 81

Figure 17. Remote sensing reflectance spectrum [$R_{rs}(\lambda)$] of filtered seawater (baseline) obtained during the *C. polykrikoides* culture experiment for determinations of $R_{rs}(\lambda)$. 83

Figure 18. Remote sensing reflectance spectra [$R_{rs}(\lambda)$] measured during the five-step *C. polykrikoides* culture addition sequence. 84

Figure 19. Second-derivative plots corresponding to the $R_{rs}(\lambda)$ spectra measured during the five-step addition sequence of *C. polykrikoides* cultures..... 87

Figure 20. Second-derivative plots of the $R_{rs}(\lambda)$ spectra measured during the five-step addition sequence of *C. polykrikoides* cultures, illustrating the enhancement in magnitude of the most prominent spectral features in direct response to increasing cell abundances. 92

Figure 21. Spectral absorption coefficients [$a(\lambda)$] for the ten-step addition sequence of *C. polykrikoides* cultures measured with the ac-9. 96

Figure 22. Spectral attenuation coefficients [$c(\lambda)$] for the ten-step addition sequence of *C. polykrikoides* cultures measured with the ac-9. 98

Figure 23. Spectral scattering coefficients [$b(\lambda)$] for the ten-step addition sequence of *C. polykrikoides* cultures measured with the ac-9. 99

Figure 24. Backscattering (b_b) spectra of 0.2 µm filtered seawater measured with the HS6. .. 101

Figure 25. Spectral backscattering coefficients [$b_b(\lambda)$] for the ten-step addition sequence of *C. polykrikoides* cultures measured with the HS6. 102

Figure 26. Average $R_{rs}(\lambda)$ spectra measured at the six stations studied in Bahía Fosforescente from May 2002 to July 2003. 104

Figure 27. Complete set of $R_{rs}(\lambda)$ spectra measured at the six stations studied in Bahía Fosforescente from May 2002 to July 2003. 107

Figure 28. $R_{rs}(\lambda)$ spectra representative of blooms of *C. polykrikoides*, *A. sanguinea*, and *C. furca* var. *hircus-P. bahamense* corresponding to similar chlorophyll *a* concentrations, collected in Bahía Fosforescente during the monthly samplings period. 109

Figure 29. Second-derivative plots of the $R_{rs}(\lambda)$ spectra of *C. polykrikoides*, *A. sanguinea* and *C. furca* var. *hircus-P. bahamense* blooms. 111

Figure 30. $R_{rs}(\lambda)$ spectra measured at Bahía Fosforescente on May 16 and 18, 2007 during a bloom of *C. polykrikoides*..... 115

Figure 31. Second-derivative plots of the average $R_{rs}(\lambda)$ spectra for the *C. polykrikoides* bloom and reference stations. 117

Figure 32. Spectral absorption coefficients [a (λ)] measured with the ac-9 at the *C. polykrikoides* bloom and reference stations. 119

Figure 33. Spectral attenuation coefficients [c (λ)] measured with the ac-9 at the *C. polykrikoides* bloom and reference stations. 121

Figure 34. Spectral scattering coefficients [b (λ)] measured with the ac-9 at the *C. polykrikoides* bloom and reference stations. 122

Figure 35. Spectral backscattering coefficients [b_b (λ)] measured with the HS6 at the bloom and reference stations. 124

Figure 36. Relationship between *C. polykrikoides* cell abundance and chlorophyll *a* concentration corresponding to the data set used for the quantitative analysis for estimations of *C. polykrikoides* abundance based on in situ hyperspectral R_{rs} data. 126

Figure 37. Comparison of algorithms that showed the best relationships for estimations of *C. polykrikoides* cell abundance based on *in situ* hyperspectral R_{rs} data. 129

Appendix List

Appendices **Page**

Appendix 1. Chlorophyll *a* concentrations measured at Bahía Fosforescente throughout the study period by spectrophotometric, fluorometric and HPLC methods. 160

Appendix 2. SIMPER analysis of dissimilarities among sampling stations based on physical-chemical properties. 161

Appendix 3. SIMPER analysis of dissimilarities among sampling dates based on physical-chemical properties. 162

Appendix 4. Summary of two-way ANOVA for *C. polykikoides* abundance data. 165

Appendix 5. Comparison of physical-chemical parameters measured in Bahía Fosforescente in previous studies and during the current study. 166

General Introduction

Among the thousands (~5000) of marine phytoplankton species, roughly 60 to 80 are considered harmful or toxic (Hallegraeff, 1993; Smayda, 1997). Although diatoms, cyanobacteria, dinoflagellates, prymnesiophytes, raphidophytes, chrysophytes and silicoflagellates are included in this category, dinoflagellates represent the most prominent noxious group, comprising about 75% (45-60 species) of all harmful algal bloom (HAB) species (Smayda, 1997). The harmful properties of these algae involve the production of biotoxins or hemolytic/hemagglutinating compounds, physical structures that cause physical or mechanical damage to higher trophic levels, and/or extreme biomass accumulations (i.e. blooms). The deleterious impacts of these harmful algae and/or their blooms include: negative ecological consequences (e.g. displacement of indigenous species, habitat and trophic structure alterations, oxygen depletion, water quality deterioration, mass mortalities of fish and shellfish, and deaths of birds and mammals); human health problems (e.g. paralytic, neurotoxic, diarrhetic, amnesic and azaspiracid shellfish poisoning, and ciguatera fish poisoning); and vast economic losses (particularly in the aquaculture, recreation and tourism industries) (Hallegraeff, 1993; Anderson, 1994, 1995; Smayda, 1997; Glibert et al., 2005).

Harmful algal blooms (also known as red or brown tides) have become a widespread issue throughout coastal waters worldwide (Smayda, 1990; Hallegraeff, 1993). This trend seems to be related to both natural and anthropogenic causes including: biological species dispersal mechanisms; natural variability of climatic patterns; changing environmental conditions promoting species dispersal through currents and storms; enhanced eutrophication of coastal waters (land runoff, domestic, industrial and agricultural wastes, and aquaculture practices); transport of species via ship ballast water; and increased scientific attention to harmful species,

concurrent with improved instrumentation and analytical techniques facilitating their detection (Hallegraeff, 1993; Anderson, 1994, 1995; Glibert et al., 2005). Consequently, understanding the bloom dynamics of harmful algae, as well predicting, detecting and monitoring their blooms is essential to minimize their adverse effects on human health and ecology, and economic losses to coastal communities. Conventional approaches for HAB assessments primarily rely on field samplings, chemical analyses or mouse bioassays for toxin detection and microscopic cell examinations (Schofield et al., 1999). Unfortunately, these methods are arduous and time consuming, with a poor spatial and temporal resolution. Therefore, alternative methods allowing faster detection and characterization of these harmful outbreaks over broad spatial scales would be more suitable.

The fact that phytoplankton strongly influences the optical properties of natural waters through their striking water discolorations, usually when they reach bloom densities, led to an enhanced interest in the bio-optical assessment of HAB's (Roesler and McLeroy-Etheridge, 1998). Once established, blooms are largely mono-specific, reaching extremely high biomass over small spatial scales. As a result, their bio-optical signatures are distinct and usually persist for an extended period of time providing a means of optical detection (Millie et al., 1995). Ocean color remote sensing is of particular utility for the assessment of the HAB phenomena, measuring the amount and quality of the light reflected from near the sea surface. This allows an extensive monitoring of coastal waters on a regular basis enhancing our capabilities for rapid determinations of HAB's presence and the extent of their distribution, and to trace their evolution (Cullen et al., 1997; Schofield et al., 1999).

Puerto Rico has no known reports of toxic algal events, except for those regarding ciguatera fish poisoning (Tosteson et al., 1997, and references therein). However, dense

accumulations of the dinoflagellate *Cochlodinium polykrikoides* (= *C. heterolobatum*) were recurrently observed since 1958 at Bahía Fosforescente, a bioluminescent bay in southwestern Puerto Rico (Figure 1) (Margalef, 1961; Burkholder et al., 1967; Cintrón, 1969; Cintrón et al., 1970; Seliger et al., 1971; Seixas, 1983). *Cochlodinium polykrikoides* (Figure 2) was reported as the causative species of numerous HAB occurrences and/or massive fish kills in many regions including Barnegat Bay, New Jersey (Silva, 1967); York River and Chesapeake Bay, Virginia (Ho and Zubkoff, 1979; Marshall, 1995); Japan (Yuki and Yoshimatsu, 1989); China (Du et al., 1993); Guatemala (Rosales-Loessener et al., 1996); Gulf of Olbia, Sardinia, Italy (Sannio et al., 1997); Korea (Kim, 1998; Kim et al., 1999); Vancouver Island, British Columbia, Canada (Whyte et al., 2001); the Gulf of California, Mexico (Gárate-Lizárraga et al., 2000; Gárate-Lizárraga et al., 2004); Peconic Estuary and Shinnecock Bay, New York (Nuzzi, 2004; Gobler et al., 2008); California, USA (Curtiss et al., 2008); Pettaquamscutt Cove, Rhode Island (Tomas and Smayda, 2008); Palawan, Phillipines (Azanza et al., 2008); and Sabah, Malaysia (Anton et al., 2008). So far, the most catastrophic blooms of this species occurred in Korea during 1995, where mass mortalities of wild and farmed finfish and shellfish resulted in an economic loss of about 95 million dollars (Kim et al., 2000). The potential impacts of this dinoflagellate in Puerto Rico have yet to be investigated.

Despite the potential deleterious effects of *C. polykrikoides*, no previous efforts have been dedicated to understand the population dynamics of this organism in Bahía Fosforescente. Although numerous studies were conducted to understand the dinoflagellates dynamics in this bay (Seliger et al., 1971; Seixas, 1983; Seixas, 1988; Walker, 1997; Soler, 2006), they mostly address the bioluminescent species *Pyrodinium bahamense* and other species coexisting within the central part of the bay including *Ceratium furca* var. *hircus*, *Dinophysis caudata*, *Akashiwo*

Figure 1. Bloom of *Cochlodinium polykrikoides* in the northwest inlet of Bahía Fosforescente.

Figure 2. Two-celled chain of *Cochlodinium polykrikoides* (Photo courtesy of Carmelo R. Tomas).

sanguinea (= *Gymnodinium splendens*/*G. sanguineum*), *Prorocentrum micans* and *Peridinium divergens*. As a result, the factors influencing *C. polykrikoides* blooms have remained unclear. Also, no previous attempts to develop monitoring strategies for *C. polykrikoides* blooms in this bay have been conducted.

The present study characterizes the optical properties of *C. polykrikoides* and evaluates whether it is possible to discriminate and quantify the blooms of this species in Bahía Fosforescente based on *in situ* hyperspectral remote sensing reflectance (R_{rs}) measurements. In addition, the role of climatological and physical-chemical parameters on the population dynamics of *C. polykrikoides* in Bahía Fosforescente is assessed.

This dissertation is written in a manuscript format and consists of two major chapters, each with its own abstract, introduction, materials and methods, results, discussion and conclusions. Chapter one examines the influence of climatological and physical-chemical parameters on the population dynamics of *C. polykrikoides* in Bahía Fosforescente. In the second chapter, the optical properties of *C. polykrikoides* are characterized based on pure culture measurements. This chapter also evaluates the feasibility of *in situ* hyperspectral R_{rs} data to discriminate and quantify the blooms of this species in Bahía Fosforescente.

1 Population dynamics of the harmful dinoflagellate *Cochlodinium polykrikoides* (Margalef) in Bahía Fosforescente, southwestern Puerto Rico

1.1 Introduction

Blooms of the dinoflagellate *Cochlodinium polykrikoides* (= *C. heterolobatum*) were recurrently observed since 1958 at Bahía Fosforescente, a bioluminescent bay in southwestern Puerto Rico (Margalef, 1961; Burkholder et al., 1967; Cintrón, 1969; Cintrón et al., 1970; Seliger et al., 1971; Seixas, 1983). Although numerous studies were conducted to understand the dinoflagellates dynamics in Bahía Fosforescente (Seliger et al., 1971; Seixas, 1983; Seixas, 1988; Walker, 1997; Soler, 2006), they mostly address the bioluminescent species *Pyrodinium bahamense* and other species coexisting within the central part of the bay including *Ceratium furca* var. *hircus*, *Dinophysis caudata*, *Akashiwo sanguinea* (= *Gymnodinium splendens*/*G. sanguineum*), *Prorocentrum micans* and *Peridinium divergens*. As a result, the factors influencing *C. polykrikoides* blooms remain unclear.

Cochlodinium polykrikoides is an unarmored, chain-forming dinoflagellate, varying in size from 30-40 µm long and 20-30 µm wide that is regarded as potentially ichthyotoxic and is extensively distributed along warm temperate and tropical waters (Steidinger and Tangen, 1997). It was reported as the causative species of numerous harmful algal bloom (HAB) occurrences and/or massive fish kills in many regions including Barnegat Bay, New Jersey (Silva, 1967); York River and Chesapeake Bay, Virginia (Ho and Zubkoff, 1979; Marshall, 1995); Japan (Yuki and Yoshimatsu, 1989); China (Du et al., 1993); Guatemala (Rosales-Loessener et al., 1996); Gulf of Olbia, Sardinia, Italy (Sannio et al., 1997); Korea (Kim, 1998; Kim et al., 1999); Vancouver Island, British Columbia, Canada (Whyte et al., 2001); the Gulf of California, Mexico (Gárate-Lizárraga et al., 2000; Gárate-Lizárraga et al., 2004); Peconic Estuary and

Shinnecock Bay, New York (Nuzzi, 2004; Gobler et al., 2008); California, USA (Curtiss et al., 2008); Pettaquamscutt Cove, Rhode Island (Tomas and Smayda, 2008); Palawan, Phillipines (Azanza et al., 2008); and Sabah, Malaysia (Anton et al., 2008). So far, the most catastrophic blooms of this species occurred in Korea during 1995, where mass mortalities of wild and farmed finfish and shellfish resulted in an economic loss of about 95 million dollars (Kim et al., 2000). The potential impacts of this dinoflagellate in Puerto Rico are yet to be assessed.

The precise toxic mechanisms of *C. polykrikoides* are poorly understood at present. While some scientists postulate that it produces neurotoxic, hemolytic and hemagglutinating substances, others propose that reactive oxygen species (O_2^-, ^-OH and H_2O_2) generated from this organism are responsible for its noxious effects. Suffocation due to copious secretions of mucus-like substances in fish exposed to this species was also reported as a possible cause for fish mortalities (Kim et al., 1999; Kim et al., 2000).

Bahía Fosforescente is characterized by high concentrations of resident dinoflagellates, differing notably from the contiguous coastal waters where the phytoplankton biomass tends to be relatively lower. This differs specially from the waters farther off the coast, in the nearby extensive coral reef area of La Parguera, where not only is the phytoplankton biomass significantly lower, but also is predominantly constituted by pelagic diatoms. According to Margalef (1961), this is indicative of a mature community, occupying an advanced level in the natural succession of phytoplankton. Within the bay premises, *P. bahamense*, the main species responsible for the bioluminescence in these waters, and the non-luminescent *C. furca* var. *hircus*, represent the most abundant species in the center of the main bay area. Only during sporadic events, when the abundance of these two species was found to decrease drastically, other species outnumber them (Margalef, 1961; Seliger et al., 1971). Towards the northern part of the bay,

however, the abundance of these two species remains low in a consistent manner and *Peridinium quinquecorne* usually dominates particularly in the northeast margin (Seliger et al., 1971; Seixas, 1983), whereas very localized blooms of *C. polykrikoides* frequently occur in the northwest corner (Margalef, 1961; Burkholder et al., 1967; Cintrón et al., 1970; Seliger et al., 1971; Seixas, 1983).

Multiple mechanisms were proposed to explain this densification of dinoflagellates in Bahía Fosforescente. According to Coker and González (1960), the prevalent tidal conditions (tidal amplitude in La Parguera is ~30 cm), the absence of rivers, and the low precipitation and land runoff characteristic of the area, limit water exchange rates between Bahía Fosforescente and open waters, thus promoting the accumulation of phytoplankton. Margalef and González (1958) and Margalef (1961) postulated that such densification respond to the physiographic characteristics of the bay and the particular circulation pattern of this shallow marine environment. Margalef (1961) postulated a density distribution based circulation pattern for this area, generated by evapo-transpiration factors associated with the red mangroves encircling the bay and the high evaporation typical of the region, where less dense offshore water flow into the bay at the surface, driven by the prevailing winds, and accumulates in the rear part of the bay. Saltier, denser water flows out of the bay as a bottom current. This circulation pattern, together with the highly secluded nature of this bay (having a narrow and shallow entrance), strongly reduce diffusion rates and increases the retention time to maintain large concentrations of dinoflagellates. Seliger et al. (1971), on the other hand, emphasized the motility and phototactic capabilities of dinoflagellates as having an influential role in their accumulation in Bahía Fosforescente. Other studies also suggested that abundant dinoflagellate populations are maintained within the bay by a supply of organic matter from the mangrove community and

decomposing phytoplankton, inorganic nutrients from episodic rainfall runoff, remineralization processes in the bottom sediments, availability of vitamin B_{12} produced *in situ* and wind patterns (Burkholder and Burkholder, 1958; Seixas, 1988; San Juan and González, 2000).

Previous work revealed a complex temporal succession of dinoflagellates in Bahía Fosforescente, particularly in the main central region (Seliger et al., 1971; Seixas, 1988). These successional patterns were attributed to the rainfall regime, tidal effects, alterations in the prevailing wind patterns and the phototactic properties of the different dinoflagellate species. Nevertheless, very little is known about the temporal variations and dynamics of the dinoflagellate populations inhabiting predominantly the northern margin of the bay. In the specific case of *C. polykrikoides*, Burkholder et al. (1967) reported dense blooms of this species several days after a heavy rainfall and attributed them to nutritional factors entering the northern part of the bay from inundated mangrove areas, though no measurements were made to support this contention. The aim of this study was to assess the role of climatological and physical-chemical parameters on the bloom dynamics of *C. polykrikoides* in Bahía Fosforescente.

1.2 Materials and Methods

1.2.1 Study area

Bahía Fosforescente is located about 3.2 km east of La Parguera, a small fishing village in the southwest coast of Puerto Rico (17° 58' 30" N; 67° 01' 10" W) (Figure 3). This bay is irregular in shape, having three inlets or arms oriented towards the north of the main central body, and a narrow (~150 m wide) and shallow outlet that connects with the ocean. The bay occupies an estimated area of 0.19 km^2 and has an average depth of 3.5 m, with a maximum depth of about 4 m near the western margin. It is fringed by a mangrove forest predominantly comprised by *Rhizophora mangle* (red mangrove), which support a rich fauna and flora, and is of vital importance for the survival of this delicate and fragile ecosystem (Burkholder and Burkholder, 1958; US Department of Interior, 1968). The bottom is devoid of macrovegetation and larger benthic animals except for the western side where turtle grass (*Thalassia testudinum*) and marine algae, including the genera *Penicillus*, *Dictyota*, *Aurainvillea*, and *Udotea* grow abundantly (Cintrón et al., 1970). Bottom sediments are mainly composed of fine mud, large amounts of sponge spicules, diatoms, ostracods, seagrass remains and mangrove leaves (Margalef, 1961). The bay is highly turbid due to high phytoplankton concentrations, debris from the bordering mangroves, infrequent rainfall runoff and stirring of loose sediments by wind and fishes (San Juan and González, 2000). It is characterized by high evaporative rates, driven by the arid conditions prevalent throughout the southwestern region of the island. Surface circulation patterns are controlled primarily by the prevailing winds from the east and southeast (Glynn, 1973), which tend to move water in a west-northwest direction. Since there is no river discharge to the sea in La Parguera or adjacent areas, freshwater inputs to the bay are negligible.

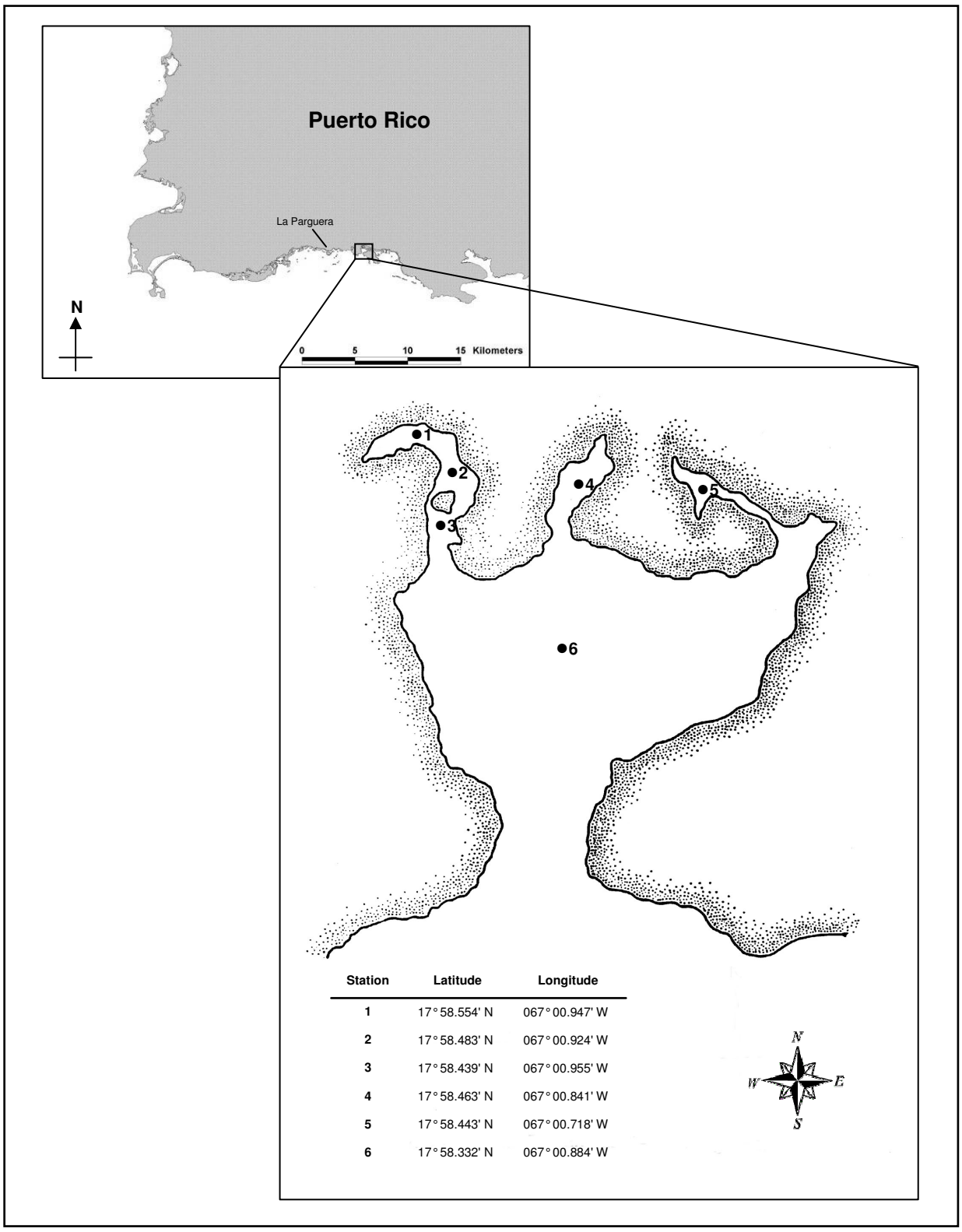

Station	Latitude	Longitude
1	17° 58.554' N	067° 00.947' W
2	17° 58.483' N	067° 00.924' W
3	17° 58.439' N	067° 00.955' W
4	17° 58.463' N	067° 00.841' W
5	17° 58.443' N	067° 00.718' W
6	17° 58.332' N	067° 00.884' W

Figure 3. Map of Bahía Fosforescente illustrating the location of the sampling stations.

1.2.2 Field work

Monthly samplings took place at six stations in Bahía Fosforescente (Figure 3) from May 2002 to July 2003. These samplings were conducted during the morning using small boats provided by the Department of Marine Sciences of the UPRM. At each station, surface water samples for cell counts, chlorophyll *a* and nutrient analyses were collected using a battery operated portable water pump system. Triplicate 1-5 L water samples, depending on the station and/or on apparent microalgal concentrations, were fixed with acid Lugol's solution (by adding ~4 ml per liter of seawater), filtered through a 25 µm mesh and concentrated to about 50 ml for subsequent *C. polykrikoides* cell counts. For determinations of nutrient concentrations, triplicate 500 ml water samples were collected in polyethylene bottles, fixed with 50 µl of $HgCl_2$ and immediately refrigerated until further processing. A 4 L water sample for chlorophyll *a* determinations was also taken in an amber plastic bottle and refrigerated for immediate processing upon return to the laboratory.

Surface seawater temperature, salinity and dissolved oxygen concentration were measured at each station using a thermometer, a hand-held refractometer and a dissolved oxygen meter, respectively. Measurements for determinations of the vertical attenuation coefficient of downwelling irradiance, K_d (PAR) [PAR - photosynthetic active radiation (400 –700 nm)], were performed at two different depths (just below the surface and at 0.5 or 1m depth, depending on the station's depth) with a LiCor 1400 underwater irradiance meter (~10 measurements were recorded at each depth once the instrument readings were stable). Precipitation and wind data were obtained from the Magueyes Island meteorological station operated by NOAA.

1.2.3 Laboratory work

1.2.3.1 Nutrient analyses

Determinations of nitrite, phosphate and silicate concentrations were performed according to the methods described by Strickland and Parsons (1972) using a double-beam spectrophotometer (model UV-1601, Shimadzu, Inc.). Ammonium concentrations were measured by fluorometric methods (Holmes et al., 1999) using a spectrofluorometer (model F-2000, Hitachi, Inc.). Nitrate analyses were performed using a nitrate/nitrite analyzer (model 745, Antek, Inc.) and following the methodology described by Braman and Hendrix (1989). N:P ratios (atoms) were calculated by adding up the total dissolved inorganic nitrogen (i.e. nitrate, nitrite and ammonium) divided by the phosphate concentration.

1.2.3.2 K_d (PAR) calculations

K_d (PAR) values, which are indicative of the penetration of solar radiation in natural waters, were calculated for each station from the *in situ* downwelling irradiance measurements (E_d) at two different depths. Prior to the calculations, average E_d values were computed from the data set collected at each depth. Then, K_d (PAR) values were obtained from the following equation:

$$K_d\,(PAR) = 1/(z_2 - z_1) * \ln (E_d1/E_d2) \qquad (1)$$

where E_d1 and E_d2 represent the measured downwelling irradiance values at depths z_1 (just below the surface) and z_2 (0.5m/1m), respectively.

1.2.3.3 Chlorophyll *a* determinations

Water samples for chlorophyll analysis were vigorously stirred prior to processing in order to assure homogeneity. From each sample, two sub-samples were filtered onto GF/F filter pads and frozen at -80 ºC until extraction. Pigments were extracted in ~4 ml of 90% acetone by grinding the filters in an aluminum foil-covered glass homogenization tube, with a motor-driven

Teflon pestle rotating at about 500 rpm. During the grinding process the tube was kept in an ice bath to avoid pigment degradation by overheating. The extract was then filtered to remove filter remains and analyzed simultaneously by fluorometric, spectrophotometric and HPLC methods. This provided the opportunity to corroborate the efficiency of these three methods (Appendix 1).

Chlorophyll *a* concentrations were determined by the standard fluorometric method (Welschmeyer, 1994) using a field fluorometer (model 10-AU, Turner Designs). For the spectrophotometric analysis, absorbances were measured using a double-beam spectrophotometer (model UV-1601, Shimadzu, Inc.) equipped with 1 cm quartz cells. Then, chlorophyll *a* concentrations were estimated with the trichromatic equations reported by Jeffrey and Humphrey (1975) for mixed phytoplankton populations. HPLC analysis of chlorophyll *a* was performed using a Waters C18 column (symmetry 3.9 x 150 mm) and an HPLC system consisting of a Shimadzu LC-10 AT pump and a SPD-M10AU diode array detector connected to a Waters WISP 712 injector. The analysis was based on a modified version of the methodology described by Wright et al. (1991). The HPLC was calibrated with a solution of pure chlorophyll *a* in 90% acetone. Chlorophyll *a* was identified by comparing its retention time and absorption spectrum (400-700nm) to published data.

1.2.3.4 Determinations of *C. polykrikoides* abundance

Triplicate water samples were used for quantitative determinations of *C. polykrikoides* cell abundance and for the qualitative assessment of other phytoplankton species. Prior to cell counts**,** sample volumes were adjusted depending on apparent cell concentrations. Samples were gently mixed to give a homogeneous distribution of cells and subsequently, two 1ml aliquot replicates were counted in a Sedgewick-Rafter counting chamber using an inverted microscope (model CK40, Olympus, Inc.). Determinations of cell abundance were based on average cell counts calculated from the replicate samples.

1.2.4 Data analysis

A log (sqrt^4+1) transformation was applied to the monthly *C. polykrikoides* abundance data in order to normalize distributions. Two-way analysis of variance (ANOVA) with replication was used to test for differences in *C. polykrikoides* abundance between stations, dates, and/or interaction effects.

Non-parametric multivariate analyses were used to analyze the physical-chemical data set. These analyses were performed on standardized data and were based on Euclidean distances. Non-metric principal component analysis (PCA) was used to examine spatial and temporal patterns in the physical-chemical seawater properties. Differences in the physical-chemical properties among stations and dates were tested using a two-way crossed analysis of similarity (ANOSIM) without replication (a multivariate non-parametric analogue of ANOVA), which is a permutation-based test between *a priori* defined groups (stations and dates) where generated R statistic values are indicative of how similar the groups are (the closer to 1 the greater the differences; 0 indicates no difference among groups). A similarity percentage (SIMPER) analysis was used to determine which physical-chemical parameters primarily contributed to dissimilarity wherever statistical differences were found. Physical-chemical data corresponding to the period between May and July 2002 was not included in the analyses, due to the lack of nutrient data for those dates.

PCA was further used to evaluate patterns in the physical-chemical properties between *C. polykrikoides* bloom and non-bloom periods. Bloom periods represent all stations and dates sampled where *C. polykrikoides* abundance was 1 x 10^5 cells L^{-1} or higher. To determine which physical-chemical parameters, if any, differentiate *C. polykrikoides* bloom and non-bloom periods, discriminant function analysis (DFA) was used. DFA is a parametric method that

distinguishes between *a priori* defined groups (bloom and non-bloom) using linear combinations of the variables. The procedure finds discriminant functions which account for as much of the variability between groups as possible. To explore relationships between *C. polykrikoides* abundance and the rainfall and wind patterns, as well as between the climatological and physical-chemical parameters, Spearman rank correlation analysis was used. All data were analyzed using the statistical packages from Statistica software version 7 (StatSoft) and PRIMER-E (Plymouth routines in multivariate ecological research) version 6 (PRIMER-E, Ltd., UK).

1.3 Results

1.3.1 Climatological parameters

The precipitation regime observed for La Parguera during the sampling period (Figure 4) was characterized by frequent high to moderate rainfall episodes extending from April to September 2002 (monthly values ranged from 24.3 to 105 mm) and throughout April 2003 (cumulative monthly value of 217 mm). Maximum precipitation occurred in April 2003 during an event of heavy rainfall that lasted several days and produced ~117 mm of rainfall in the area. An extended period of very low precipitation persisted from October 2002 through the last week of March 2003, with minimum values registered for November 2002 (cumulative monthly value of 3.6 mm). Another period of very low rainfall occurred between May and June 2003, with cumulative monthly values of 7.1 and 16.3 mm, respectively. July 2003 exhibited moderate precipitation (cumulative monthly value of 38.3 mm).

Prevailing winds from the east-southeast (ranging from 98.51° to 124.07°) were measured for this region throughout the study period, except for October 2002 when winds were predominantly from the east-northeast (74.6°) (Figure 5). Maximum wind speeds were measured during November 2003 (3.19 m/s), while minimum wind speeds were recorded in October and December 2002 (1.71 and 1.89 m/s, respectively). These values represent the average of wind data for the seven days prior to the samplings.

1.3.2 Physical-chemical parameters

1.3.2.1 Temperature, salinity and dissolved oxygen

Surface water temperature at Bahía Fosforescente fluctuated from 25.9 to 33.5°C during the sampling period (Table 1). Higher temperatures were measured throughout the summer

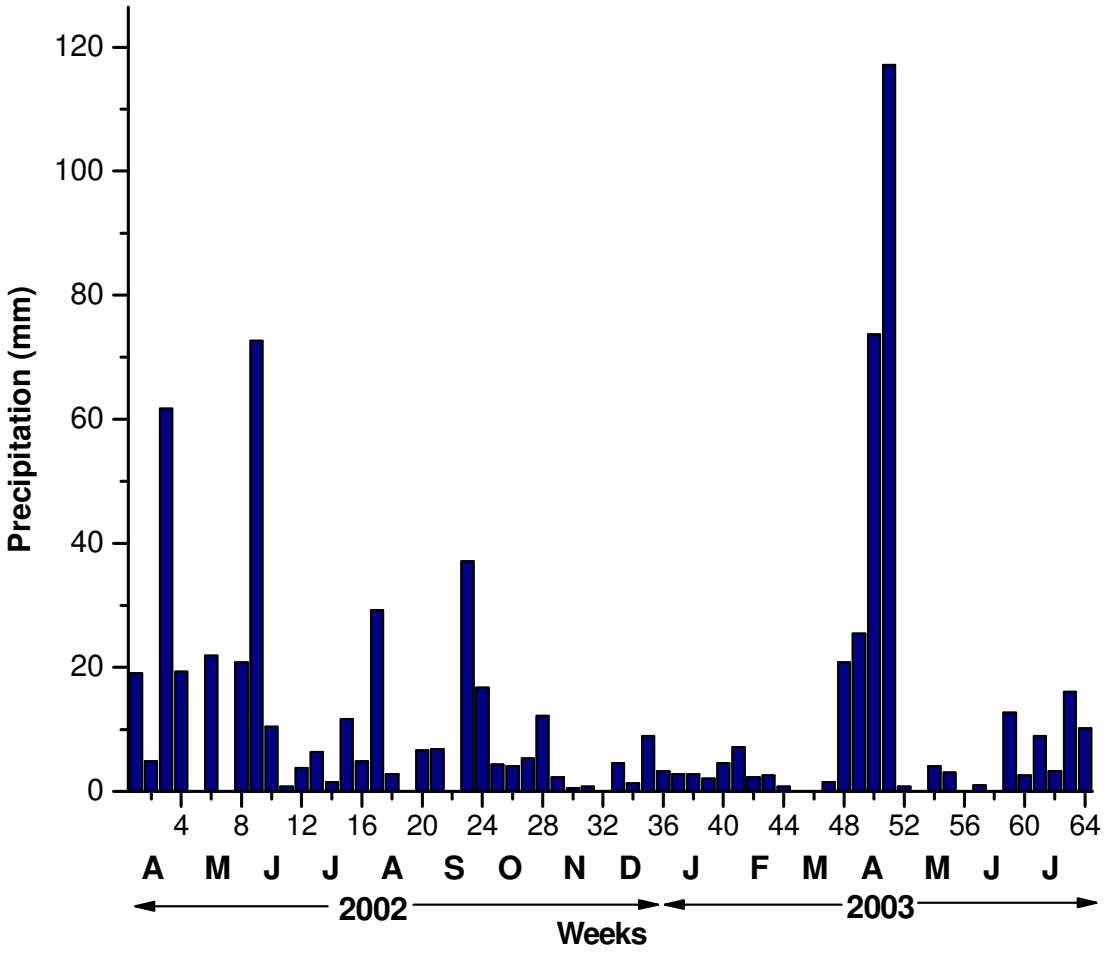

Figure 4. Distribution of weekly precipitation in La Parguera throughout the sampling period.

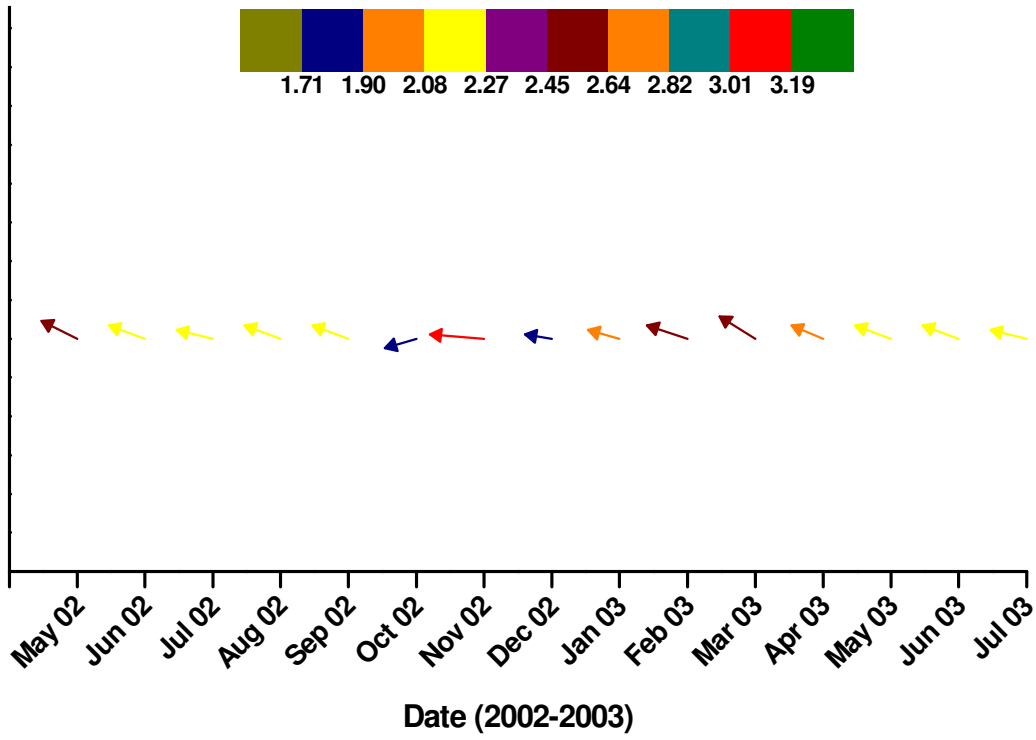

Figure 5. Vectors indicating the wind speed and direction measured in La Parguera throughout the study period. They represent the average of the data corresponding to the seven days preceding the samplings. The color scale indicates the wind speed range (m/s). The length and color of the arrows are indicative of the measured wind speed.

Table 1. Physical-chemical data measured at Bahía Fosforescente during the sampling period.

Date/Station	Temperature (ºC)	Salinity (ps)	Dissolved oxygen (mg L^{-1})	µmol L^{-1}					N:P ratio
				NH_4^+	NO_3^-	NO_2^-	PO_4^-	SiO_2	
May/ 28/2002									
* St 1	-	37	6.9	-	-	-	-	-	
* St 2	-	37	6.3	-	-	-	-	-	
St 3	-	38	6.4	-	-	-	-	-	
St 4	-	37	7.1	-	-	-	-	-	
St 5	-	37	6.9	-	-	-	-	-	
St 6	-	39	7.1	-	-	-	-	-	
Jun/27/2002									
* St 1	32	38	5.9	-	-	-	-	-	
* St 2	32	36.5	6.6	-	-	-	-	-	
St 3	31	36	6.1	-	-	-	-	-	
St 4	32	37	6.8	-	-	-	-	-	
St 5	32	38	4.5	-	-	-	-	-	
St 6	31.5	37	7.6	-	-	-	-	-	
Jul/31/2002									
* St 1	33.5	36	5.9	-	-	-	0.88	4.51	
* St 2	33	37.5	5.8	-	-	-	0.48	4.34	
St 3	32.5	38	5.6	-	-	-	0.46	4.74	
St 4	33.5	37	7.3	-	-	-	0.49	4.83	
St 5	33.5	35	5.4	-	-	-	0.20	3.91	
St 6	33.5	37	7.3	-	-	-	0.34	3.70	
Aug/28/2002									
* St 1	32	35	6.9	0.19	0.00	0.17	1.08	3.69	0.3
* St 2	32	36.5	5.6	0.09	0.00	0.06	0.22	3.54	0.7
St 3	32	36.5	5.4	0.26	0.00	0.05	0.12	3.44	2.5
St 4	33	35	6.0	0.27	0.00	0.08	0.13	3.97	2.7
St 5	32.5	35	5.9	0.44	0.00	0.13	0.22	3.96	2.6
St 6	32.5	34	-	0.18	0.00	0.05	0.19	3.85	1.2
Sep/26/2002									
* St 1	27	33.5	7.9	0.35	0.00	0.19	0.48	7.01	1.1
* St 2	27	34	3.5	0.21	0.00	0.28	0.79	7.18	0.6
St 3	27.5	35	2.8	0.79	0.08	0.19	0.12	5.04	9.0
St 4	28	35.5	4.1	1.04	0.08	0.20	0.21	5.34	6.3
St 5	28	36	3.5	1.71	0.21	0.25	0.28	5.20	7.8
St 6	28	37	5.2	0.50	0.26	0.19	0.20	4.18	4.8
Oct/22/2002									
* St 1	29	37	5.1	4.91	0.00	0.19	0.43	6.20	11.8
* St 2	28.5	37	4.2	2.10	0.05	0.16	0.21	4.05	10.7
St 3	28.5	37	4.2	2.10	0.10	0.16	0.21	3.82	11.2
St 4	29	37	5.7	1.41	0.05	0.18	0.28	3.91	6.4
St 5	29	37	5.1	2.61	0.18	0.27	0.70	3.80	4.4
St 6	29	36	6.1	0.32	0.07	0.08	0.18	3.27	2.7
Nov/14/2002									
St 1	28.5	35	4.3	2.41	0.72	0.42	0.31	5.03	11.3
St 2	28	34.5	4.4	2.97	0.76	0.38	0.18	4.43	23.0
St 3	28	35	3.6	1.23	0.17	0.14	0.12	3.61	12.6
St 4	29	35	5.1	1.97	0.18	0.23	0.34	4.29	7.0
St 5	29	35	3.7	1.23	0.42	0.34	0.39	4.48	5.1
St 6	29	34.5	6.2	0.11	0.00	0.10	0.24	4.15	0.9
Dec/19/2002									
St 1	28.6	36	6.9	3.29	0.00	0.63	0.81	4.48	4.8
St 2	28	35	5.4	2.41	0.00	0.15	0.25	3.45	10.2
St 3	27	35.5	4.9	1.85	0.08	0.14	0.18	3.40	11.8
St 4	27.5	35	6.6	1.51	0.00	0.19	0.21	3.50	8.2
St 5	28.7	35	6.0	1.37	0.21	0.17	0.27	3.77	6.5
St 6	27	34	6.6	0.98	0.41	0.10	0.14	2.72	10.5

Table 1 cont. Physical-chemical data measured at Bahía Fosforescente during the sampling period.

Date/Station	Temperature (ºC)	Salinity (ps)	Dissolved oxygen (mg L^{-1})	µmol L^{-1}					N:P ratio
				NH_4^+	NO_3^-	NO_2^-	PO_4^-	SiO_2	
Jan/27/2003									
St 1	26.8	38	4.7	4.97	0.48	0.32	0.57	4.47	10.1
St 2	26.9	36	5.7	3.81	0.42	0.27	0.25	4.08	17.9
St 3	26.9	37	5.9	2.76	0.15	0.18	0.22	3.82	14.1
St 4	27	35	4.7	4.26	0.26	0.26	0.36	4.66	13.4
St 5	27	36	4.2	3.23	0.91	0.33	0.32	5.48	13.9
St 6	27.5	35	6.5	3.26	0.42	0.15	0.24	4.10	16.0
Feb/25/2003									
St 1	26.8	36	5.3	1.75	0.40	0.25	0.79	4.74	3.0
St 2	26.7	37	5.5	1.97	0.36	0.24	0.34	3.60	7.5
St 3	25.9	37	6.4	0.65	0.07	0.09	0.23	2.97	3.5
St 4	26.5	36	7.1	0.82	0.09	0.12	0.23	3.18	4.5
St 5	27	36	4.2	2.00	0.91	0.49	0.38	5.34	8.9
St 6	26.7	36	7.9	0.06	0.00	0.13	0.22	3.11	0.9
Mar/25/2003									
* St 1	28.2	37	9.2	0.13	0.00	0.28	0.79	4.02	0.5
St 2	28	37.5	7.2	0.19	0.03	0.09	0.26	3.81	1.2
St 3	27.9	37	7.7	0.86	0.16	0.13	0.15	3.22	7.8
St 4	27.8	37	6.8	1.40	0.16	0.14	0.21	3.46	8.1
St 5	28.1	39.5	6.2	0.83	0.54	0.24	0.35	4.21	4.7
St 6	28.7	35	8.7	0.12	0.74	0.12	0.34	3.12	2.9
Apr/30/2003									
St 1	32	36	5.8	0.19	0.00	0.32	0.62	5.99	0.8
St 2	31	36	6.2	0.36	0.02	0.14	0.22	1.03	2.4
St 3	32	36	6.4	0.22	0.04	0.11	0.23	0.90	1.6
St 4	32	35	6.9	0.28	0.00	0.17	0.29	1.13	1.6
St 5	31	37	7.3	0.29	0.00	0.16	0.47	1.32	0.9
St 6	32	36	9.4	0.07	0.00	0.13	0.20	0.37	0.9
May/29/2003									
* St 1	32	38	5.7	0.11	0.00	0.10	0.63	8.63	0.3
* St 2	32	37	5.9	0.25	0.00	0.18	0.63	5.59	0.7
St 3	31.5	37	6.5	0.45	0.01	0.10	0.20	4.57	2.8
St 4	32	37	6.2	0.62	0.04	0.12	0.29	6.12	2.7
St 5	31.5	35	4.8	0.39	0.16	0.17	0.23	6.20	3.1
St 6	32	36	7.2	0.08	0.00	0.08	0.22	5.95	0.7
Jun/24/2003									
St 1	32	37	5.3	0.78	0.15	0.22	0.34	3.21	3.4
St 2	31	37	5.0	0.67	0.13	0.11	0.16	2.35	5.6
St 3	31	37	5.2	0.52	0.00	0.11	0.16	2.05	3.8
St 4	32	37	6.1	0.58	0.00	0.17	0.31	2.75	2.4
St 5	32	36	5.0	0.31	0.10	0.18	0.28	2.82	2.1
St 6	32	37	7.0	0.07	0.00	0.12	0.28	3.84	0.7
Jul/29/2003									
St 1	31	34	6.2	0.64	0.06	0.12	0.21	3.98	4.0
St 2	31	35	7.1	0.69	0.09	0.11	0.20	3.67	4.5
St 3	32	36	8.3	0.30	0.03	0.09	0.22	2.94	1.9
St 4	32	36	7.1	0.58	0.09	0.14	0.33	3.59	2.5
St 5	32	35	6.3	0.72	0.10	0.15	0.32	6.02	3.0
St 6	32	34.5	7.9	0.08	0.00	0.08	0.32	2.97	0.5

(-) Data not available. (*) *C. polykrikoides* blooms.

months (i.e. June-August 2002 and April-July 2003), with highest values occurring in July 2002. Lower temperatures corresponded to the period between September 2002 and March 2003, with lowest values occurring in February 2003. Spatial variations of temperature were minimal.

Salinity varied from 33.5 to 39.5 ps throughout the bay, with variations among the stations per sampling ranging from 0 to 4.5 ps (Table 1). The greatest temporal fluctuations (though moderate) were observed for stations 1, 5 and 6 with 33.5-38, 34-39.5 and 34-39 ps, respectively. In general, higher surface salinities occurred during May-July and October 2002, as well as from January to June 2003, whereas lower salinities mainly occurred in August-September and November-December 2002, and during July 2003. A significant negative correlation was found between salinity and the cumulative rainfall for the four weeks previous to the samplings ($r = -0.70$; $p < 0.05$).

Dissolved oxygen concentrations ranged from 2.8 to 9.4 mg L^{-1} (Table 1). Highest concentrations were typically measured at the center of the bay (station 6), though occasionally maximum values were found at station 1 (i.e. August, September and December 2002, and March 2003). Lower concentrations were invariably associated with the inlets (arms) of the bay, with lowest values usually alternating between stations 3 and 5. Significant negative correlations were found between dissolved oxygen and ammonium ($r = -0.59$; $p < 0.05$), and between dissolved oxygen and nitrate concentrations ($r = -0.71$; $p < 0.05$).

1.3.2.2 Nutrients

Ammonium (NH_4^+) concentrations at Bahía Fosforescente ranged from 0.06 to 4.97 µmol L^{-1} during the sampling period (Table 1). In general, higher values were measured at all stations between October 2002 and February 2003, particularly during January 2003. The highest concentrations were measured at station 1 during October 2002 and January 2003 (4.91 and 4.97 µmol L^{-1}, respectively). Lower ammonium values were measured at all stations between August

and September 2002 (with few exceptions), and from March through July 2003. Lowest values typically corresponded to station 6, except in August - September 2002 and January 2003.

Dissolved nitrate (NO_3^-) concentrations were extremely low overall (0- 0.91 µmol L^{-1}), mostly less than 0.5 µmol L^{-1} and often reaching undetectable levels (Table 1). Higher values were generally measured between November 2002 and March 2003 (with some exceptions, particularly at station 6), whereas lower concentrations prevailed from August to October 2002 and from April to July 2003. Undetectable or lowest concentrations were found at all stations in August 2002 and April 2003. Levels of dissolved nitrite (NO_2^-) were also very low, but always detectable (0.05-0.63 µmol L^{-1}) (Table 1). Most stations consistently exhibited concentrations less than 0.4 µmol L^{-1}, except for stations 1 and 5 where higher values were occasionally measured. During most samplings, lowest concentrations were found at stations 3 and 6 (usually < 0.2 µmol L^{-1}).

Phosphate (PO_4^-) concentrations varied between 0.12 and 1.08 µmol L^{-1} (Table 1). Dissolved phosphates were, for the most part, notably higher at station 1 relative to the other areas and were always among the highest measured values (except in July 2003). In contrast, stations 3, 4 and 6 continually exhibited very low concentrations, typically less than 0.5 µmol L^{-1}. Phosphate concentrations at stations 2 and 5 were much more variable (occasionally exhibiting highest values). N:P ratios of dissolved inorganic nitrogen to phosphate (DIN/PO_4^+) ranged from 0.3 to 23.0 throughout the bay (Table 1). With the exception of three values corresponding to the samplings of November 2002 and January 2003, N:P ratios were lower than 14.1 (Table 1).

Of all nutrients, dissolved silicate (SiO_2) concentrations reached the highest levels (0.37-8.63 µmol L^{-1}) (Table 1). Relatively high silicate values (>2 µmol L^{-1}) were consistently measured at all stations, except in April 2002 when concentrations dropped to their lowest levels

for all but station 1. Silicate concentrations were, in general, comparable among the stations though often, values tended to be higher at station 1 (particularly in October 2002 and April-May 2003) and lower at station 6.

1.3.2.3 Statistical analysis of spatial and temporal distributions of physical-chemical parameters

Principal component analysis (PCA) revealed differences in the physical-chemical properties of the seawater both in space and time (Figure 6). Two components (PC1 and PC2) explained 59% of the variation in the data, while three components (PC1, PC2 and PC3) accounted for 72.1 % of the variability (PC3 is not presented in the 2-dimensional plot). Parameters scoring high on PC1 (meaning that they were well represented in that particular PC or axis) were nitrites, ammonium, nitrates, silicates and phosphates, while on PC2 salinity and nitrates were the ones that scored higher. PCA showed a clear differentiation between station 1 and the other stations, where station 1 was preferentially represented towards the nutrient vectors, particularly those corresponding to phosphates and silicates. Station 1 also exhibited greater temporal variability in its physical-chemical properties relative to the other stations, primarily related to phosphate, silicate, ammonium, nitrate and nitrite concentrations. Spatial and temporal differences among the physical-chemical properties of the other stations were much less evident. Temperature and dissolved oxygen were the parameters that varied less in space and time, and therefore most points appeared concentrated towards the corresponding vectors in the two-dimensional plot, which were very close to each other but separated from the others.

Analysis of similarity (ANOSIM) confirmed significant differences of the physical-chemical seawater properties between stations ($R = 0.405$; $p = 0.001$) and in the temporal scale ($R = 0.313$; $p = 0.001$). Similarity percentage (SIMPER) analysis showed that the physical-chemical parameters that mostly contributed to the overall dissimilarity among stations

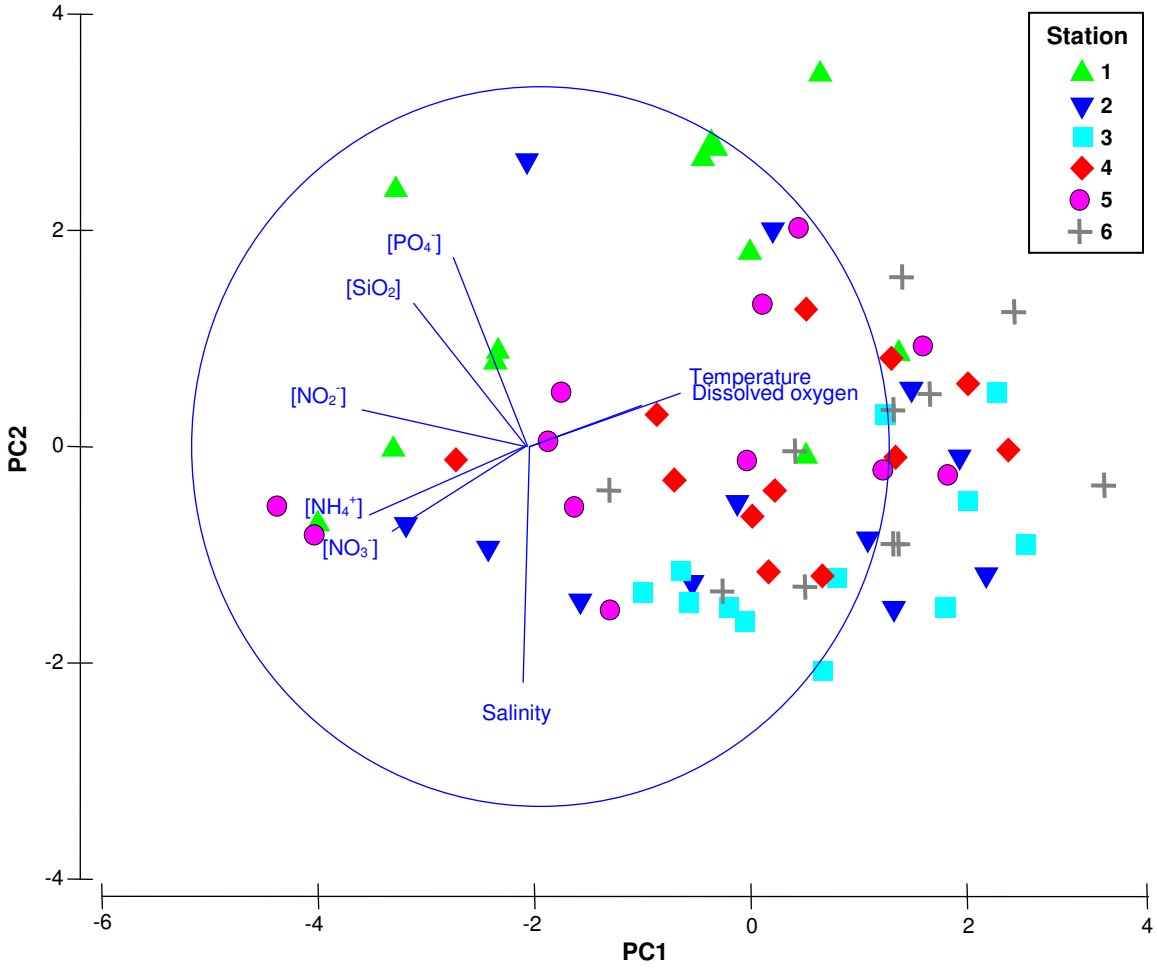

Figure 6. Principal component analysis (PCA) ordination plot of sampling stations based on physical-chemical parameters.

were the phosphates and nitrates (average contribution of 22.84 and 20.4%, respectively), though the ones that contributed most to the dissimilarity observed between station 1 and the other stations were the phosphates and nitrites (average contributions of 30.4 and 18.02%, respectively) (Appendix 2). In the temporal scale, silicates and ammonium were the parameters that mostly contributed to the overall dissimilarity with average contributions of 21.5 and 20.9 %, respectively (Appendix 3).

1.3.3 Vertical attenuation coefficient of downwelling irradiance, K_d (PAR)

K_d (PAR) values at Bahía Fosforescente showed considerable spatial and temporal variability, ranging from 0.24 to 3.96 m^{-1} (Figure 7). Spatially, PAR (photosynthetic active radiation) attenuation was least variable in May 2002 and February 2003 (values ranging from 0.68 to 1.05 and from 0.49 to 0.86 m^{-1}, respectively), and most variable in June and September 2002 (values varying from 0.53 to 3.96 and 0.33 to 2.18 m^{-1}, respectively). Temporal variability was greater for stations 1, 3 and 4, with values from 0.39 to 2.18, 0.33 to 2.13 and 0.58 to 3.96 m^{-1}, respectively, and lesser for stations 2, 5 and 6 where values ranged from 0.41 to 1.29, 0.51 to 1.30 and 0.23 to 1.05 m^{-1}, respectively. The center of the bay (station 6) typically showed the lowest or among the lower K_d (PAR) values (except in May 2002), whereas station 1 often exhibited greatest PAR attenuation (or among the higher values, except in May, June and August 2002).

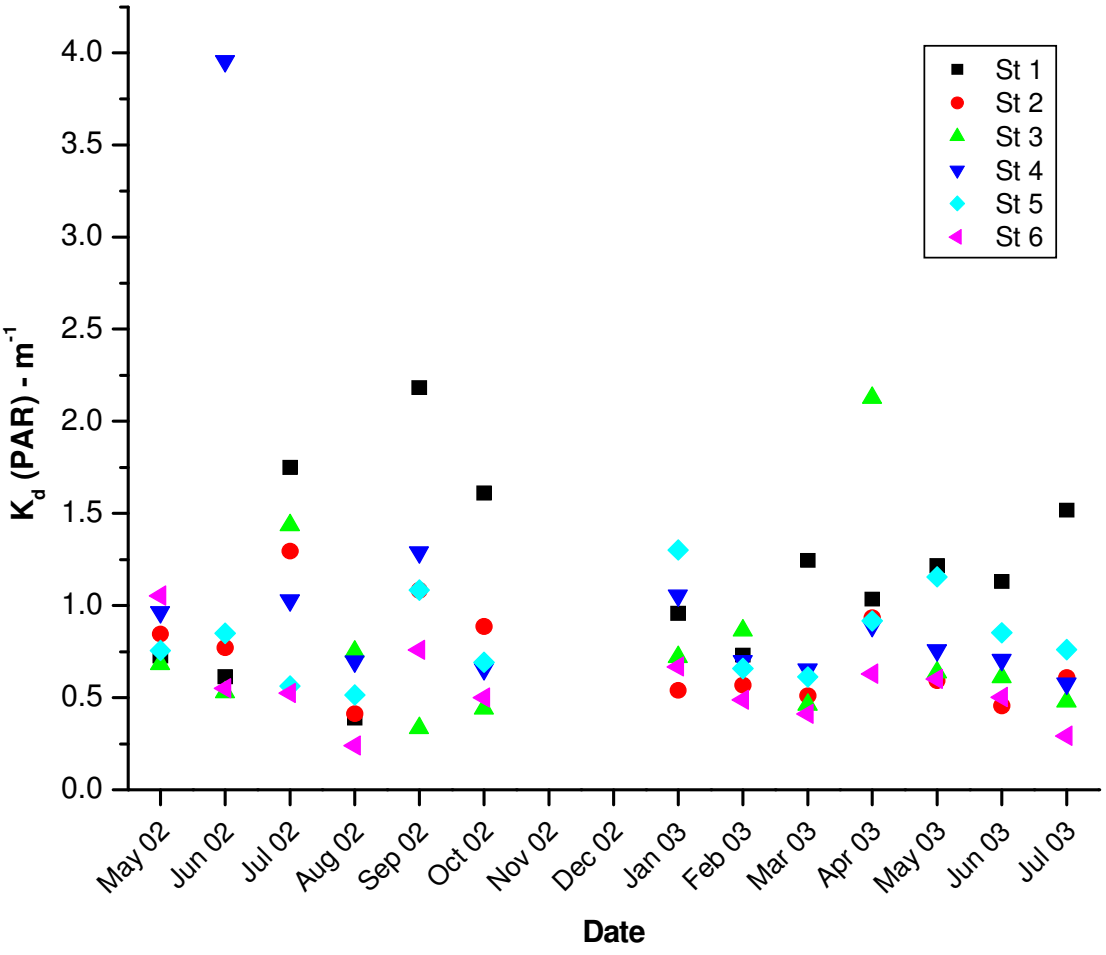

Figure 7. Vertical attenuation coefficients of downwelling PAR irradiance, K_d (PAR), measured at Bahía Fosforescente throughout the sampling period. Data corresponding to November and December 2002 is missing because the LiCor 1400 irradiance meter was sent to the manufacturer for maintenance service during that time.

1.3.4 Chlorophyll *a* concentration

Chlorophyll *a* concentrations, representing the average of fluorometric, spectrophotometric and HPLC measurements, ranged from 0.27 to 39.15 µg L^{-1} throughout the study period (Figure 8). Highest concentrations were normally found in the western-most arm of the bay at stations 1 and 2, but mainly at station 1. However, during the sampling of March 2003 comparatively high chlorophyll *a* values were also measured at station 6 (11.5 µg L^{-1}) associated with a bloom of *Ceratium furca* var. *hircus* and *Pyrodinium bahamense*, whereas in April and July 2003 highest values were measured at station 5 (10 and 4.6 µg L^{-1}, respectively). Maximum overall values occurred in August and September 2002 at stations 1 (39.15 µg L^{-1}) and 2 (34.44 µg L^{-1}), respectively. Minimum values occurred in June (0.27 µg L^{-1}) and September 2002 (0.31 µg L^{-1}) at stations 3 and 4, respectively. During the samplings of February and June 2003 chlorophyll *a* concentrations were lower than 2.5 µg L^{-1} at all stations.

1.3.5 Spatial and temporal distribution of *Cochlodinium polykrikoides* abundance

The presence of *C. polykrikoides* at the six sampling stations is presented in Figure 9. *Cochlodinium polykrikoides* was always observed as single cells or forming chains of 2 or 4 cells, with cell chains more common under bloom conditions. *Cochlodinium polykrikoides* exhibited an aggregated spatial distribution towards the northwest corner of the bay (stations 1 and 2), where cell abundances from 0 (undetectable) to 1.34 x 10^6 cells L^{-1} were found throughout the study period (Figure 9a). At the other stations, *C. polykrikoides* always occurred in substantially lower concentrations that often reached background or undetectable levels (Figure 9b), particularly at stations 5 and 6 where the lowest abundances (<1,374 cells L^{-1}) were generally found. At station 3 and 4, *C. polykrikoides* cell abundance fluctuated from 0 to 28, 210 cells L^{-1}

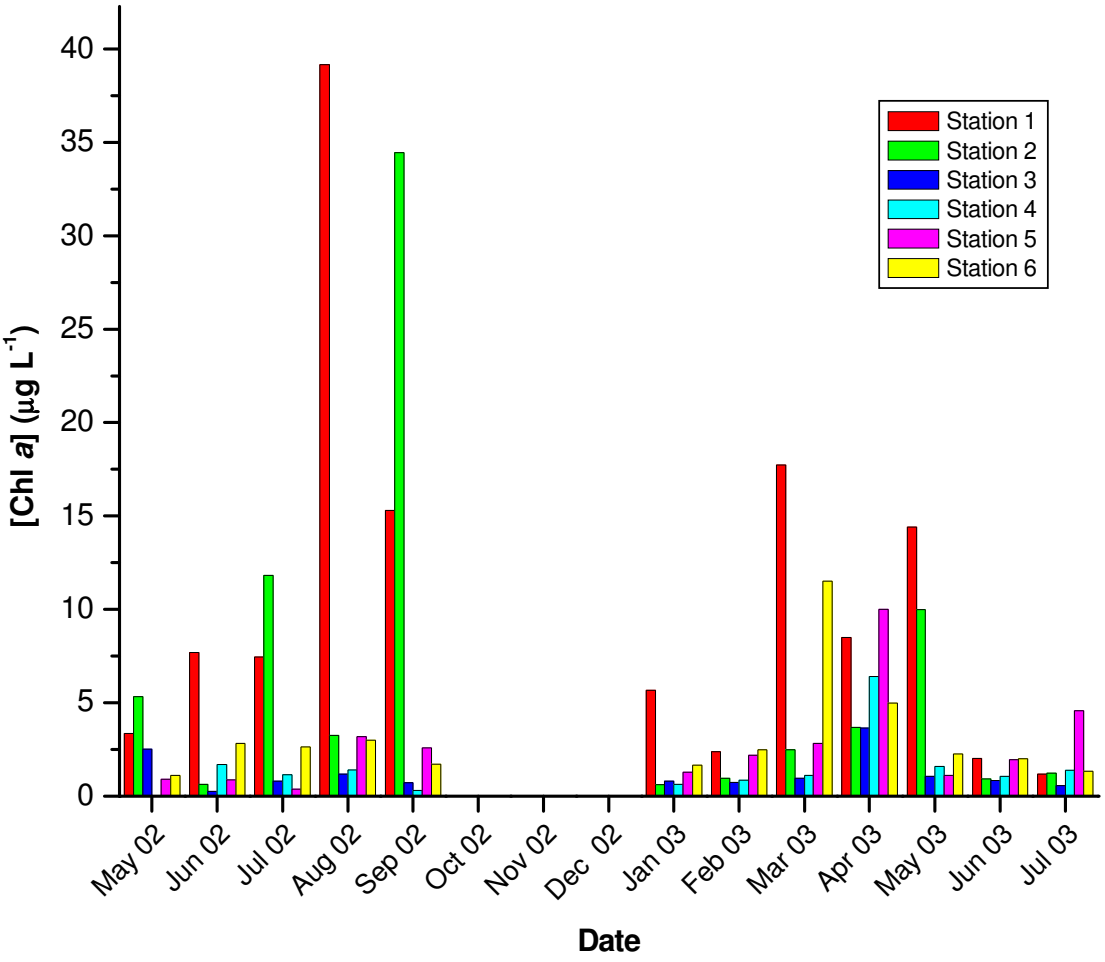

Figure 8. Chlorophyll *a* concentrations measured at Bahía Fosforescente throughout the sampling period. Values represent the average of spectrophotometric, fluorometric and HPLC measurements. Data corresponding to October, November and December 2002 was accidentally lost.

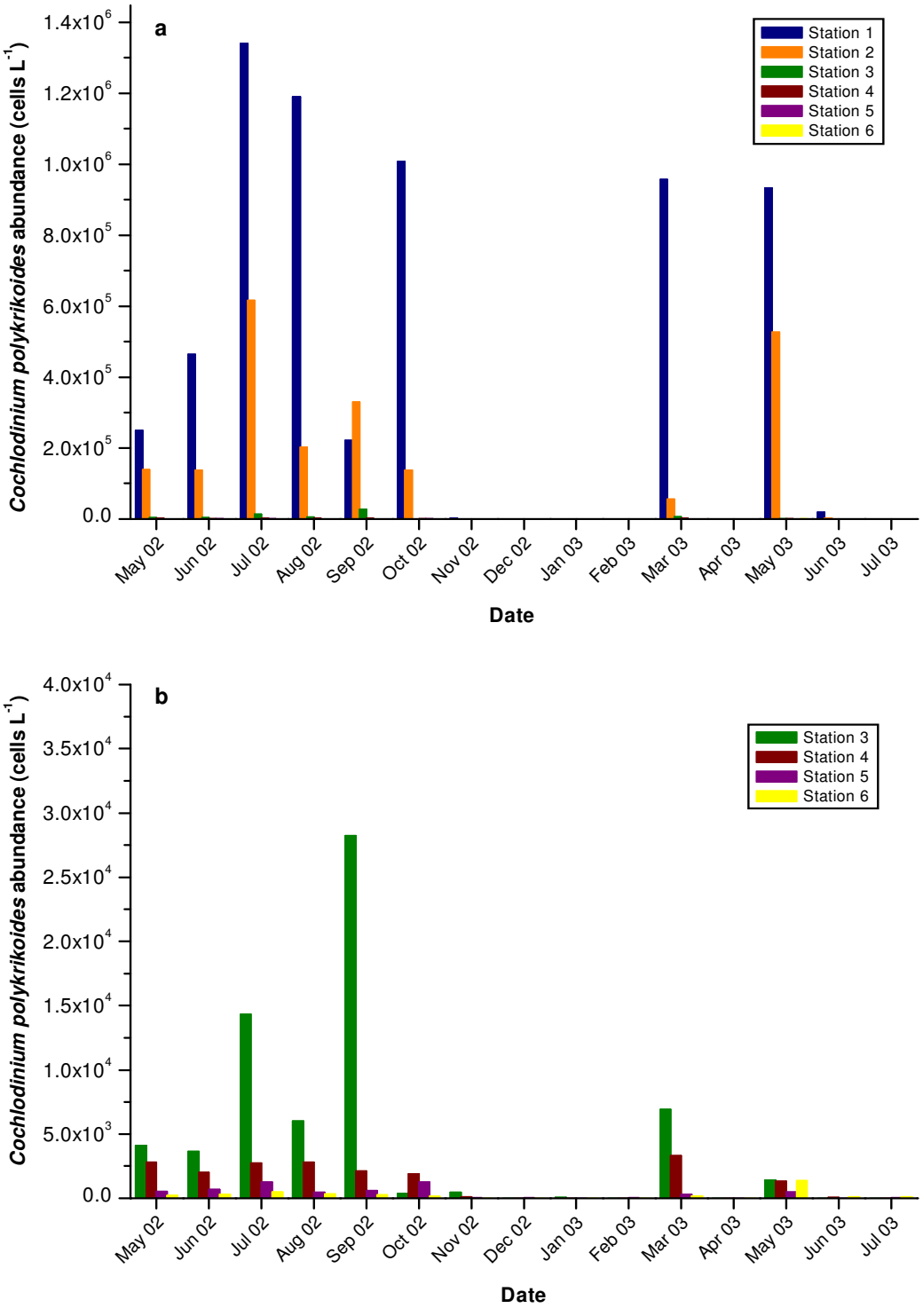

Figure 9. *Cochlodinium polykrikoides* abundances at the six sampling stations in Bahía Fosforescente during the study period. a) Cell abundances at all stations. b) Cell abundances at stations 3 to 6 with expanded scale to show low abundances.

and from 0 to 3,299 cells L^{-1}, respectively.

Very high cell densities or blooms (>10^5 cells L^{-1}) of *C. polykrikoides* were observed at stations 1 and 2 from May to October 2002, and during March and May 2003 (Figure 9a). During these blooms, *C. polykrikoides* was by far the dominant species. The most intense bloom episode occurred in July 2002, when cell densities at stations 1 and 2 were 1.34 x 10^6 and 6.16 x 10^5 cells L^{-1}, respectively. The presence of *C. polykrikoides* at other stations followed the same temporal pattern as the bloom occurrences (Figure 9b). *Cochlodinium polykrikoides* practically disappeared from November 2002 to February 2003 when cell abundances varied from 0 to 3,300 cells L^{-1} throughout the bay, and then again during April and July 2003 when cell abundances were from 0 to 96 cells L^{-1}. In June 2003, very low concentrations (<100 cells L^{-1}) of *C. polykrikoides* cells also occurred, except for station 1 where an abundance of 19,490 cells L^{-1} was found.

Two-way ANOVA revealed significant differences in the temporal and spatial pattern of *C. polykrikoides* abundance ($p < 0.0001$ and $p < 0.0001$, respectively) (Appendix 4). Additionally, the temporal and spatial patterns of *C. polykrikoides* abundance were characterized by a significant interaction between sampling dates and stations ($p = 0.005$) (Appendix 4), meaning that spatial differences of *C. polykrikoides* abundance depend upon dates, and vice versa.

1.3.6 Relationship between *C. polykrikoides* abundance and the physical-chemical and climatological parameters

PCA showed differences in the physical-chemical properties of the seawater between *C. polykrikoides* bloom and non-bloom periods (Figure 10). Two components (PC1 and PC2)

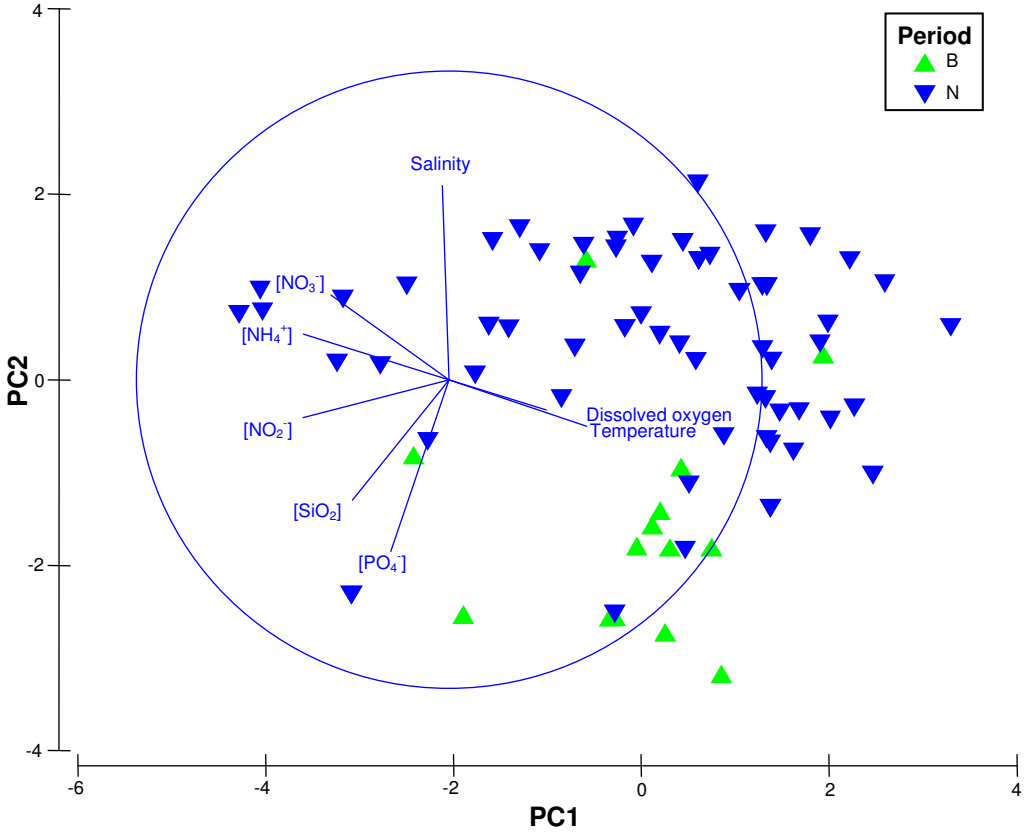

Figure 10. Principal component analysis (PCA) ordination plot of *C. polykrikoides* bloom (B) and non-bloom (N) periods based on physical-chemical parameters.

accounted for 59% of the variation in the data, while three components (PC1, PC2 and PC3) explained 72.4 % of the variability (PC3 is not presented in the 2-dimensional plot). Parameters scoring high on PC1 were nitrites, ammonium, nitrates, silicates and phosphates, while on PC2 phosphates and silicates were the ones that scored higher. PCA revealed a clear separation between bloom and non-bloom periods, where all the points corresponding to *C. polykrikoides* bloom conditions appeared mostly oriented towards the phosphate and silicate vectors. On the other hand, although the points representing non-bloom conditions appeared, in general, more dispersed through the plot, they were preferentially represented towards the temperature, dissolved oxygen and salinity vectors, and to a lesser degree toward the nitrate and ammonium vectors. Discriminant function analysis (DFA) confirmed that silicates and then phosphates are the physical-chemical parameters that better discriminate *C. polykrikoides* blooms from non-bloom periods in Bahía Fosforescente (Table 2).

No significant correlations were found between *C. polykrikoides* abundance and the cumulative rainfall corresponding to 7 days, 14 days, 21 days and 1 month prior to the samplings, nor with the average wind speed and direction for the 2 and 7 days preceding the samplings.

Table 2. Summary of discriminant function analysis (DFA) of physical-chemical parameters that better discriminate *C. polykrikoides* bloom and non-bloom periods. (Wilks' Lambda varies between 0 and 1; the closer to 0 the better the discriminant power. Partial lambda is the contribution of each variable to discrimination. Tolerance measures the redundancy of a particular variable with respect to the others).

Physical-chemical variables	Wilks' Lambda	Partial Lambda	F-ratio (df = 1, 73)	p-level	Tolerance	1-Tolerance (R-Sqr.)
Phosphates (PO_4^-)	0.82	0.59	50.16	0.00	0.66	0.34
Silicates (SiO_2)	0.54	0.90	7.86	0.01	0.92	0.09

1.4 Discussion

Characterization of climatological, physical-chemical and bio-optical parameters in Bahía Fosforescente

This is the first study addressing the population dynamics of the dinoflagellate *Cochlodinium polykrikoides* in Bahía Fosforescente. Given its potential noxious effects, it is vital to identify which factors or conditions are favorable for the formation of recurrent blooms of this species within this bay. With that in mind, a comprehensive data set including climatological, physical-chemical and bio-optical parameters was collected simultaneously with *C. polykrikoides* abundance data, and analyzed.

The precipitation and wind patterns observed for La Parguera area during the study period were, in general, consistent with the climatological conditions prevalent in the southwestern region of Puerto Rico. This area is characterized by low rainfall, with a dry season extending from December to April and a relatively wet season from May through November (Glynn, 1973). The high rainfall recorded during April 2003, as well as the very low rainfall that occurred during May 2003, represented atypical conditions. The predominating east-southeast winds measured throughout the study agreed with the wind field reported for this region which has its strongest component from the east and southeast (Glynn, 1973; Seixas, 1988).

Temperature and salinity values measured at Bahía Fosforescente were comparable with those reported by other authors (Coker and González, 1960; González, 1965; Cintrón, 1969; Smayda, 1970; Seixas, 1983; Seixas, 1988; Walker, 1997; Soler, 2006) (Appendix 5) and are indicative of the arid conditions that characterize the area. Surface temperatures changed in accordance with seasonal climatological fluctuations, exhibiting maximum values in the summer (July 2002) and minimum values in the winter period (February 2003). Even though a negative

correlation was found between salinity and rainfall, the lowest salinities did not necessarily correspond to the period of maximum precipitation, and vice versa. For instance, relatively high salinity values (35-37 ps) were measured throughout the bay during the sampling of April 2003, just about a week after a heavy rainfall episode that represented the precipitation peak for the study period. Likewise, the low salinities measured during November 2002 (34.5-35 ps) coincided with the precipitation minimum. This was probably related to seasonal changes in the evaporation rates for these waters (Margalef, 1961), where lower evaporative rates may have balanced the low precipitation during November, resulting in low salinities, whereas higher evaporative rates in April may have resulted in relatively high salinities despite the heavy rainfall.

Highest dissolved oxygen concentrations were generally found in the center of the bay (station 6) primarily as a result of being the deepest and most exposed sampling area, which makes it less affected by turbidity and more influenced by wind mixing, thus promoting oxygen diffusion in surface waters. The photosynthetic activity of the numerous dinoflagellates typically associated with this area (Seliger et al., 1971; Walker, 1997; Soler, 2006) presumably contributed to the high dissolved oxygen levels in this station. The northern part of the bay, on the other hand, is not only much shallower and protected from wind mixing by the bordering mangroves, but is also prone to the accumulation of organic material from the mangrove community, stimulating oxygen consumption by means of organic matter decomposition and remineralization processes. Nevertheless, very high levels of dissolved oxygen were occasionally measured at station 1 coinciding with blooms of *C. polykrikoides* (August and September 2002, and March 2003) and of *Akashiwo sanguinea* (December 2002). This suggested that these blooms were in early stages, when oxygen production by photosynthesis significantly exceeded consumption due to decomposing organic matter. The negative

correlation found between dissolved oxygen and ammonium/nitrate concentrations (related to a significant consumption of nitrogen by phytoplankton during photosynthesis, as well as to considerable oxygen utilization during decomposition and remineralization processes) implied the influential role of photosynthesis in supporting high dissolved oxygen levels in these waters.

Nutrient concentrations were, for the most part, within the range measured in previous studies (González, 1965; Smayda, 1970; Seixas, 1983; Seixas, 1988; San Juan and González, 2000; Soler, 2006) (Appendix 5). Overall, silicate represented the most abundant nutrient along the bay followed by ammonium. Phosphate, nitrite and nitrate levels were invariably very low ($\leq 1\ \mu mol\ L^{-1}$). These results are consistent with the findings of González (1965), who reported much higher silicate concentrations in the bay relative to the other nutrients, and of Soler (2006), who also found considerably higher levels of silicates and ammonia in the central part of the bay than of phosphates, nitrates and nitrites. These high silicate levels presumably respond to the preponderance of dinoflagellates in these waters, not known to have any particular requirements for silica. The slightly lower silicate concentrations measured in the center of the bay may be attributed to a preferential occurrence of pelagic diatoms in this area where turbulent mixing may prevent them from sinking, given their lack of locomotion capabilities. The considerably lower phosphate, nitrite and nitrate concentrations available in these waters suggested a strong utilization of these nutrients by phytoplankton, while the comparatively higher ammonium concentrations measured implied a tight coupling with *in situ* biologically mediated redox-transformations (i.e. nutrient cycling). San Juan and González (2000) had previously hypothesized that ammonification could be a key process in the release of nitrogen from the sediments to the water column in this bay, such as to sustain a very high density of phytoplankton. The general trend of N:P ratios, with most values lower than 10, diverged

notably from the requirements of phytoplankton based on the Redfield molar ratio of N:P = 15. This suggests a strong nitrogen limitation in these waters.

Vertical light attenuation coefficients [K_d (PAR)] for Bahía Fosforescente were consistently very high, exhibiting values typical of productive coastal waters. The central part of the bay often showed lowest K_d (PAR) values, presumably due to its higher depth, susceptibility to wind mixing and water exchange, and less proximity to the surrounding mangroves compared to the other stations. These factors help reduce sediment resuspension and the accumulation of color dissolved organic matter (CDOM) and suspended materials (i.e. phytoplankton cells and detritus from the mangroves), thus allowing deeper light penetration. In contrast, station 1 frequently showed greatest PAR attenuation given its very secluded location (which facilitates the accumulation of suspended and dissolved materials), prevalence of dinoflagellate blooms, close proximity to the surrounding mangroves and shallow depth (~1m), all of which promote a strongly reduced light penetration.

Chlorophyll *a* concentrations showed high spatial and temporal variability, sporadically reaching considerably elevated values (>15µg L^{-1}). There was a tendency for higher chlorophylls to occur towards the northern margin of the bay, predominantly in the northwest corner, concurrent with red tide blooms of *C. polykrikoides* and of *A. sanguinea*. Nevertheless, in few occasions higher values also occurred at station 6. This general spatial pattern of chlorophyll *a* coincided, to a large extent, with the spatial distribution of the physical-chemical parameters. Results indicated that station 1 differed substantially from the other stations in relation to its physical-chemical characteristics, particularly in its nutrient content. This station often exhibited higher concentrations of nutrients, mainly phosphates and silicates, and less frequently of ammonium, nitrites and nitrates. This suggests a direct supply of nutrients in that

particular area, probably related to land drainage during rainfall events (Cintrón, 1969), coupled with a significant contribution of organic mangrove materials and a very efficient nutrient cycling associated with bottom microbial activity (Burkholder and Burkholder, 1958; Burkholder et al., 1967).

Relationship between *C. polykrikoides* blooms and the climatological and physical-chemical parameters

The blooms of *C. polykrikoides* in Bahía Fosforescente constitute an interesting phenomenon given their recurrent and constrained occurrence towards the northwest margin of the bay (Margalef, 1961; Burkholder et al., 1967; Cintrón, 1969; Cintrón et al., 1970; Seliger et al., 1971; Seixas, 1983). Even though this study demonstrates the presence of *C. polykrikoides* in other areas of Bahía Fosforescente, it consistently occurred in very low or background concentrations. This species only reached high densities in the northwestern arm of the bay, particularly toward the inner part of this cove.

The characteristics of Bahía Fosforescente that makes it an ideal location for the occurrence of dense populations of dinoflagellates have been well documented (Margalef and González, 1958; Margalef, 1961; US Department of Interior, 1968; Seliger et al., 1971). Fundamentally, it is understood that the physical characteristics of the bay, consisting of its small size, shallow basin and narrow entrance with a sill, interact with the prevailing winds and arid conditions, absence of riverine discharge and the prevalent small tidal range, to restrict its diffusion and flushing rates. The fringe of mangrove trees encircling the bay, periodic land runoff and microbial nutrient cycling processes, provide plenty of nutrients and growth factors to these waters (Burkholder and Burkholder, 1958; Burkholder et al., 1967). All these factors result in a fairly stable water mass, able to develop markedly different characteristics from that of

adjacent waters, that furthers the growth and retention of large numbers of dinoflagellates (US Department of Interior, 1968; Cintrón et al., 1970).

Margalef (1961) further emphasized that the inlets (or arms) of the bay represent optimal settings for the initiation of dinoflagellate blooms. As discrete, semi-isolated areas within the main water body of the bay they offer twice as favorable diffusivity conditions, such as to reduce the horizontal dispersion of dinoflagellate cells, plus the minimum nutritional requirements to support the accumulation of these organisms. This seems to explain, at least partially, the occurrence of *C. polykrikoides* blooms in the northern part of the bay. However, it does not provide an explanation for their limited distribution towards the northwestern corner, despite the fact that the three inlets share similar physical characteristics.

Overall, the spatial distribution of *C. polykrikoides* blooms in Bahía Fosforescente appears to be highly related to the observed spatial patterns of nutrients in these waters. As explained previously, the inner part of the northwestern inlet (station 1) was characterized by often showing relatively higher phosphate and silicate levels than the other stations. Occasionally, higher concentrations of ammonium, nitrite and nitrates were also observed. Since *C. polykrikoides* does not have any known requirements for silica, high levels of this nutrient are not expected to have any influence on the blooms of this species. Phosphorus and nitrogen, on the other hand, are essential nutrients of all phytoplankters and are most often implicated in the constraint of phytoplankton growth in marine environments (Reynolds, 2006). The fact that *C. polykrikoides* preferentially grows in this particular area of the bay, where phosphate levels tend to be higher, suggest that these blooms are primarily controlled by phosphorus and not by nitrogen. This is in agreement with the findings of Gárate-Lizarraga et al. (2004), who found higher levels of phosphates in a coastal lagoon in Bahía de La Paz, Gulf of California, during the

onset of a *C. polykrikoides* bloom than previously measured for that area. On the other hand, the very low N:P ratios (0.3-11.8) typically observed during *C. polykrikoides* blooms (Table 1) strongly implied a limitation by nitrogen and not by phosphorus. This is consistent with Tomas and Smayda (2008), who found that *C. polykrikoides* blooms in a coastal cove in Rhode Island occurred or developed towards nitrogen-limiting environments, but rarely occurred in phosphorus-limited environments.

Other factors contributing, to a greater or lesser extent, to the limited spatial distribution of *C. polykrikoides* in Bahía Fosforescente are the prevailing winds and tides. Seixas (1988) pointed out the relevance of wind patterns in generating and maintaining dense patches of dinoflagellates in surface waters, and their movement within the bay. Under the influence of the southeast winds, the water in Bahía Fosforescente tends to move towards the northwest. Even though the wind does not seem to have an effect by itself on the generation of blooms of *C. polykrikoides*, supported by the no correlation found between *C. polykrikoides* abundance and wind speed/direction, it is an important factor in maintaining the cells aggregated in the northwestern margin. Correspondingly, the small tidal amplitude characteristic of the area (~30 cm) prevents these blooms from extreme advective losses.

Some specific life-form characteristics of *C. polykrikoides* may also have an influential role in its strongly aggregational or patchy distribution towards the northwestern margin of the bay. *Cochlodinium polykrikoides* is highly motile (Margalef, 1961) and was usually observed forming chains of up to four cells, particularly under bloom conditions. Chain formation has been recognized as an adaptational strategy of some bloom-forming dinoflagellates to increase their motility (Fraga et al., 1989). *Cochlodinium polykrikoides* also tended to form large clumps or strips of cells embedded in mucilaginous secretions when in high densities. Mucilage

production is considered another adaptative strategy of red tide dinoflagellate species to dampen turbulence (Smayda, 2002). Furthermore, this species has been reported to be positively phototactic (Seliger et al, 1971) and to migrate vertically in the water column (Park et al., 2001). All these life-form characteristics represent important mechanisms to overcome advective losses and to promote the spatial accumulation of this organism.

A comparison between qualitative trends of rainfall and *C. polykrikoides* abundance during the study period (Figs. 4 and 9) revealed that the occurrence of *C. polykrikoides* blooms followed a similar tendency to that observed for the precipitation regime. Moreover, *C. polykrikoides* practically disappeared from November 2002 to February 2003 and from June to July 2003, coincidentally with extended periods of very low rainfall. This implies that precipitation is an important factor influencing the population dynamics of *C. polykrikoides*, most likely promoting the availability of essential nutrients, vitamins and chelating substances (humic and fulvic acids) required for its growth, as previously proposed by Burkholder et al. (1967). Since no correlation was found between cell abundance and the cumulative rainfall for the 7, 14, 21 and 30 days preceding the samplings, it is inferred that the intensity and delay in the response (i.e. proliferation of cells) of *C. polykrikoides* to these nutrient pulses is highly variable. This may be due to variations in nutrient input during rainfall events, and/or in the lag periods needed for sedimentation to reduce water turbidity and for *C. polykrikoides* to adapt to conditions of enhanced nutrient concentrations (i.e. preconditioning), lower salinity and adequate light penetration. It also may be related to competition of *C. polykrikoides* with other dinoflagellate species in the area that may prevent it from proliferating.

Although *C. polykrikoides* was usually the dominant bloom-forming species in the northwestern arm of the bay, blooms of *A. sanguinea* were observed in this same area during

December 2002 and April 2003. The bloom of April 2003 concurred with the peak precipitation event for the study period. A common observation during both bloom episodes was the virtual absence of *C. polykrikoides* (367 and 24 cells L^{-1}, respectively). In the same way, *A. sanguinea* was never found to occur during *C. polykrikoides* blooms. Cintrón (1969) and Seliger et al. (1971) also reported the occurrence of *A. sanguinea* blooms in the northwestern arm in complete absence of *C. polykrikoides* and vice versa. Moreover, Cintrón (1969) reported the transition between blooms of these two species to be abrupt. This strongly suggests that these species are mutually exclusive in this area. This apparent exclusion may involve the production of allelopathic exudates released into the water that inhibit the growth of competing species (Glibert et al., 2005 and references therein). However, it may also be related to differences in adaptability to salinity changes between these two species. Cintrón (1969) compared the salinity tolerance of both species and concluded that *A. sanguinea* appears to be better able to survive rapid salinity reductions than *C. polykrikoides*. This agrees with the trend observed after the heavy rainfall episode of April 2003, where an *A. sanguinea* bloom developed immediately after the rainfall and was followed by a *C. polykrikoides* bloom several weeks later (May 2003). Although this seems a plausible explanation to the delayed proliferation of *C. polykrikoides* after this heavy rainfall episode, it does not necessarily represent the only mechanism responsible for the sporadic prevalence of *A. sanguinea* over *C. polykrikoides* in this area. Salinities in the northwestern arm do not appear to vary much, even during heavy rainfall events due to the high evaporative and transpiration rates in this area, as to explain the occasional alternation between the blooms of these two species. Additionally, a dense bloom of *A. sanguinea* occurred in December 2003 during a period of very low precipitation, when typical salinity values (St 1 = 36 ps; St 2 = 35 ps) for these waters were measured. This implies that other mechanisms such as

differences in specific growth rates, action of allelopathic substances and/or sudden changes in wind velocity favoring the movement and accumulation of large numbers of *A. sanguinea* cells towards the northwest arm (Cintrón, 1969), most likely control or assist the proliferation of this species in the absence of *C. polykrikoides*, or by out-competing it.

The fact that a *C. polykrikoides* bloom occurred during March 2003, in the absence of a previous rainfall episode, denote the relevance of other factors in initiating blooms of this organism. Relatively high phosphate concentrations were measured at station 1 during the sampling of March 2003, implying that rainfall is not necessarily a prerequisite for the availability of high nutrients in this area. These are very shallow waters receiving a continuous supply of organic matter from the adjacent mangrove community. Therefore, the decomposition of these mangrove materials and dead phytoplankton cells, along with the redox transformations that take place in bottom sediments, must contribute considerable amounts of dissolved organic and inorganic nutrients to these waters. A sudden increase in wind velocity capable of inducing enough turbulent mixing such as to bring ample nutrients from bottom sediments to surface waters may trigger the onset of a *C. polykrikoides* bloom. After the bloom initiates and nutrient levels start to decrease due to excessive consumption, dense concentrations of *C. polykrikoides* may be sustained given its propensity to undertake vertical migrations (Park et al., 2001). Nocturnal migrations to bottom waters by this species in Bahia Fosforescente have been suggested (Cintrón, 1969), and may represent an important nutrient gathering strategy affecting its population dynamics in this area. *Cochlodinium polykrikoides* is also capable of mixotrophy, ingesting preferentially small phytoplankton (<11µm). This species has been demonstrated to increase its growth rates considerably with increasing prey densities, from 0.17 without prey to 0.32 doublings per day, with prey (Jeong et al., 2004). Although the relevance of mixotrophy as

a supplementary strategy to fulfill the nutritional requirements of *C. polykrikoides* is recognized, the potential mixotrophic behavior of *C. polykrikoides* in Bahía Fosforescente remains an open question.

The recurrent nature of *C. polykrikoides* blooms in Bahía Fosforescente points out to a temporary cyst formation strategy. Temporary cysts are nonmotile life stages produced by some dinoflagellates to withstand adverse conditions (Kim et al., 2002) and have been regarded as potentially important for the initiation of dinoflagellate blooms (Anderson and Wall, 1978). The generation of temporary cysts by *C. polykrikoides* has been documented in other areas and were suggested as the cause of recurrent blooms of this species (Kim et al., 2002; Tomas and Smayda, 2008). According to Kim et al. (2002), these cysts can survive extended periods of time (up to 6 months) prior to regenerate motile cells when exposed to favorable conditions. Even though this study did not assess the existence of *C. polykrikoides* cysts in bottom sediments of Bahía Fosforescente, it seems plausible for *C. polykrikoides* to settle down at the bottom as temporary cysts under unfavorable circumstances (e.g. sudden changes in salinity, paucity of essential nutrients or growth factors, and/or the production of allelochemical substances by other co-occurring species). Cysts could regenerate motile cells when favorable conditions reappear, thus providing a recurrent seed source or inoculum for *C. polykrikoides* blooms. However, very low or background concentrations of *C. polykrikoides* cells were frequently found in the northwest arm during periods of no bloom occurrences. Therefore, the possibility that *C. polykrikoides* blooms may be seeded from this small residual motile population or from a population introduced from other areas cannot be ignored. If the proper chemical and physical conditions meet, such as to allow this small population of *C. polykrikoides* to proliferate in a way that active

growth compensates losses due to advection and predation (Tomas and Smayda, 2008), a bloom would initiate.

This study demonstrates the influential role of nutrients and the processes that contribute to enhance their availability (i.e. precipitation, nutrient cycling and turbulent mixing), in regulating the spatial and temporal distribution of *C. polykrikoides* blooms in Bahía Fosforescente. Although this certainly represents an important first step in the aim of understanding the factors that dictate the bloom dynamics of *C. polykrikoides* in these waters, much research is still needed. For instance, the specific effects of temporal fluctuations in the concentration of vitamins, micronutrients and humic substances in regulating these blooms must be evaluated. Likewise, the potential formation of temporary cysts by *C. polykrikoides*, as well as its vertical migration and mixotrophic behavior in these waters need to be assessed. Lastly, the use of more robust meteorological data, obtained *in situ*, instead of using the available data from the Magueyes Island station (obtained haphazardly) is strongly recommended for future studies, as it could contribute to minimize errors in the relationships between rainfall/wind and bloom dynamics of *C. polykrikoides* in Bahía Fosforescente.

1.5 Conclusions

- This is the first study addressing the population dynamics of the dinoflagellate *Cochlodinium polykrikoides* in Bahía Fosforescente.

- *Cochlodinium polykrikoides* exhibited a strongly aggregational spatial distribution at the northwest inlet of the bay, particularly towards the inner margin, occurring only in very low concentrations outside this area. This spatial pattern appears to be highly related to the distribution of nutrients in these waters, especially phosphates, which frequently showed higher concentrations in the inner part of this inlet.

- The aggregational pattern of *C. polykrikoides* seems to be assisted by the favorable diffusivity conditions of the area, prevailing southeast winds, small tidal amplitude and specific life-form characteristics of this organism that promote its accumulation.

- The occurrence of *C. polykrikoides* blooms coincided, in general, with the precipitation regime. This implies rainfall as an important factor influencing the population dynamics of this organism, most likely promoting the availability of nutrients, vitamins and humic substances essential for its growth.

- The absence of correlation between *C. polykrikoides* abundance and the cumulative rainfall for the 7, 14, 21 and 30 days preceding the samplings suggest that the intensity (i.e. proliferation of cells) and delay in the response of *C. polykrikoides* to these nutrient pulses is highly variable.

- *Cochlodinium polykrikoides* bloom episodes were mainly differentiated from non-bloom episodes by higher silicate and phosphate levels. Since *C. polykrikoides* does not have any known requirements for silica, this strongly suggests that *C. polykrikoides* blooms require high phosphorus levels, although low N:P ratios suggest nitrogen limitation.

- Other factors aside from rainfall (e.g. sudden changes in wind velocity promoting turbulent mixing coupled with organic matter decomposition and redox transformations in bottom sediments) may provide ample nutrients to these waters and trigger blooms of this species.

- Nocturnal migrations to bottom waters for nutrient gathering and mixotrophic behavior represent potential adaptational strategies that may help sustain dense accumulations of *C. polykrikoides* in Bahía Fosforescente.

- The recurrent nature of *C. polykrikoides* blooms in Bahía Fosforescente suggests a temporary cyst-type survival strategy. Under unfavorable circumstances *C. polykrikoides* may form cysts and settle down at the bottom, to regenerate motile cells when favorable conditions reappear. This would provide a recurrent seed source or inoculum for *C. polykrikoides* blooms.

- The presence of small numbers of *C. polykrikoides* cells in the northwest inlet during non-bloom periods implies that this small residual population may also be responsible for the recurrent blooms of this species.

2 Optical properties of the harmful dinoflagellate *Cochlodinium polykrikoides* (Margalef)

2.1 Introduction

The dinoflagellate *Cochlodinium polykrikoides* was reported as the causative species of numerous harmful algal bloom (HAB) occurrences and/or massive fish mortalities in many warm temperate and tropical waters (Silva, 1967; Ho and Zubkoff, 1979; Yuki and Yoshimatsu, 1989; Du et al., 1993; Marshall, 1995; Rosales-Loessener et al., 1996; Sannio et al., 1997; Kim, 1998; Gárate-Lizárraga et al., 2000; Whyte et al., 2001; Nuzzi, 2004; Anton et al., 2008; Azanza et al., 2008; Curtiss et al., 2008; Gobler et al., 2008; Tomas and Smayda, 2008). Since 1958, blooms of *C. polykrikoides* were recurrently observed in Bahía Fosforescente, a bioluminescent bay considered one of the main tourist attractions in southwestern Puerto Rico (Margalef, 1961; Burkholder et al., 1967). Despite the potential deleterious effects associated with this organism, no previous attempts to develop monitoring strategies for *C. polykrikoides* blooms in this bay have been conducted.

Conventional approaches for HAB assessments primarily rely on field samplings, chemical analyses or mouse bioassays for toxin detection and microscopic cell examinations. Unfortunately, these methods are arduous and time consuming, with a poor spatial and temporal resolution. Alternative methods allowing faster detection and characterization of these harmful outbreaks over broad spatial scales would be more suitable.

Phytoplankton strongly influences the optical properties of natural waters through their striking water discolorations, usually when they reach bloom densities. This fact suggests that optical methods are well suited to assess HAB's. Once established, blooms are largely mono-specific, reaching very high biomass over small spatial scales. As a result, their bio-optical

signatures are distinct and usually persistent for an extended period of time providing a means of optical detection (Millie et al., 1995). Of particular utility for the assessment of HAB phenomena is ocean color remote sensing, which measures the amount and quality of the light reflected from near the sea surface. It allows an extensive monitoring of coastal waters on a regular basis enhancing our capabilities for rapid determinations of HAB's presence and the extent of their distribution, and to trace their evolution (Cullen et al., 1997; Schofield et al., 1999).

Ocean color is defined radiometrically by remote sensing reflectance [R_{rs} (λ)], an apparent optical property (AOP). R_{rs} (λ) depends on the substances comprising the aquatic medium and the angular distribution of the light field. It is represented as the ratio of water-leaving radiance [L_w (λ)] to incident downwelling irradiance [E_d (λ)], or:

$$R_{rs}(\lambda) = L_w(\lambda) / E_d(\lambda) \qquad (1)$$

R_{rs} (λ) is primarily influenced by two inherent optical properties (IOP's) (i.e. those that depend on the constituents of the aquatic medium, but not on the angular distribution of the light field), the absorption (a) and backscattering (b_b) coefficients. The absorption coefficient is defined as the flow of incident light that is absorbed, divided by the thickness of the medium. In contrast, the backscattering coefficient is equivalent to the flow of incident light that is dispersed in a backward direction, divided by the thickness of the medium. The main constituents of the water column that contribute to absorb and backscatter light, and thereby control R_{rs} (λ) are: water itself, organic particulates (phytoplankton and detritus), color dissolved organic matter (CDOM) and inorganic particulate matter. Theoretical studies demonstrated that the relationship between R_{rs} (λ) and the IOP's can be described by the ratio of backscattering to absorption (Morel and Prieur, 1977), such that:

$$R_{rs}(\lambda) \approx b_b(\lambda) / [a(\lambda) + b_b(\lambda)] \quad (2)$$

Therefore, variations in ocean color associated with HAB's must be a function of changes in these IOP's.

Phytoplankton has evolved a variety of light-harvesting pigments which are classified in three main categories: chlorophylls, carotenoids (carotenes and xanthophylls) and phycobiliproteins. Some of these pigments are recognized as taxonomic markers because they are unique to a small group of closely related organisms or to a specific taxonomic group. Given that each pigment has a particular light absorption spectrum, detection of specific optical features may distinguish individual pigments and can be used as a diagnostic tool to characterize phytoplankton composition (Johnsen et al., 1994b; Richardson, 1996). Differentiation to the species level can only be attained if the organism represents a significant fraction of the phytoplankton biomass and/or if it has discriminating spectral features (e.g. unique pigments, or the light acclimation state associated with the ecological niche occupied by the species) (Schofield et al., 1999).

Previous laboratory studies suggest the viability of using pigment absorption features to differentiate amongst phytoplankton classes, and to some extent, species (Johnsen et al., 1994b; Millie et al., 1997). However, the discriminatory features identified in these studies correspond to spectral regions associated with absorption by accessory chlorophylls and carotenoids. This fact results in significant limitations for the characterization of microalgal composition since the absorption contributed by these pigments tends to be minor compared to that of the major light-harvesting pigment chlorophyll *a*, and hence their signals are usually masked in the overall cellular absorption spectra. Besides, the absorption of carotenoid pigments tend to overlap in the blue-green region (~ 450-550 nm) of the visible spectrum, thus spectral features attributable to

unique or diagnostic pigments would be difficult to discern. Derivative analysis, a mathematical technique that amplifies and resolves the weak signals caused by the extensive overlapping of pigment absorption spectra (Butler and Hopkins, 1970), has proven useful in overcoming the aforementioned difficulties (Bidigare et al., 1988; Bidigare, 1989; Millie et al., 1995; Aguirre-Gómez et al., 2001). It was successfully applied in recently developed *in situ* methods for the detection of phytoplankton species from mixed assemblages (Millie et al., 1997; Kirkpatrick et al., 2000; Stæhr and Cullen, 2003). Therefore, derivative analysis represents a powerful tool for bio-optical determinations of phytoplankton taxa, particularly in those areas where a limited number of species dominate the phytoplankton assemblage.

Although most research emphasized the pigment compositions and spectral absorption characteristics of harmful algae as responsible for the distinct bio-optical signatures frequently observed during HAB events, most harmful species have rather similar pigment compositions as their harmless counterparts (Roesler and McLeroy-Etheridge, 1998). In consequence, their absorption signatures are hardly unique and cannot be relied on as a sole discrimination criterion. This is particularly true within the chlorophyll *c*-containing algae (including prymnesiophytes, chrysophytes, diatoms, dinoflagellates, raphidophytes and chryptophytes) whose spectral absorption properties exhibit very similar patterns (Johnsen et al., 1994b). The only known exceptions are the toxic dinoflagellates *Karenia brevis*, *K. mikimotoi* and *Karlodinium micrum*, that unlike most dinoflagellates which have peridinin as their major light-harvesting carotenoid pigment, contain fucoxanthin and 19'-acylofucoxanthins instead, as well as a unique minor carotenoid pigment, gyroxanthin-diester (Millie et al., 1995).

There is sustaining evidence regarding the limited potential of absorption signatures for the discrimination of harmful taxa based on ocean color measurements. Garver et al. (1994)

demonstrated that accessory pigment absorptions are challenging to discern from remotely sensed ocean color data. Additionally, while measuring the IOP's of four harmful algal species of various sizes and growth phases, McLeroy-Etheridge and Roesler (1998) observed slight differences in the shape of the absorption spectra between species or growth phase but substantial variations in their scattering and backscattering spectra. They concluded that the scattering and backscattering properties of harmful algae have a significant role in the distinct ocean colors observed during HAB events. Moreover, simulations of ocean color corresponding to blooms of these four harmful species suggested that the enhanced concentrations of uniform-size cells in surface waters and their unique backscattering spectra are the specific bloom properties influencing ocean color (Roesler and McLeroy-Etheridge, 1998).

Despite the fact that spectral backscattering was pointed out as having an influential role in the unique spectral signatures of HAB's, essentially because it is controlled by specific properties of the harmful algae such as cell abundance, cell size, shape, refraction index and physiological status (Ahn et al., 1992; McLeroy-Etheridge and Roesler, 1998; Roesler and McLeroy-Etheridge, 1998; Boss et al., 2004; Vaillancourt et al., 2004), it has been largely ignored in ocean color efforts to discriminate toxic phytoplankton species. This is most likely related to the fact that the algal backscattering contribution to R_{rs} (λ) is weak compared to that of absorption (Ahn et al., 1992). Also, commercial instrumentation for *in situ* determinations of optical backscattering has only recently become available (Maffione and Dana, 1997). Nevertheless, in an attempt to identify waters dominated by blooms of *K. brevis*, Cannizaro (2004) was able to develop a classification technique based on the unique optical properties of the blooms of this species given by their characteristically low backscattering to absorption ratio.

This confirms the feasibility of using backscattering signatures as part of bio-optical strategies to identify harmful phytoplankton species.

Ocean color remote sensing have long been criticized for providing only bulk composite signals (including contributions by phytoplankton, detritus, suspended sediments, and CDOM) for a particular water mass. Therefore, signatures corresponding to different phytoplankton groups or species are difficult to determine (Garver et al., 1994; Schofield et al., 1999). Still, many different approaches were developed during recent years for the remote detection and assessment of phytoplankton blooms in both coastal and open ocean waters. Some of these methods involve the development of robust protocols based on unique optical properties of harmful algae (Subramaniam and Carpenter, 1994; Cannizaro, 2004), monitoring of chlorophyll anomalies in SeaWiFS imagery combined with climatological data analyses (Stumpf et al., 2003; Suh et al., 2004), or the application of spectral enhancement/classification techniques and/or red tide index (RI) algorithms (Ahn et al., 2006; Ahn and Shanmugam, 2006) to satellite imagery data. Additionally, a technique to differentiate among different phytoplankton groups based on spectral variations of SeaWiFS normalized water-leaving radiances was developed (Alvain et al., 2005).

Novel strategies based on the use of hyperspectral remote sensing reflectance data collected *in situ* were also established. For instance, Roesler et al. (2004) demonstrated the application of an ocean color inversion model to a time series of hyperspectral reflectance data obtained during a HAB event to delineate the presence and abundance of harmful algae. Lubac et al. (2005) compared second-derivative transformations of R_{rs} (λ) spectra corresponding to natural blooms of diatoms and the prymnesiophyte *Pheocystis globosa* and found notable differences among spectra at 469 nm, which allowed differentiating blooms of *P. globosa* from

diatoms dominated waters. In a recent study by Craig et al. (2006), a quasi-analytical algorithm was employed to derive a phytoplankton absorption spectrum for blooms of *K. brevis* from *in situ* measurements of R_{rs} (λ). Subsequently, they used a similarity index to compare the fourth-derivatives of reflectance-derived absorption spectra to a fourth-derivative of a reference *K. brevis* spectrum. With this technique they were not only able to detect this organism, but also to estimate its abundance.

There are very few studies on optical assessments of *C. polykrikoides* blooms (Suh et al., 2004; Ahn et al., 2006; Ahn and Shanmugam, 2006). Suh et al. (2004) demonstrated the viability of detecting blooms of this species in Korean waters utilizing a combination of satellite-derived sea surface temperature (SST) and chlorophyll *a* concentration anomalies together with *in situ* observations of the blooms distribution. Ahn et al. (2006) and Ahn and Shanmugam (2006) employed the Forward Principal Component Analysis/Minimum Spectral Distance classification techniques and red tide index (RI) algorithms, respectively, to differentiate *C. polykrikoides* blooms from non-bloom or turbid waters from satellite images.

Except for the work of Suh et al. (2004), who suggested a detection method based on specific absorption characteristics of these blooms at 340 nm, no other evidence of previous efforts to discriminate *C. polykrikoides* blooms from particular optical signatures was found. Absorption between 310-360 nm is likely due to the presence of mycosporine-like amino acids (water soluble substances for UV protection), which are widespread in many phytoplankton species (Hannach and Sigleo, 1998). Unfortunately, the ultraviolet region is not suitable for airborne or satellite remote sensing due to the pronounced effects of atmospheric (Raleigh) scattering below 400 nm.

Given the need for effective strategies to monitor the blooms of *C. polykrikoides* in Bahía Fosforescente, and the alleged potential of optical methods for these purposes, this study has established the following objectives:

1. To characterize the inherent and apparent optical properties (AOP's and IOP's) of *C. polykrikoides* from pure cultures.
2. To evaluate whether it is possible to discriminate and quantify the blooms of this species in Bahía Fosforescente based on *in situ* hyperspectral remote sensing reflectance data.

2.2 Materials and Methods

2.2.1 Cultures

2.2.1.1 Culturing of *C. polykrikoides*

Waters samples were collected from Bahía Fosforescente in June 2004 during a bloom of *C. polykrikoides*. A few cells were isolated under an inverted microscope using capillary pipettes and cultured in polystyrene well plates filled with enriched L1 medium (Guillard and Hargraves, 1993) at 26 °C and a salinity of about 36 ps. These plates were exposed to 74 µmol m^{-2} s^{-1} of photosynthetically active radiation (PAR) provided by cool-white fluorescent lamps (Phillips F20T12/CW) in a 12:12 light:dark cycle. When numerous cells were observed, they were transferred to 125 ml culture flasks and grown under the same conditions. A batch culture technique was subsequently used until maximum culture volumes of 1 L were reached. From this point on, exponential growth phase cultures were maintained in 2 L glass Fernbach flasks until all the optical measurements were performed.

2.2.1.2 Bio-optical characterization of cultures

Cultures of *C. polykrikoides* were used for determinations of pigment composition, spectral absorption coefficients, CDOM, and the relationship between cell abundance and chlorophyll *a* concentration. Culture samples were filtered through 25 mm Whatman glass-fiber filters (GF/F) with a nominal pore size of 0.7 µm, wrapped in aluminum foil and immediately stored in a -80 °C freezer for characterizations of pigment composition. These filters were shipped in dry ice, within less than fours hours, to an external laboratory (Horn Point Laboratory, Center for Environmental Science, University of Maryland) for analysis. Pigment analyses were carried out using high-performance liquid chromatography (HPLC) following the method described in Van Heukelem and Thomas (2001).

Spectral absorption coefficients of *C. polykrikoides* were determined based on the quantitative filtering technique (Trüper and Yentsch, 1967). Culture samples were collected onto GF/F filters and stored at -80 °C until analysis. Optical density (OD) measurements corresponding to total particulates and detritus were performed on these filters (referenced to a blank filter saturated with 0.2 µm filtered seawater) before and after pigment extractions (by slowly passing ~ 40 ml of hot methanol through the filters) (Kishino et al., 1985), respectively. Optical densities were recorded between 350 and 850 nm with a 1 nm spectral resolution using a double-beam spectrophotometer (model UV/Vis Lambda 18, Perkin-Elmer, Inc.) equipped with an integrating sphere. All OD spectra were corrected for differential scattering by subtracting the corresponding average value measured between 800 and 820 nm. Spectra of total particulate absorption [$a_p(\lambda)$] and detritus absorption [$a_d(\lambda)$] were then obtained as follows:

$$a_{p/d}(\lambda) = ((2.303 * OD_{p/d}(\lambda))/(\beta * vol)) * A \qquad (3)$$

where:

2.303 is the conversion factor to transform Log_{10} to Log_e,

$OD(\lambda)$ represents Log_{10} (scan reference/scan sample),

vol is the culture volume filtered in liters,

A is the clearance area of the filter, and

β is the pathlength amplification correction factor (that compensates for multiple scattering inside the filters).

In this study a constant β factor of 2, as proposed by Roesler (1998), was used. Spectral absorption coefficients due to *C. polykrikoides* pigments [$a_{ph}(\lambda)$] were estimated as the difference between $a_p(\lambda)$ and $a_d(\lambda)$ spectra. An average a_{ph} spectrum was calculated from six culture samples collected during different dates.

Determinations of CDOM absorption coefficients [$a_g(\lambda)$] were done to investigate the presence of CDOM and to elucidate its potential contribution to the bio-optical measurements from these cultures. A total of six culture samples were collected during different dates and processed immediately according to the methodology presented in section 2.2.6. Simultaneously, triplicate samples for cell abundance determinations were obtained and fixed in acid Lugol's solution. The L1 culture medium was prepared with 0.2 µm filtered natural seawater and it could represent a potential source of CDOM. Therefore, duplicate samples of the L1 medium were also collected and analyzed following the same method to evaluate its CDOM absorption signal.

The relationship between chlorophyll *a* concentration and *C. polykrikoides* cell abundance was determined based on linear regression analysis. This also helped to develop an equation from which estimations of cell abundance could be obtained based on chlorophyll *a* measurements. With this purpose, a series of nine dilutions were prepared, starting with a highly concentrated culture that was sequentially diluted with equal volumes of 0.2 µm filtered seawater. During each dilution step, the culture was homogenized using a manual stirring device and then water samples were collected for cell enumerations and chlorophyll *a* determinations. Triplicate samples for cell counts were fixed with a few drops of acid Lugol's solution, while duplicate chlorophyll *a* samples were stored in amber plastic bottles and refrigerated until processed.

2.2.2 Mesocosm experiments for determinations of apparent and inherent optical properties of *C. polykrikoides*

2.2.2.1 Remote sensing reflectance measurements

Data acquisition for determinations of $R_{rs}(\lambda)$ took place on November 6, 2006 from 10:30 to 12:00 local time, under clear sky conditions, at the research facilities of the Marine

Sciences Department, located at La Parguera, southwestern Puerto Rico (latitude 17º 57' N and longitude 067º 02' W). The specific site selected to carry out the experiment was at the end of a boat pier away from possible shadow effects.

Radiometric measurements were conducted in a fiberglass cylinder measuring 44.5 cm in diameter, 61 cm in height and with a volume of ~100 L, with a flat-black painted interior and a 45º angle bottom (to reduce spurious bottom contribution). To maintain homogeneous conditions, water was kept circulating using a mechanical pump-driven set-up consisting of a 700 GPH (~2650 L/hour) submersible utility pump, two black hose rings attached to the interior of the cylinder at different depths and black connecting hoses (Figure 11). This system pulled water into the pump through a suction hose positioned at the bottom of the cylinder, and then forced it out through a series of perforations distributed along the hose rings and through a hose located on the top of the cylinder (just below the water surface). Precautions were taken, so that no bubbles or turbulence were created at the surface that could affect the measurements.

Optical data was recorded in the spectral range of 293–1095 nm, with a spectral resolution of 2.8 nm, using a portable spectroradiometer (model 1500, Geophysical Environmental Research Corp., hereafter abbreviated GER 1500). Only the 400-700 nm (visible spectrum) range was used for analysis.

At the beginning, the cylinder was filled with 80 liters of seawater, previously filtered in three steps: an initial filtration through 0.4 μm membrane filters (the day before the experiment), followed by two additional filtrations using 0.2 μm membrane filters (just before the experiment). Subsequently, 2 liters of seawater were removed and replaced with an equal volume of cultures of *C. polykrikoides*. This procedure was repeated five times. This five-step sequence was used to achieve a wide range of microalgal concentrations and corresponding R_{rs}.

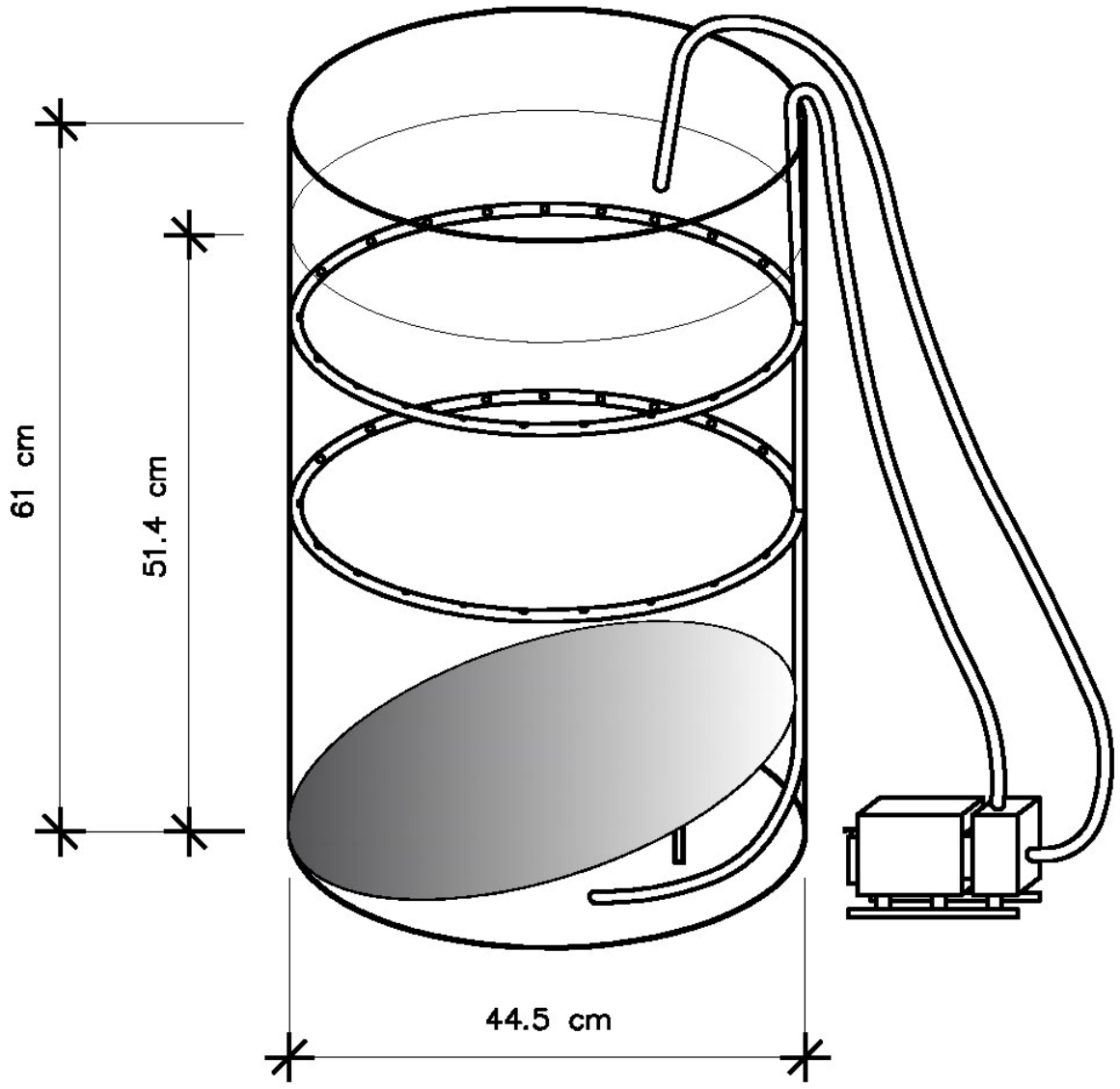

Figure 11. Experimental set-up for $R_{rs}(\lambda)$ measurements of pure cultures of *C. polykrikoides*.

Spectral measurements were performed for the filtered seawater (baseline spectrum) and for each of the five microalgal additions as follows: 10 replicate scans of the downwelling irradiance [$E_d(0^+, \lambda)$] were recorded pointing directly upward using a Teflon cosine collector diffuser fixed to the entrance optics of the GER 1500. Thereafter, 5 replicate scans of both the radiance from a Spectralon 50% reference panel (Labsphere, Inc.) above the water surface [$L_{ref}(0^+, \lambda)$], and the upwelling radiance just below the water surface [$L_w(0^-, \lambda)$] were measured using a nadir-viewing fiber optic cable attached to the instrument. Each set of scans was averaged and the mean was used for R_{rs} determinations.

Concurrent with the scans, water samples were collected (from the 2 liters of water removed during each step of the additions sequence) for further analyses: three 5 or 10 ml (10 ml for the first two additions and 5 ml for the others) replicate samples were fixed in acid Lugol's solution for cell counts, and a 1 L sample was used for determinations of chlorophyll *a* concentration. Chlorophyll *a* samples were placed in a dark, cold ice chest and transported to the laboratory for processing. Water temperature was monitored throughout the experiment to avoid drastic changes that may affect the physiological status of the cells.

Remote sensing reflectance calculations were based on the following equation:

$$R_{rs}(0^+, \lambda) = [L_w(0^-, \lambda)*(t/n^2)]/[L_{ref}(0^+, \lambda)*2*\pi] \qquad (4)$$

where:

$t/n^2 = 0.54$

n = refractive index of seawater = 1.34

t = transmittance of the air-water interface = 0.97

In order to propagate $L_w(0^-, \lambda)$ values through the air-water interface to obtain the water-leaving radiance just above the water surface [$L_w(0^+, \lambda)$], they were multiplied by 0.54 to account for

refraction and loss of light as it passes through the air-water interface. Additionally, $L_{ref}(0^+, \lambda)$ data were transformed to $E_d(0^+, \lambda)$, by multiplying them by 2, to get a 100% reflectance from the 50% reference panel, and then by π, which is the measured angular distribution factor of spectral radiance, that can be used to relate upwelled spectral radiance to irradiance (Vertucci and Likens, 1989; Toole et al., 2000). Once $L_{ref}(0^+, \lambda)$ measurements were converted to $E_d(0^+, \lambda)$, they were compared to the measured $E_d(0^+, \lambda)$ with the cosine collector to evaluate their differences. As a final step, $R_{rs}(0^+, \lambda)$ spectra were corrected by subtracting the seawater reflectance spectrum (baseline) to remove any spurious signal provided by the cylinder and the seawater itself.

2.2.2.2 Inherent optical properties measurements

Spectral backscattering (b_b) measurements of *C. polykrikoides* cultures were made using a submersible backscattering meter (model Hydroscat-6, HOBI Labs, Inc., henceforth abbreviated HS6). The HS6 measures the volume scattering function (which in simple terms, characterizes the scattered radiant intensity as a function of angle), β, at a fixed angle of 141° in six wavelengths (10 nm bandwidth) centered at 442, 470, 510, 589, 620 and 675 nm, from which the backscattering coefficient [$b_b(\lambda)$] is determined (Maffione and Dana, 1997).

HS6 measurements were carried out in the same ~100 L flat-black painted fiberglass cylinder used for the $R_{rs}(\lambda)$ measurements. The HS6 was suspended above the cylinder so that its faceplate (where the optical windows are located) was always submerged below the air-water interface. Precautions were taken, such as to cover the set-up with black fabric, to prevent extraneous light from entering the cylinder. To determine the backscattering contribution from the container, it was filled with 60 liters of 0.2 µm twice-filtered seawater, and then the HS6 was lowered such that its faceplate was about 2.5 cm from the bottom. The instrument was then raised in steps and the backscattering measured until no further changes in instrument readings

were observed. Backscattering reached minimum values and remained constant with the HS6 faceplate positioned ≥ 25 cm above the bottom. All subsequent readings on *C. polykrikoides* cultures were made with the faceplate of the HS6 suspended 30 cm above the cylinder's bottom.

To measure the backscattering of *C. polykrikoides* cultures, the cylinder was filled with 80 liters of previously filtered seawater (first through a 0.45 µm filter and then twice through 0.2 µm filters, just before the experiment). After a clean-seawater backscattering baseline was obtained, 1 L culture volumes were added, the mixture was stirred to distribute the cells homogeneously, and then backscattering readings were performed. A total volume of 10 liters of culture were added incrementally in this fashion in ten independent additions. Small bubbles that formed on the HS6 and cylinder sides were always carefully removed so that they did not affect the readings. Also, water temperature was monitored before and after cell additions to make sure it did not differ significantly from the growth temperature of the cultures. To maintain a constant water volume, 1 L water samples were removed from the cylinder at each addition, subsequent to the optical measurements, and used for chlorophyll *a* determinations. Backscattering readings were recorded in periods of five minutes to ensure representative values, and the median of those values was computed. Filtered seawater measurements were subtracted from the additions data to remove the signal provided by the cylinder and the seawater itself.

Immediately after performing the backscattering measurements, absorption and attenuation (an IOP that represents the sum of the absorption and scattering coefficients, $c = a + b$) were measured using an absorption and attenuation meter (model ac-9, WET Labs, Inc.). The ac-9 simultaneously determines the spectral absorption [$a(\lambda)$] and spectral attenuation [$c(\lambda)$] coefficients of water over nine wavelengths (412, 440, 488, 510, 532, 555, 650, 676 and 715 nm). The instrument collected data for filtered seawater (baseline) and for each of the ten culture

additions during five minutes in a flow-thru mode, by means of a submersible pump attached to the flow tubes of the instrument that kept the water circulating from the cylinder. Median values were computed for each five-minute dataset. After that, temperature and salinity corrections (Pegau et al., 1997), and spectral scattering corrections (WET Labs Inc., 2008) were applied to the resulting values. Spectral scattering [b (λ)] coefficients (which is the sum of forward (b_f) and backward (b_b) scattering) were calculated by difference [b (λ) = c (λ) – a (λ)].

2.2.3 Field Work

Field data were collected at six stations in Bahía Fosforescente during monthly samplings conducted between May 2002 and July 2003 as part of a monitoring study of the population dynamics of *C. polykrikoides* in this bay (Figure 3). At each station, measurements for R_{rs} determinations were performed and surface water samples were collected using a portable water pump system. Triplicate 1-5 L water samples (depending on the station and/or on microalgal concentrations) were filtered through a 25 µm mesh, concentrated to about 50 ml and fixed with acid Lugol's solution for subsequent *C. polykrikoides* cell counts. In addition, a 4 L water sample was stored in an amber plastic bottle and refrigerated for further chlorophyll determinations.

Further samplings were carried out in May 16 and May 18, 2007 concurrent with a bloom episode of *C. polykrikoides*. During these dates three stations were assessed, two of them located within the extent of the bloom area and one away from it (Figure 12). Data collection included measurements for determinations of both apparent [R_{rs} (λ)] and inherent optical properties [b_b (λ), a (λ), b (λ) and c (λ)], as well as water samples for cell counts (3/250 ml-5 L), chlorophyll *a* concentration (1/1 L), CDOM (2/250 ml), and total suspended solids (TSS) (1/1 L)

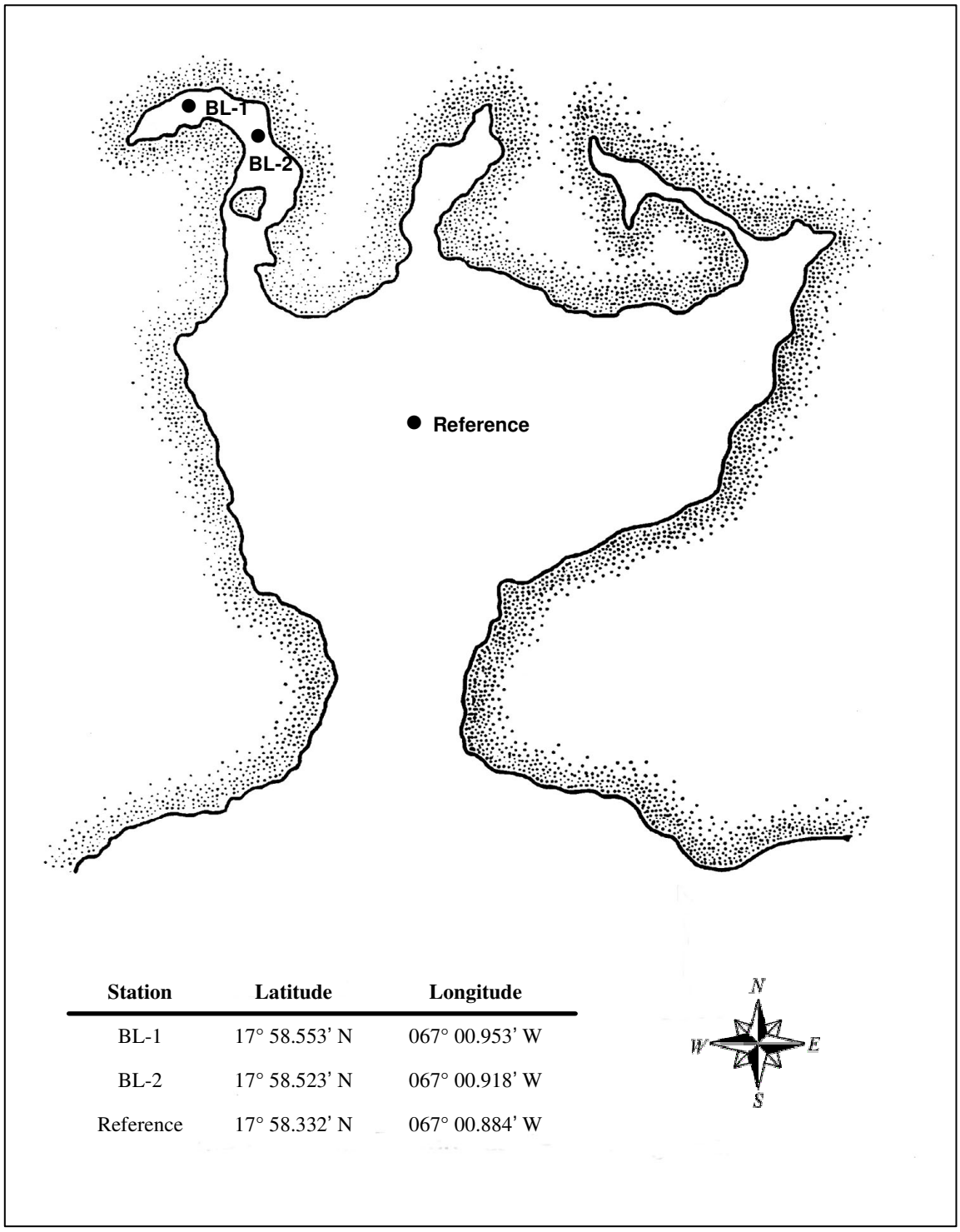

Station	Latitude	Longitude
BL-1	17° 58.553' N	067° 00.953' W
BL-2	17° 58.523' N	067° 00.918' W
Reference	17° 58.332' N	067° 00.884' W

Figure 12. Map of Bahía Fosforescente indicating the location of the stations sampled during May 16 and 18, 2007.

determinations. Samples for chlorophyll *a* and CDOM analyses were stored in amber plastic bottles and pre-combusted amber glass bottles, respectively, and refrigerated until processed.

2.2.3.1 Remote sensing reflectance measurements

The $R_{rs}(\lambda)$ measurements were carried out during daylight hours between 8:00 and 15:00 local time. Upwelling radiance [$L_0(\lambda)$], downwelling sky radiance [$L_s(\lambda)$] and the above surface downwelling irradiance [$E_d(0^+, \lambda)$] were measured using the spectroradiometer GER 1500. $L_0(\lambda)$ was measured at 45º from nadir to minimize sun glint, and $L_s(\lambda)$ at 45º from zenith, both maintaining an azimuth of 90º from the solar plane. $E_d(0^+, \lambda)$ was measured aiming directly upward using a Teflon cosine collector diffuser attached to the entrance optics of the GER 1500. Three replicate scans for each measurement were recorded and averaged, and the mean used for $R_{rs}(\lambda)$ determinations, which was calculated as follows:

$$R_{rs}(\lambda) = L_0(\lambda) - f\,L_s(\lambda)/\,E_d(0^+, \lambda) \qquad (5)$$

where $L_0(\lambda) - f\,Ls(\lambda)$ represents the water-leaving radiance, $L_w(\lambda)$, and f is the Fresnel number, the percent of sky radiance reflected off the water's surface. For a 45º angle the Fresnel number has a value of 0.028. A final correction to remove any residual reflected sky radiance still contained in the $R_{rs}(\lambda)$ spectra was performed by subtracting the $R_{rs}(\lambda)$ at 860 nm (for monthly samplings data) or 890 nm (for bloom episode samplings data). Traditionally, the $R_{rs}(\lambda)$ at 750 nm has been used for this correction based on the assumption that the water-leaving radiance at that wavelength is zero. However, the signal at 750 nm was not negligible in this study, because of backscattering due to high suspended particulate loads typical of coastal environments (referred to as Case 2 waters). A careful evaluation of all $R_{rs}(\lambda)$ spectra indicated that the chosen wavelengths were the most appropriate for each particular data set (Toole et al., 2000).

2.2.3.2 Inherent optical properties measurements

Backscattering measurements [$b_b(\lambda)$] were performed by submerging the HS6 to about 10 cm below the air-water interface using a manual winch positioned at one side of the boat. The HS6 recorded data for five minutes, and the median of those readings (after removal of noisy data) was computed.

Absorption [$a(\lambda)$] and attenuation [$c(\lambda)$] data were collected using the ac-9 in flow-thru mode. Surface seawater was pumped into the instrument flow tubes using a submersible water pump system, while the instrument was on board. The ac-9 collected readings in periods of five minutes, from which median values were calculated (after removal of noisy data). Temperature, salinity and flat scattering (by subtracting a (715) from $a(\lambda)$) corrections were subsequently applied to the resulting absorption and scattering values (Pegau et al., 1997; WET Labs Inc., 2008). Spectral scattering [$b(\lambda)$] was determined as the difference between $c(\lambda)$ and $a(\lambda)$.

2.2.4 Chlorophyll *a* determinations

Samples for chlorophyll analyses were vigorously stirred prior to processing in order to assure homogeneity. From each sample, two sub-samples were filtered onto GF/F filter pads and frozen at -80 ºC until extraction. Pigments were extracted in ~4 ml of 90% acetone by grinding the filters in an aluminum foil-covered glass homogenization tube, with a motor-driven Teflon pestle rotating at about 500 rpm. During the grinding process the tube was kept in an ice bath to avoid pigment degradation by overheating. The extract was then filtered to remove filter remains, and analyzed by fluorometry, spectrophotometry and/or HPLC.

Throughout this study, chlorophyll *a* concentrations were consistently determined by the standard fluorometric method (Welschmeyer, 1994), using a field fluorometer (model 10-AU,

Turner Designs). In many occasions, however, chlorophyll *a* measurements were also made spectrophotometrically and/or by HPLC. This provided the opportunity to corroborate the efficiency of these three methods. For the spectrophotometric analysis, absorbances were measured using a double-beam spectrophotometer (model UV-1601, Shimadzu, Inc.) equipped with 1cm quartz cells. Chlorophyll *a* concentrations were estimated with the trichromatic equations reported by Jeffrey and Humphrey (1975) for mixed phytoplankton populations.

HPLC analyses of chlorophyll *a* were done using a Waters C18 column (symmetry 3.9 x 150 mm) and an HPLC system consisting of a Shimadzu LC-10 AT pump and a SPD-M10AU diode array detector connected to a Waters WISP 712 injector. The analysis was based on a modified version of the methodology described by Wright et al. (1991). The HPLC was calibrated with a solution of pure chlorophyll *a* in 90% acetone. Chlorophyll *a* was identified by comparing its retention time and absorption spectrum (400-700 nm) to published data.

2.2.5 Cell abundance determinations

Triplicate samples were used for both quantitative determinations of *C. polykrikoides* cell abundance and/or for the quantitative/qualitative assessment of other phytoplankton species. Prior to cell counts**,** sample volumes were adjusted depending on apparent cell concentrations. Samples were gently mixed to give a homogeneous distribution of cells and subsequently, two 1ml aliquot replicates were counted in a Sedgewick-Rafter counting chamber using an inverted microscope (model CK40, Olympus, Inc.). Determinations of cell abundance were based on average cell counts calculated from the replicate samples.

2.2.6 CDOM determinations

CDOM absorption measurements were performed based on the method described by Del Castillo et al. (1999). Seawater/culture samples were filtered onto pre-combusted (500 ºC for 6h) GF/F filters using a glass filtration unit that was previously acid-washed, and rinsed with HPLC grade distilled water and methanol. Filtered samples were drained into pre-combusted (500 ºC for 6h) 250 ml amber glass bottles and refrigerated until analysis.

CDOM absorption spectra were determined between 250 and 750 nm at 1 nm intervals using a Perkin-Elmer Lambda 18 double-beam spectrophotometer equipped with matching 10 cm quartz cells. Each sample was scanned two times, referenced to HPLC grade distilled water. The resulting absorbance spectra [$A_g(\lambda)$] were corrected for scattering and baseline fluctuations by subtracting the corresponding value at 700nm. CDOM absorption coefficients [$a_g(\lambda)$] were then obtained as follows:

$$a_g(\lambda) = (2.303 * A_g(\lambda))/l \qquad (6)$$

where 2.303 is the conversion factor to transform Log_{10} to Log_e, $A_g(\lambda)$ represents Log_{10} (scan reference/scan sample) and l is the pathlength in meters. For each set of replicate samples (seawater samples)/from all samples (culture samples), an average $a_g(\lambda)$ was calculated.

2.2.7 Total suspended solids (TSS) determinations

Well-mixed replicate seawater samples were filtered through pre-weighed dried (60 ºC overnight) 47 mm GF/F filters. These filters were transferred to aluminum weighing dishes (for support) and placed in an oven to dry at 60 ºC overnight. After cooling to room temperature in a desiccator, filters were weighed again. The increase in weight, representing the TSS, was calculated by difference. Subsequently, filters were returned to the weighing dishes and ignited

in a furnace at 500 ºC for six hours to remove the volatile fraction (organic suspended solids). Filters were let to partially cool inside the furnace until most of the heat was dissipated and then the cycle of cooling, desiccating and weighing was repeated once again. The weight of the remaining inorganic suspended solids (ISS) was obtained by difference. To calculate the concentration of TSS and/or ISS, their corresponding weights were divided by the volume of filtered seawater. For each station, a mean concentration value was calculated from the replicates.

2.2.8 Spectral deconvolution

Derivative spectroscopy techniques were used in this study to deconvolve the R_{rs} (λ) data for the qualitative and quantitative assessment of *C. polykrikoides* absorption and reflectance features. The derivative of a spectrum is basically its rate of change (spectral slope) with respect to wavelength. It has been proven a powerful tool to enhance minute fluctuations in R_{rs} (λ) spectra, differentiating closely related pigment absorption features, eliminate background signals, and to reduce the effects of turbidity in coastal aquatic environment pigment investigations (Demetriades-Shah et al., 1990).

Prior to derivative analysis, R_{rs} (λ) spectra were smoothed by means of an adjacent-averaging of 5 or 9 points (depending on the data) and subsequently interpolated at 1 nm intervals using the Origin 7 scientific graphing and analysis software (OriginLab Corp.). The smoothing was intended to reduce noise in the original R_{rs} (λ) spectra and the interpolation changed the irregularly spaced spectroradiometric data with evenly spaced data. In order to enhance overlapping spectral features, second, fourth and fifth derivatives of the smoothed spectra were computed following the method of Savitsky and Golay (1964), using the Grams AI

8.0 spectroscopy software. A differentiation interval of 23 nm (at each derivative order) was found to be optimal to maximize the signal to noise amplification ratio in R_{rs} (λ) derivative spectra of cultures, while differentiation intervals of 19 and 41 nm were chosen, respectively, to calculate second and fourth/fifth derivatives of field R_{rs} (λ) spectra.

Peaks in the derivative spectra were distinguished from spectroradiometer noise following the method described by Huguenin and Jones (1986). Positive peaks in the second derivative spectra were examined in the fourth and fifth derivatives. If the magnitude of the peak was negative in the fourth and equal or close to zero in the fifth derivative, then the peak was classified as an absorption feature and not noise related. Conversely, a negative peak in the second derivative, which was positive on the fourth and close to zero in the fifth, indicated a local reflectance feature.

Qualitative pigment information was obtained based on the wavelength position of absorption features in the derivative spectra. Absorption features were compared to reported *in vivo* absorption peaks for individual pigments, as well as to pigment absorption features identified in derivative spectra by several authors. Second derivative peaks were also explored for quantitative estimations of chlorophyll *a* concentration and *C. polykrikoides* cell abundance.

2.3 Results

2.3.1 Bio-optical characterization of cultures

2.3.1.1 Pigment composition

Cochlodinium polykrikoides exhibited the characteristic pigment profile of typical dinoflagellates (Jeffrey and Vesk, 1997) including chlorophyll *a*, chlorophyll c_2, peridinin, diadinoxanthin, diatoxanthin, dinoxanthin and β,β-carotene (Figure 13). Predominant pigments in *C. polykrikoides* cultures, other than chlorophyll *a* (211.3 µg L^{-1}), were peridinin (163.7 µg L^{-1}), chlorophyll c_2 (47.14 µg L^{-1}) and diadinoxanthin (26.6 µg L^{-1}). Minor concentrations of the photoprotective carotenoids diatoxanthin (16.7 µg L^{-1}) and β,β-carotene (7.02 µg L^{-1}) were observed. Dinoxanthin (a minor carotenoid in dinoflagellates) could not be quantified because no standard for this pigment was available.

2.3.1.2 Spectral absorption properties of *Cochlodinium polykrikoides*

The absorption coefficient spectrum of *C. polykrikoides* revealed several distinct features including major peaks at 435, 463 and 670 nm, minor peaks at 590 and 628 nm, and a shoulder around 416 nm (Figure 14). The peak located at 435 (absorption maximum) and the shoulder observed near 416 nm both correspond to absorption maxima for chlorophyll *a* (Jeffrey and Vesk, 1997). The peak at 463 nm mainly responds to the combined absorptions of chlorophyll c_2 and peridinin. However, given that all carotenoid pigments absorb light between ~ 450 and 550 nm, diadinoxanthin, diatoxanthin, dinoxanthin and β,β-carotene may also have contributed to this feature. After ~500 nm, pigment absorption decreased sharply and reached minimum values around 600 nm. The two subtle features observed within this region of minimal absorption, positioned at 590 and 628 nm, most likely resulted from the mutual contributions of chlorophylls *a* and c_2. The peak observed at 670 nm denotes another absorption maximum for chlorophyll *a*.

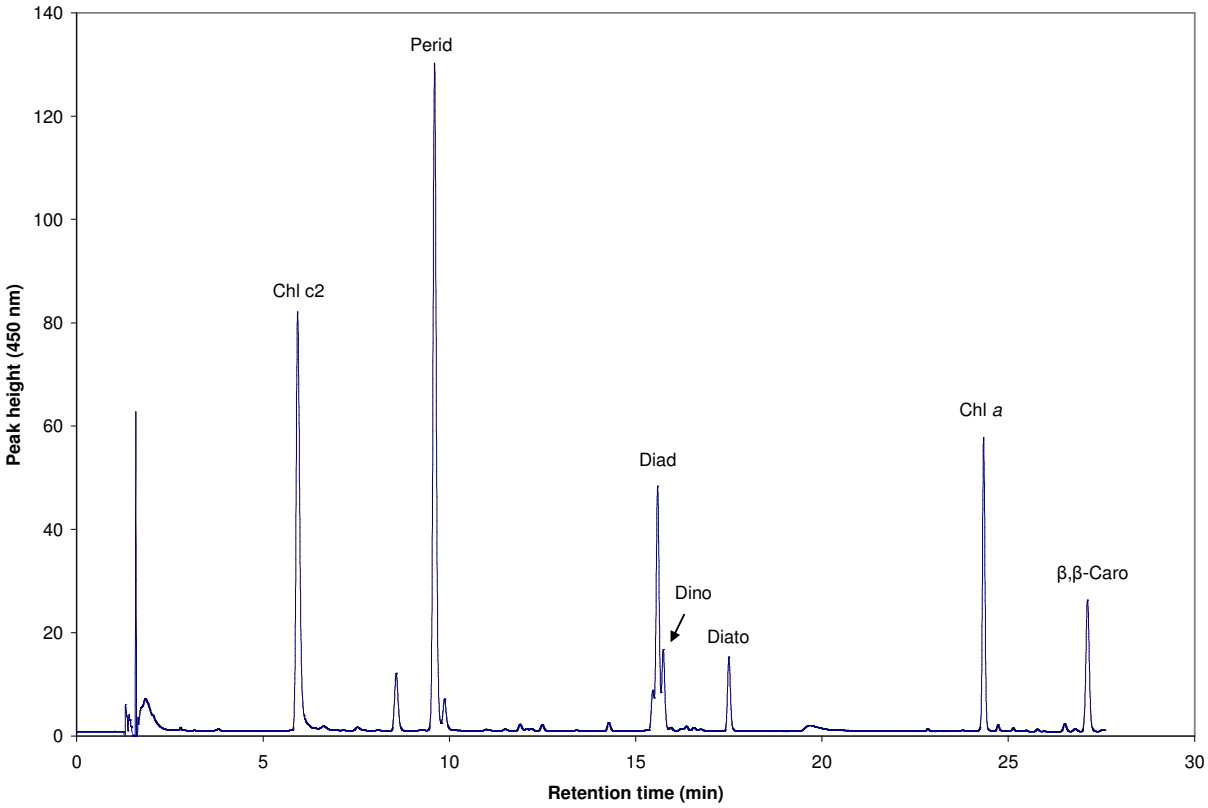

Figure 13. Representative HPLC chromatogram of pigment extracts obtained from *C. polykrikoides* cultures. The pigments detected were: chlorophyll *a* (Chl *a*), chlorophyll c_2 (Chl c_2), peridinin (Perid), diadinoxanthin (Diad), dinoxanthin (Dino), diatoxanthin (Diato) and β,β-carotene (β,β-Caro).

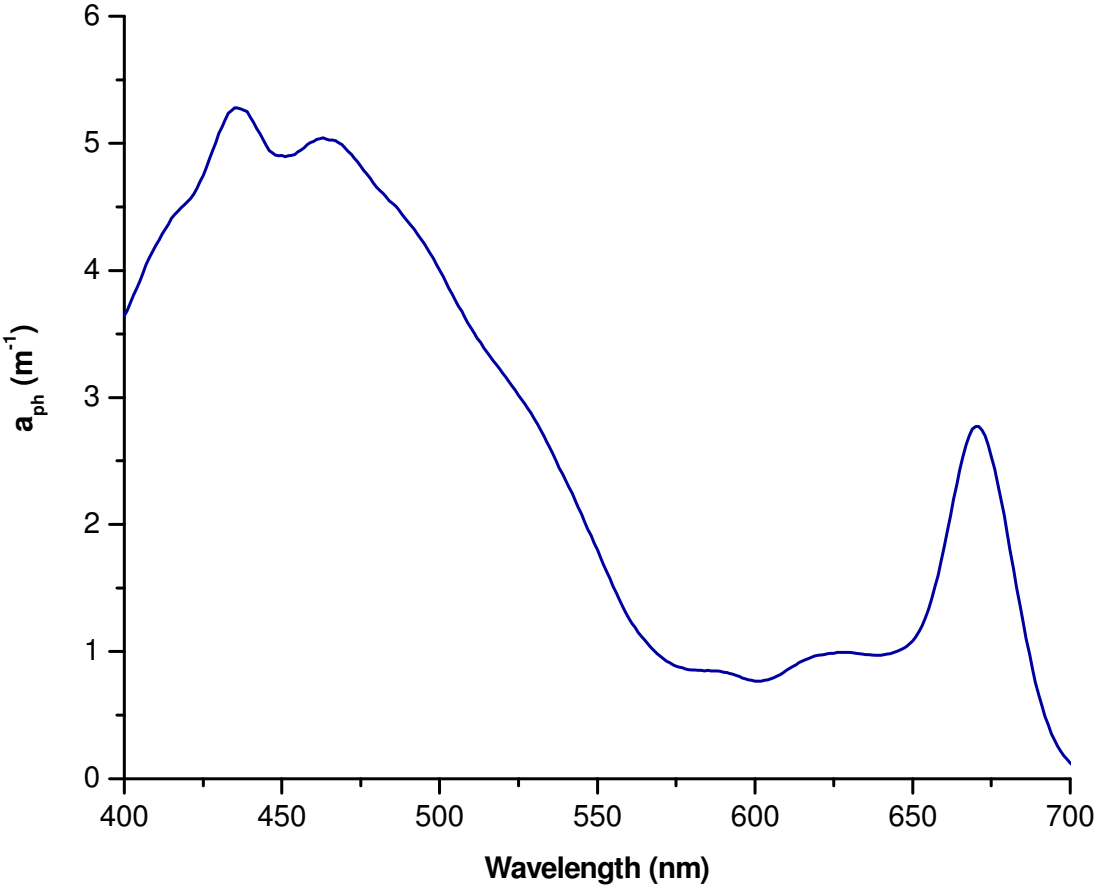

Figure 14. Mean absorption spectrum [a_{ph} (λ)] of *C. polykrikoides* cultures obtained from six culture samples collected during different dates.

2.3.1.3 Color dissolved organic matter (CDOM) absorption coefficients

Absorption measurements demonstrated the presence of CDOM in both *C. polykrikoides* cultures and the L1 medium. Both spectra revealed the characteristic shape of CDOM absorption, which strongly absorbs blue light and exhibits an exponentially decreasing trend with increasing wavelength (Figure 15). CDOM absorption coefficients were higher overall for *C. polykrikoides* cultures (values ranging from 0.85 to 0.001 m^{-1} - corresponding to an average cell abundance of 7.8 x 10^6 cells L^{-1}) than for the L1 medium (values ranging from 0.26 to 0.005 m^{-1}), clearly indicating CDOM production in the cultures.

2.3.1.4 Relationship between cell abundance and chlorophyll *a* concentration

A broad range of chlorophyll *a* concentrations (1.7- 87.8 µg L^{-1}) and cell abundances (8.02 x 10^4- 2.65 x 10^6 cells L^{-1}) were attained throughout the nine-step dilution sequence of a culture of *C. polykrikoides* (Table 3). Chlorophyll *a* concentration revealed a strong positive correlation ($r^2 = 0.98$, $p < 0.0001$) with cell abundance. The resulting linear regression equation for cell abundance estimations was as follows:

C. polykrikoides cell abundance = 29.38* [Chl *a*] + 37.97 (7)

The reported chlorophyll *a* concentration values represent averaged fluorometric and spectrophotometric data to cancel out possible discrepancies associated with instrumental calibrations. The fluorometer used was calibrated for oligotrophic waters with very low pigment concentrations, and it tended to underestimate chlorophyll *a* values over 3 µg L^{-1}. On the other hand, the spectrophotometer was less sensitive at very low chlorophyll *a* concentrations.

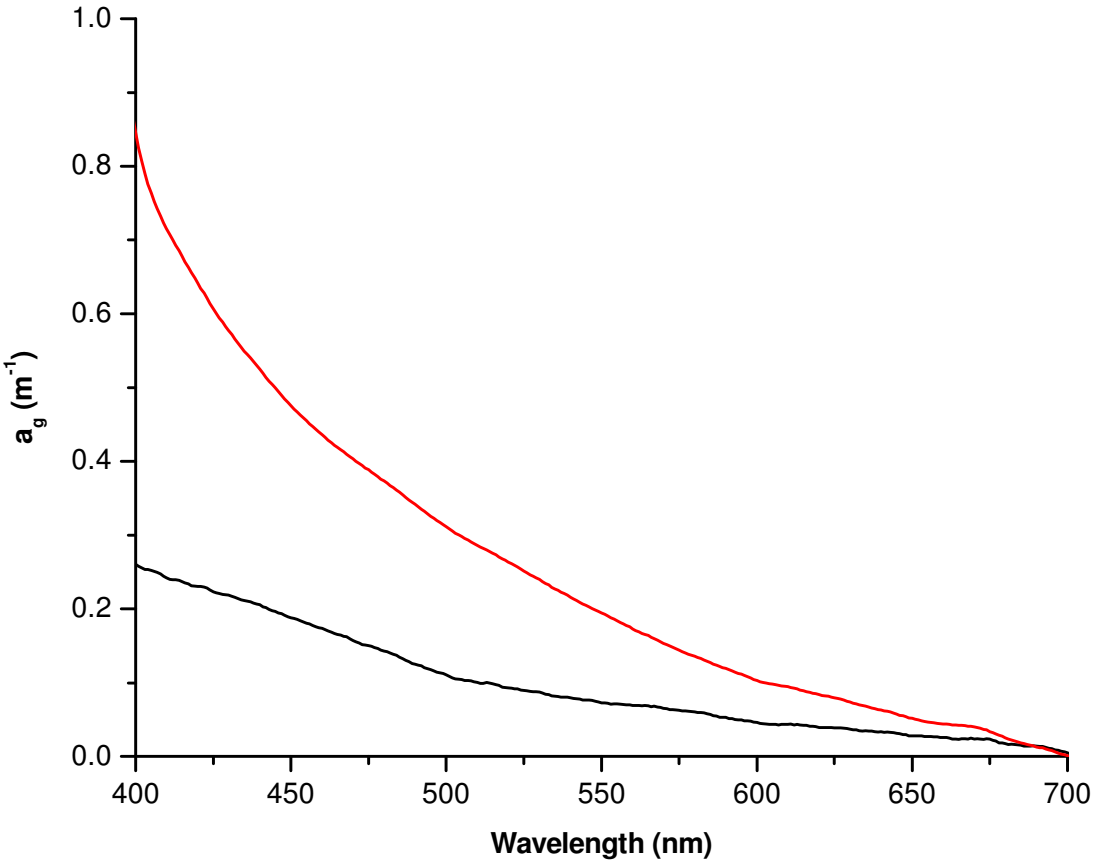

Figure 15. CDOM absorption spectra [a_g (λ)] corresponding to *C. polykrikoides* cultures (red line) and to the L1 culture medium (black line). The curves represent an average value of six and two samples, respectively.

Table 3. Summary of cell abundances and chlorophyll *a* concentrations obtained during the nine-step dilution sequence of a pure culture of *C. polykrikoides* used to determine a linear regression equation for estimations of cell abundance based on chlorophyll *a* measurements. Chlorophyll *a* concentrations represent mean values for fluorometric and spectrophotometric measurements.

Dilution step	**Cell abundance (cells L^{-1})**	**[Chl *a*] (µg L^{-1})**
original culture	2.65×10^6	87.8
1st dilution	2.20×10^6	68.2
2nd dilution	1.40×10^6	55.7
3rd dilution	1.37×10^6	44.8
4th dilution	9.92×10^5	32.0
5th dilution	7.50×10^5	22.3
6th dilution	5.77×10^5	19.2
7th dilution	2.76×10^5	6.8
8th dilution	8.02×10^4	1.7

2.3.2 Mesocosm experiments for determinations of the apparent and inherent optical properties of *C. polykrikoides*

2.3.2.1 Determinations of remote sensing reflectance (R_{rs})

2.3.2.1.1 Cell abundance and chlorophyll *a* concentration

During this experiment, a wide range of chlorophyll *a* concentrations and cell abundances were obtained, which were used to interpret changes in the spectral R_{rs} features of *C. polykrikoides* associated with variations in microalgal densities. Chlorophyll *a* concentrations ranged from 3.04 to 18.99 μg L^{-1}, while cell abundances varied from 183 x 10^3 to 927 x 10^3 cells L^{-1} (Table 4). A strong positive correlation ($r^2 = 0.97$, $p = 0.002$) was found between cell abundance and chlorophyll *a* concentration.

2.3.2.1.2 Temperature

Temperature fluctuated from 26 to 31 ºC throughout the data collection period (Table 4). The increase of temperature during the experiment was inevitable and responded to the combined effects of ever-increasing irradiances (as a function of an increasing solar elevation angle from 10:30 till noon) and the black-painted cylinder, which strongly absorbs solar radiation. Therefore, potential physiological damages related to temperature were not taken into consideration in this experiment.

2.3.2.1.3 Comparison of measured and estimated downwelling irradiances (E_d)

Measured $E_d(0^+, \lambda)$ values were spectrally very similar to those estimated from $L_{ref}(0^+, \lambda)$ (Figure 16). However, in terms of magnitude they were consistently lower, with differences ranging from ~0 to 10.6%. This might be attributed to poor cosine response (Toole et al., 2000) and/or to fluctuations in the reference panel calibration. Given that $L_w(0^+, \lambda)$ measurements were collected using the fiber optic cable, estimated $E_d(0^+, \lambda)$ values (also collected with the fiber optic cable) were chosen to calculate $R_{rs}(0^+, \lambda)$.

Table 4. Summary of parameters measured during the five-step *C. polykrikoides* culture addition sequence for determinations of R_{rs} (λ).

Addition number	[Chl *a*] (μg L^{-1})	Cell abundance (cells L^{-1})	Temperature (°C)
1	3.04	183 x 10^3	26
2	6.15	374.5 x 10^3	27
3	10.69	642 x 10^3	28
4	15.67	897 x 10^3	29.5
5	18.99	927 x 10^3	31

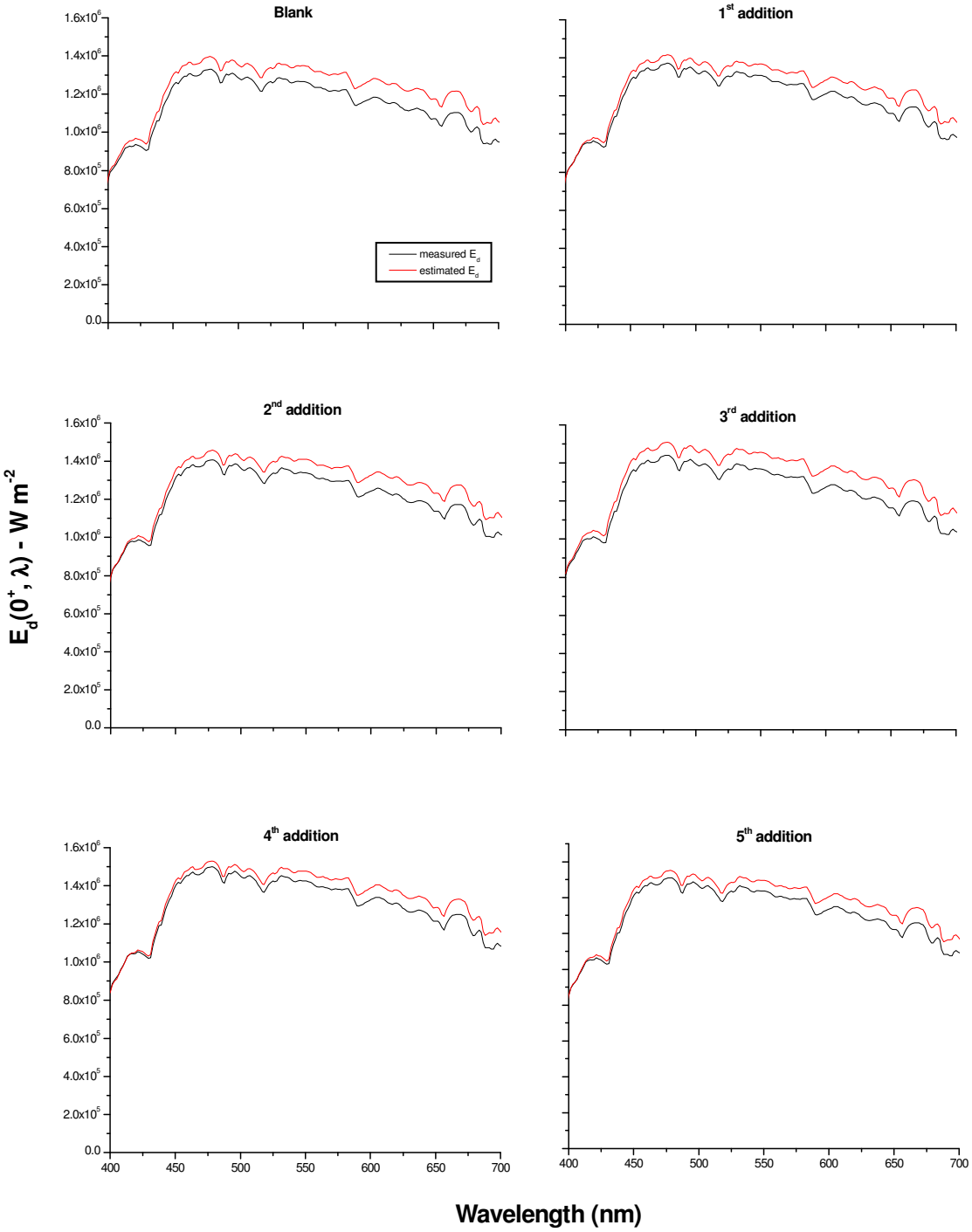

Figure 16. Comparison between measured and estimated downwelling irradiances, $E_d(0^+, \lambda)$, during the *C. polykrikoides* culture experiment for determinations of $R_{rs}(\lambda)$.

2.3.2.1.4 Baseline R_{rs} (λ) spectrum

The filtered-seawater R_{rs} (λ) spectrum showed maximum values in the blue region and minimal values in the red region, with a decreasing trend inversely related to wavelength (Figure 17). This is due to the increasing absorption properties of water molecules from shorter to longer visible wavelengths (Pope and Fry, 1997). In the absence of particles or any other absorbing substances, more blue light remained available for backscattering by the water molecules (Morel, 1974). The shape of this baseline spectrum suggested that any signal coming from the cylinder was negligible.

2.3.2.1.5 *C. polykrikoides* R_{rs} (λ) spectra

Spectral R_{rs} curves showed an overall increment in magnitude as a function of increasing cell abundance and chlorophyll *a* concentration (Figure 18a). The following spectral features were observed: a strong depression in the range of 400 to 500 nm; a prominent peak at 570 nm; a shoulder around 650 nm; a distinct trough at ~663 nm; and a peak in the red/near-infrared (NIR) region at ~690 nm. Variations in the magnitude of these spectral features as a function of cell density and chlorophyll *a* concentration were clear (Figure 18b).

The low R_{rs} (λ) observed in the blue/blue-green range of the spectrum were the outcome of the interacting absorption characteristics of both chlorophyll and carotenoid pigments. The strengthening of this R_{rs} depression feature with an increment in pigment concentration (and cell abundance) was evident. Subtle absorption features associated with *in vivo* absorption maxima for chlorophyll *a*, chlorophyll c_2 and carotenoids were identified at 436, 465, and 496 and ~530 nm, respectively (Jørgensen and Des Marais, 1988; Hoepffner and Sathyendranath, 1991).

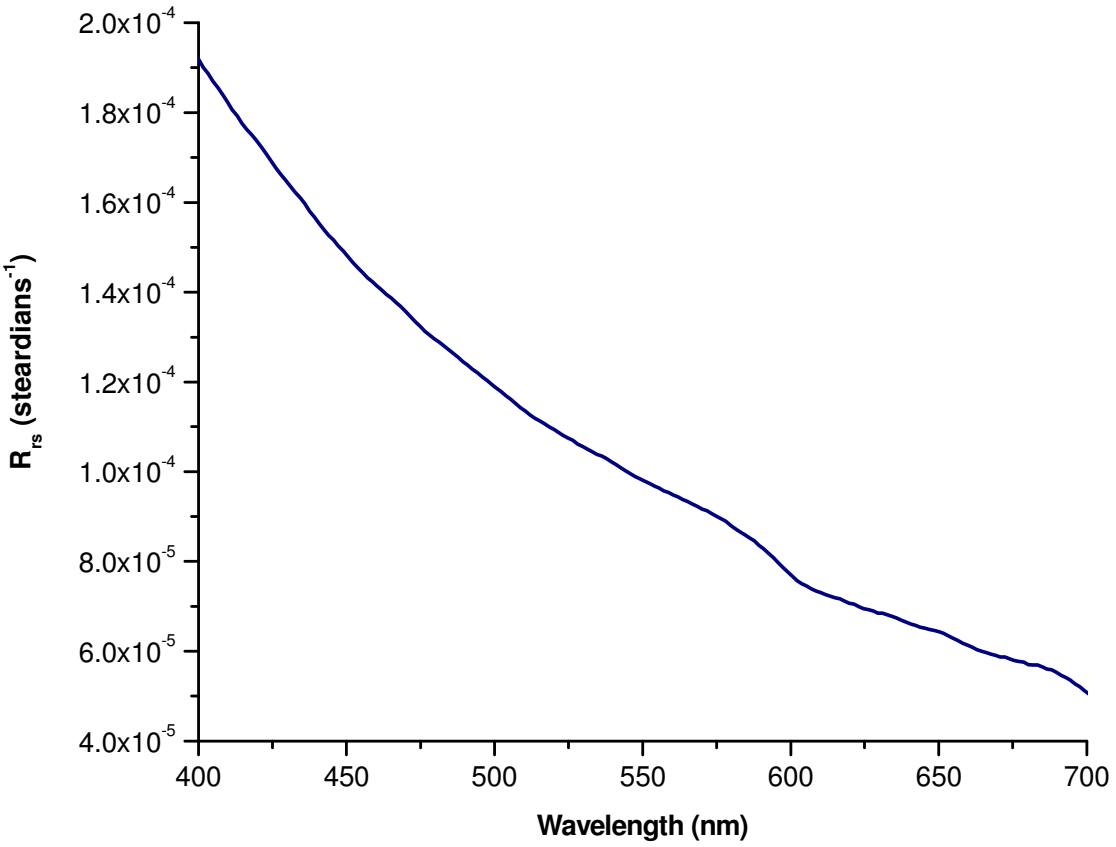

Figure 17. Remote sensing reflectance [R_{rs} (λ)] spectrum of filtered seawater (baseline) obtained during the *C. polykrikoides* culture experiment for determinations of R_{rs} (λ).

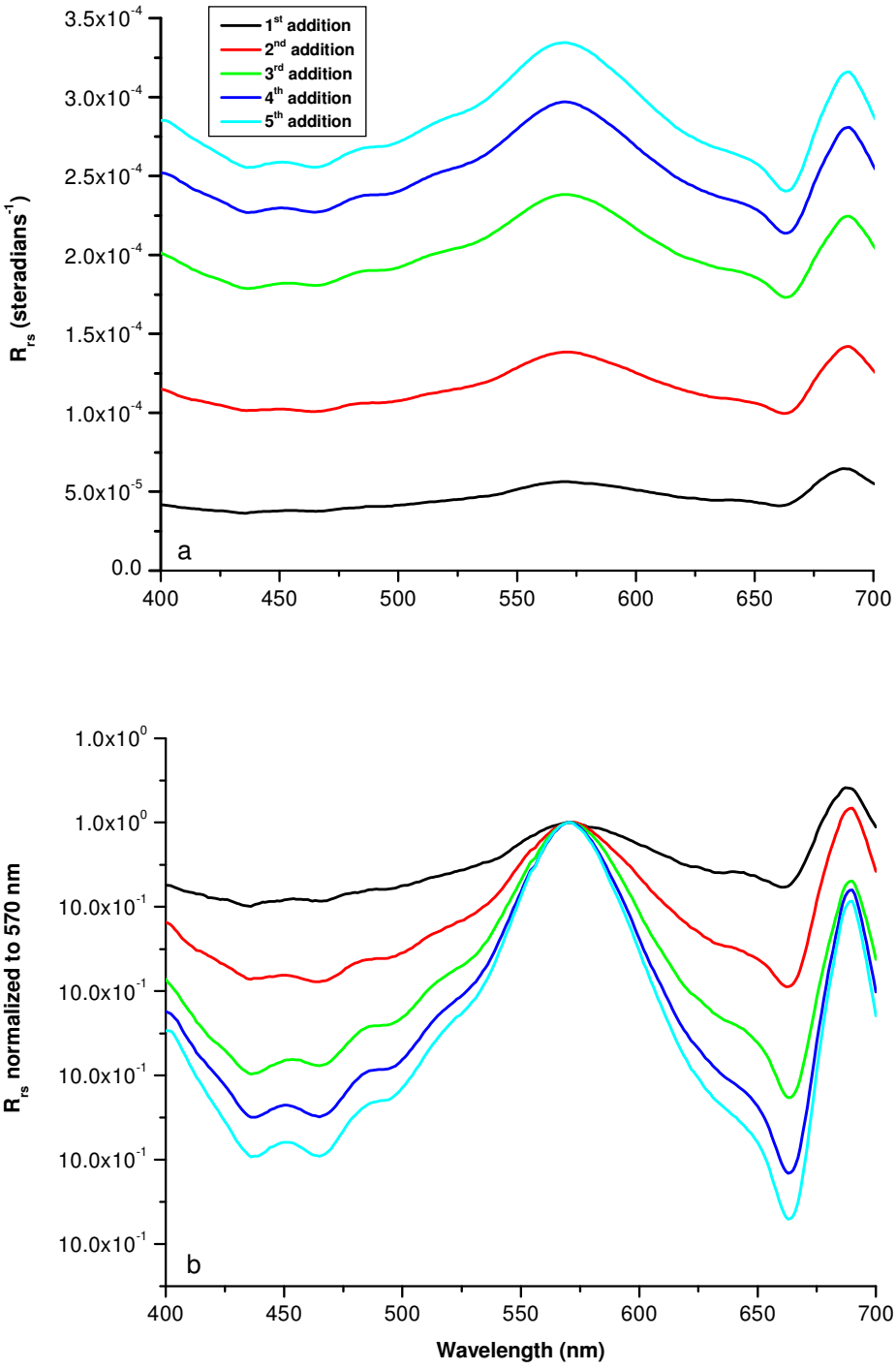

Figure 18. Remote sensing reflectance spectra [$R_{rs}(\lambda)$] measured during the five-step *C. polykrikoides* culture addition sequence. a) Original spectra showing variations in reflectance magnitude associated with increasing cell densities; b) Spectra normalized to 570 nm illustrating variations in the magnitude of the spectral features associated with increasing cell densities.

Within the spectral range of 530-600 nm, absorption by chlorophylls and carotenoids was minimal. In consequence, backscattering by cells remained the main factor governing R_{rs} (λ) (Gitelson et al., 1999; Gitelson et al., 2000). This resulted in a noticeable increment in R_{rs} (λ) (that peaked at 570 nm) with an increase in cell density. The position of this green peak near 570 nm is considered a distinctive feature of chlorophyll *c*-containing algae and is regarded as an indicator of their presence in natural waters (Gitelson et al., 1999). The shift of this peak in relation to the red/NIR peak (690 nm) toward higher R_{rs} (λ) values, in response to an increase in chlorophyll *a* and/or cell abundance, was apparent.

The shoulder appearing around 650 nm represents a region of moderate pigment absorption located between important absorption features for chlorophylls *a* and c_2 around 620-640 nm, and a well-defined absorption maximum (reflectance trough) of chlorophyll *a* positioned at 663 nm (Hoepffner and Sathyendranath, 1991; Johnsen et al., 1994a). These pigment absorption features (at both sides of the shoulder) were strengthened with an increase in cell density and chlorophyll *a* concentration.

The R_{rs} (λ) peak occurring at 690 nm is situated amid two prominent absorption features: the chlorophyll *a* absorption maximum at 663 nm (above mentioned) and the region around 700 nm, characterized by a sharp increase in water absorption (Pope and Fry, 1997). The precise nature of this peak remains uncertain. It has been attributed to natural chlorophyll fluorescence, anomalous scattering caused by absorption minima around 675-680 nm, or a minimum in the combined absorption curves of algae and water (Morel and Prieur, 1977; Gordon, 1979; Vasilkov and Kopelevich, 1982). Gitelson (1992) demonstrated, however, that fluorescence is an insignificant component of this feature. More recently, Rundquist et al. (1995) and Gitelson et al. (1999) agreed that this peak results from the interaction between cell scattering (which is

relatively independent of wavelength in this spectral region) and a minimum combined effect of pigment and water absorption. The magnitude of this peak (quantified as the difference between R_{rs} at the wavelength where the maximum value is observed and a baseline interpolated from 663 to 750 nm) showed a positive correlation with chlorophyll *a* ($r^2 = 0.97$) and cell abundance ($r^2 = 0.98$).

2.3.2.2 Derivative analysis of *C. polykrikoides* $R_{rs}(\lambda)$ spectra

2.3.2.2.1 Qualitative pigment analysis of second-derivatives

Second-derivative plots revealed eight sharp peaks attributable to *in vivo* absorption features of different chlorophyll and carotenoid pigments. They were located at 409-415, 435, 466-467, 497-498, 533-540, 614-621, 630-633 and 665-666 nm (Figure 19; Table 5). A comparison of these values with published *in vivo* pigment absorption maxima presented in Table 6 showed that the peaks located at 409-415, 435 and 614-621 nm, (peaks 1, 2 and 6, respectively), as well as the prominent peak occurring at 665-666 (peak 8), approximately coincide with the expected absorption maxima of chlorophyll *a*. The positions of these peaks were also in agreement with the (chlorophyll *a*) derivative peaks reported by many authors, which are summarized in Table 7.

The peak appearing at 466-467 nm (peak 3) most likely reflects the combined absorptions of chlorophyll c_2 and carotenoids (i.e. peridinin, diadinoxanthin, dinoxanthin, diatoxanthin, β-carotene), where the overlap of multiple absorption features prevented further separation of pigments (see Tables 6 and 7). Although no information regarding the *in vivo* absorption properties of dinoxanthin and diatoxanthin was found, it is well known that their *in vitro* absorption spectra strongly resemble that of diadinoxanthin (Jeffrey et al., 1997). Therefore,

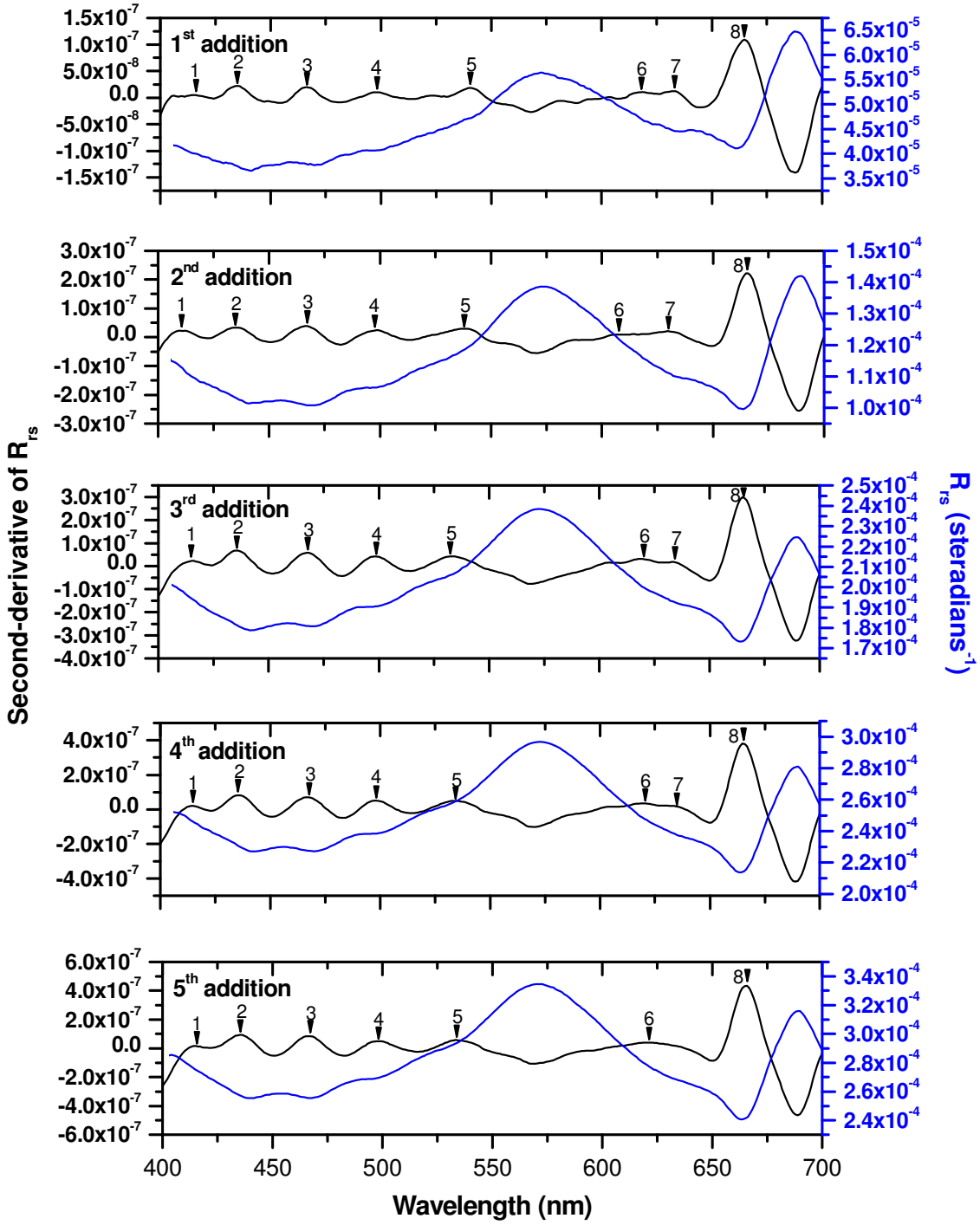

Figure 19. Second-derivative plots (black line) corresponding to the $R_{rs}(\lambda)$ spectra (blue line) measured during the five-step addition sequence of *C. polykrikoides* cultures. Numbers on derivative spectra indicate pigment peak identifications as follows: 1, 2, 6 and 8 = Chl *a*; 3 = Chl c_2, diadinoxanthin, diatoxanthin, dinoxanthin, peridinin and β-carotene; 4 = diadinoxanthin, diatoxanthin, dinoxanthin, peridinin and β-carotene; 5 = peridinin; 7 = Chl c_2.

Table 5. Wavelength positions (nm) of pigment absorption features identified in the second-derivative plots of $R_{rs}(\lambda)$ spectra measured during the five-step addition sequence of *C. polykrikoides* cultures. Pigment abbreviations: Chl *a* = chlorophyll *a*; Chl c_2 = chlorophyll c_2; Per = peridinin; Diad = diadinoxanthin; Diato = diatoxanthin; Dino = dinoxanthin; β-Car = β-carotene.

Peak	Pigment	Addition number				
		1	2	3	4	5
1	Chl *a*	415	409	415	415	415
2	Chl *a*	435	435	435	435	435
3	Chl c_2/Diad/Diato/ Dino/ Per/β-Car	466	466	467	467	466
4	Diad/Diato/Dino/Per/β-Car	497	498	498	498	498
5	Per	540	538	533	533	533
6	Chl *a*	619	614	619	620	621
7	Chl c_2	633	630	633	633	
8	Chl *a*	665	666	665	665	666

Table 6. *In vivo* absorption maxima of phytoplankton pigments as reported in the literature.

Pigment	Absorption maxima (nm)	Reference
Chlorophyll *a*	418, 437, 618, 673	Goedheer, 1970 [1]
	419, 437, 618, 675	Prézelin, 1980 [1]
	418, 440, 670-678	Owens and Wold, 1986 [1]
	430, 670	Jørgensen and Des Marais, 1988
	440, 674	Bidigare et al., 1990
	412, 435, 623, 675	Hoepffner and Sathyendranath, 1991
	415-420, 440, 625, 675 (small features at 590 and 635 nm)	Johnsen et al., 1994a
	415, 437, 676	Johnsen et al., 1994b
Chlorophyll *c*	460, 640	Mann and Myers, 1968 [2]
	585 (small feature)	Goedheer, 1970 [2]
	467, 630	Bidigare, 1989
	460, 636	Bidigare et al., 1990
	461, 583, 644	Hoepffner and Sathyendranath, 1991
	460-470, 586, 635	Johnsen et al., 1994b and references therein
Chlorophyll c_2	460, 590, 625, 635	Johnsen et al., 1994a
Carotenoids (general)	425-530	Mann and Myers, 1968 [2]
	450-500	Jørgensen and Des Marais, 1988
	490, 532	Hoepffner and Sathyendranath, 1991
	450-550	Johnsen et al., 1994b and references therein
Carotenes		
β-carotene	425-500	Mann and Myers, 1968 [2]
	490	Owens and Wold, 1986 [1]
	462	Bidigare et al., 1990
Xanthophylls		
Diadinoxanthin	440, 460, 490	Johnsen et al., 1994a
	481	Johnsen et al., 1994b
Peridinin	440, 460, 490, 540	Johnsen et al., 1994a
	481, 535	Johnsen et al., 1994b

[1] Reference obtained from Hoepffner and Sathyendranath (1991). [2] Reference obtained from Aguirre-Gomez et al. (2001).

Table 7. Summary of wavelength positions (nm) of pigment absorption features identified in derivative plots by several authors. Pigment abbreviations: Chl *a* = chlorophyll *a*; Chl c_2 = chlorophyll c_2; Per = peridinin; Fuc = Fucoxanthin; Diad = diadinoxanthin; β-Car = β-carotene. Fucoxanthin (although not present in the majority of dinoflagellates) is included since its absorption spectrum is very similar to that of peridinin and consequently, their absorption features tend to coincide.

Pigment	Reference	Derivative peak position (nm)
Chl *a*	Bidigare et al., 1988	675
	Millie et al., 1995	412, 438, 677
	Aguirre-Gómez et al., 2001	
	pure cultures	415-425, 440-455, 620, 675
	natural populations	428, 674
	Louchard et al., 2002	420-430, 445-460, 680
	Stephens et al., 2003	422, 444, 676
Chl *c*	Bidigare et al., 1988	467
	Millie et al., 1995	466, 589, 639
	Aguirre-Gómez et al., 2001	
	pure cultures	470, 640
	natural populations	454, 588, 630
	Stephens et al., 2003	468
Chl *c*/Chl *a*	Aguirre-Gómez et al., 2001	
	pure cultures	590-600
	Louchard et al., 2002	575, 585
	Stephens et al., 2003	643
Carotenoids (general)	Aguirre-Gómez et al., 2001	
	pure cultures	505, 530, 545, 590
	natural populations	482, 494, 514, 530, 556
	Louchard et al., 2002	495
Per/Fuc	Millie et al., 1995	495
	Aguirre-Gómez et al., 2001	
	pure cultures	545-555
	natural populations	514, 530, 556
	Louchard et al., 2002	510-520, 530-540
	Stephens et al., 2003	538
Diad	Millie et al., 1995	438, 466, 495
	Stephens et al., 2003	492
β-Car	Louchard et al., 2002	495
	Stephens et al., 2003	492

their *in vivo* absorption features are also expected to concur. Another absorption feature presumably entirely caused by chlorophyll c_2 was noticed at 630-633 nm (peak 7) (see Tables 6 and 7).

Absorption features related to carotenoids were identified at 497-498 nm (peak 4) and 533-540 nm (peak 5). Peak 4 resulted from a combination of peridinin, diadinoxanthin, dinoxanthin, diatoxanthin and β-carotene, given their spectral features tend to overlap in this region. In contrast, peak 5 may be most likely attributed to absorption by peridinin (see Tables 6 and 7).

2.3.2.2.2 Quantitative derivative analysis

Further evaluations of the second-derivative spectra revealed an enhancement in the magnitude of most major spectral features, directly proportional to the microalgal additions (Figure 20). Based on these observations, prominent derivative peaks associated with chlorophyll *a* absorption, as well as with natural chlorophyll fluorescence and/or cell scattering processes (i.e. reflectance features) were used to explore the feasibility of derivative techniques for accurate estimations of chlorophyll *a* concentration and *C. polykrikoides* cell abundance. The concentration of chlorophyll *a* showed significant correlations with the second derivative values at 435, 665-666 and 688-689 nm (Table 8). Likewise, *C. polykrikoides* cell abundance exhibited a strong correlation with the second derivative values at 435, 665-666 and 688-689 nm.

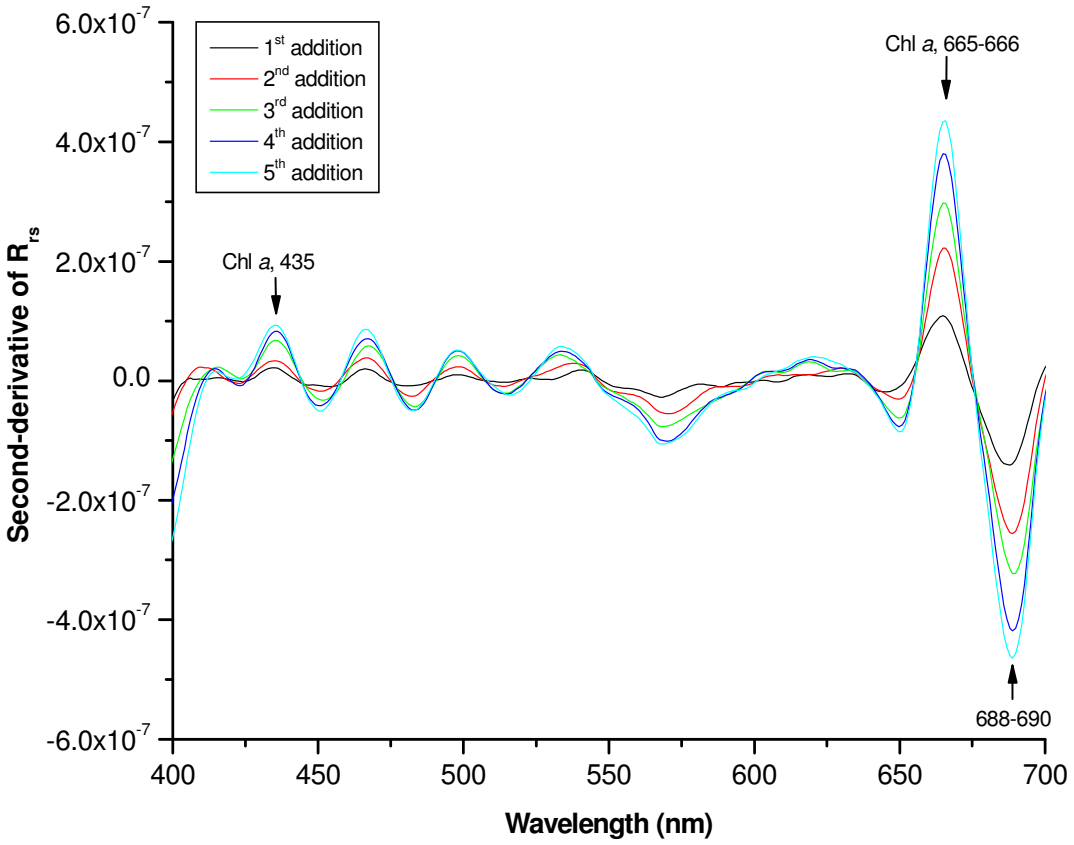

Figure 20. Second-derivative plots of the R_{rs} (λ) spectra measured during the five-step addition sequence of *C. polykrikoides* cultures, illustrating the enhancement in magnitude of the most prominent spectral features in direct response to increasing cell abundances. Identified peaks correspond to the spectral features used for quantitative estimations of chlorophyll *a* concentrations and *C. polykrikoides* cell abundance.

Table 8. Summary of linear regression analyses of *C. polykrikoides* cell abundance/ chlorophyll *a* concentration versus second-derivative peak magnitudes of R_{rs} (λ) spectra based on pure cultures.

Parameter	**Derivative position (nm)**	**Linear regression analysis $y = a + bx$; r^2; p**
Chlorophyll *a*		
	435	$y = -1.69 + 2.1E8x$; $r^2 = 0.97$; $p = 0.002$
	665-666	$y = -3.62 + 5.03E7x$; $r^2 = 0.97$; $p = 0.002$
	688-699	$y = -5.2 – 5.02E7x$; $r^2 = 0.97$; $p = 0.002$
Cell abundance		
	435	$y = -22.1 + 1.05E10x$; $r^2 = 0.98$; $p = 0.001$
	665-666	$y = -113.4 + 2.5E9x$; $r^2 = 0.97$; $p = 0.002$
	688-699	$y = -192.7 – 2.5E9x$; $r^2 = 0.98$; $p = 0.001$

2.3.2.3 Determinations of inherent optical properties

2.3.2.3.1 Chlorophyll *a* concentration and cell abundance

Chlorophyll *a* concentrations incremented progressively from 1.96 to 17.62 µg L^{-1} (Table 9) throughout the ten-step culture additions sequence. These concentrations represent the average of fluorometric and spectrophotometric measurements. Since no samples for cell counts were collected during this experiment, approximations of cell abundance were obtained from the chlorophyll *a* concentrations using equation 7. Estimated values of *C. polykrikoides* cell abundance ranged from 9.56 x 10^4 to 5.56 x 10^5 cells L^{-1} (Table 9).

2.3.2.3.2 Spectral absorption coefficients

Absorption coefficients for all ten culture additions (Figure 21) showed higher values in the blue spectral region (absorption maxima at 412 and 440 nm), and followed a decreasing tendency towards longer wavelengths. An exception to this trend was the presence of a secondary absorption maximum at 676 nm, associated with the red absorption maximum of chlorophyll *a*. Minimum absorption values within the visible spectrum occurred at 650 nm, although the lowest absorptions occurred in the near-infrared region, at 715 nm. An overall increment in absorption with increasing cell abundance and chlorophyll *a* concentration was evident. In addition, it was observed a progressive enhancement in the magnitude of the absorption maxima (relative to the other wavelengths) with an increase in cell abundance and chlorophyll *a* concentration.

Table 9. Summary of cell abundances and chlorophyll *a* concentrations obtained during the ten-step addition sequence of *C. polykrikoides* cultures for determinations of inherent optical properties [a (λ), b_b (λ), b (λ) and c (λ)]. Chlorophyll *a* concentrations represent mean values of fluorometric and spectrophotometric measurements. Cell abundances were estimated using the following equation: *C. polykrikoides* cell abundance = (29.38*[Chl *a*]) + 37.97.

Addition step	**[Chl *a*] (μg L^{-1})**	**Estimated cell abundance (cells L^{-1})**
1st addition	1.96	9.56×10^4
2nd addition	2.89	1.23×10^5
3rd addition	3.90	1.53×10^5
4th addition	6.37	2.25×10^5
5th addition	7.71	2.65×10^5
6th addition	9.65	3.21×10^5
7th addition	10.69	3.52×10^5
8th addition	10.45	3.45×10^5
9th addition	14.50	4.64×10^5
10th addition	17.62	5.56×10^5

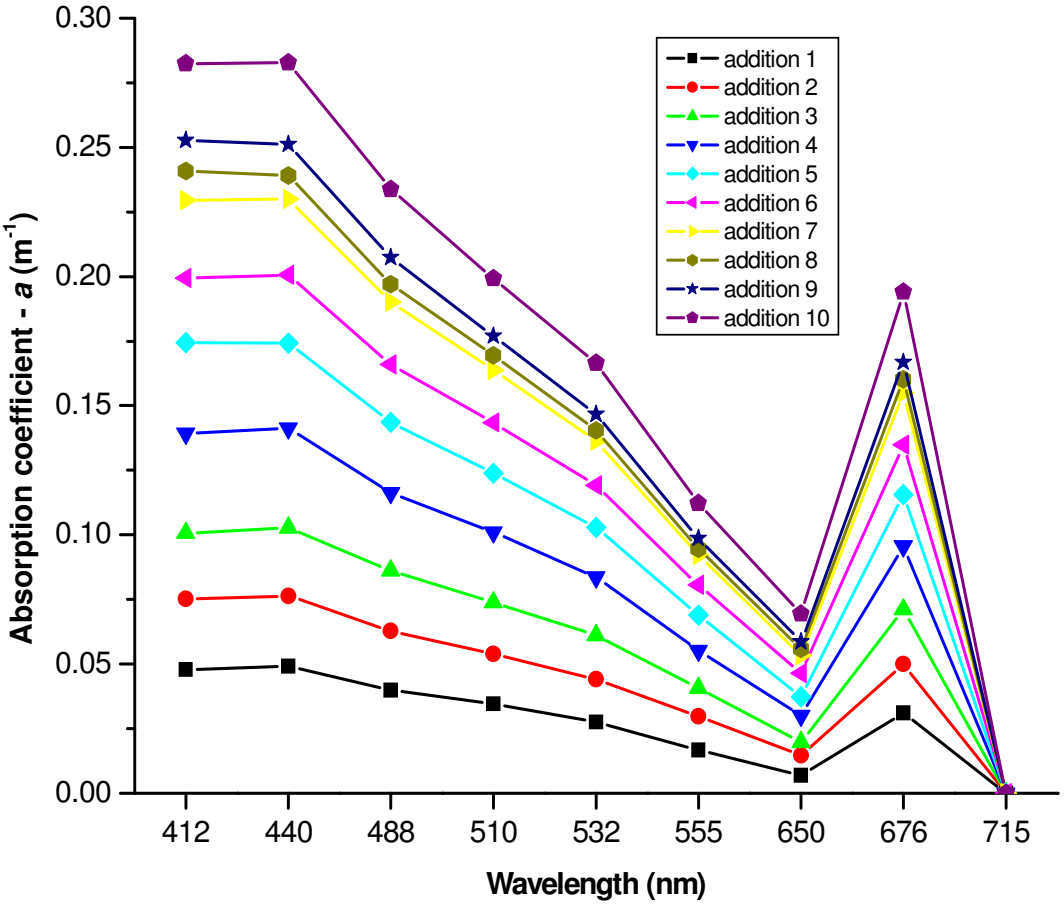

Figure 21. Spectral absorption coefficients [*a* (λ)] for the ten-step addition sequence of *C. polykrikoides* cultures measured with the ac-9. Values represent the median of the measurements recorded during periods of five minutes after the baseline correction.

2.3.2.3.3 Spectral attenuation coefficients

Spectral attenuation coefficients measured for the ten culture additions are shown in Figure 22. Light attenuation was always higher in the shorter wavelengths and decreased with increasing wavelength in a near-monotonous fashion. No prominent spectral features were observed. Attenuation coefficient values showed a progressive increment (at all wavelengths) with increasing chlorophyll *a* concentration and cell abundance.

2.3.2.3.4 Spectral scattering coefficients

Spectral scattering coefficients consistently showed maximum values at 412 nm and minimum values at 676 nm (Figure 23). Scattering exhibited an increasing tendency towards the shorter wavelengths of the visible region. At 715 nm (near-infrared region), however, scattering values were slightly higher than the minimum. An overall increment in the magnitude of the scattering coefficients with increasing chlorophyll *a* concentration and cell abundance was observed. The intensification of the spectral scattering features (in relation to the other wavelengths) with an increment in cell abundance and chlorophyll *a* concentration was also evident.

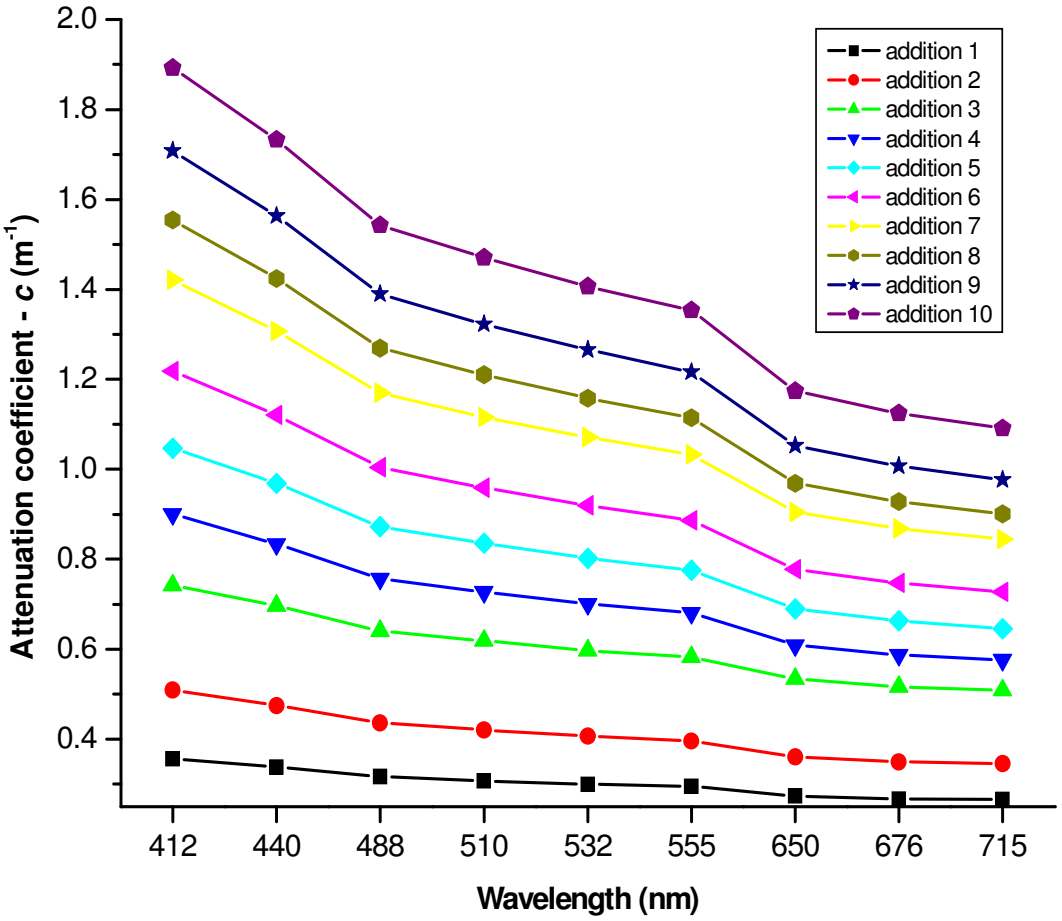

Figure 22. Spectral attenuation coefficients [*c* (λ)] for the ten-step addition sequence of *C. polykrikoides* cultures measured with the ac-9. Values represent the median of the measurements recorded during periods of five minutes after the baseline correction.

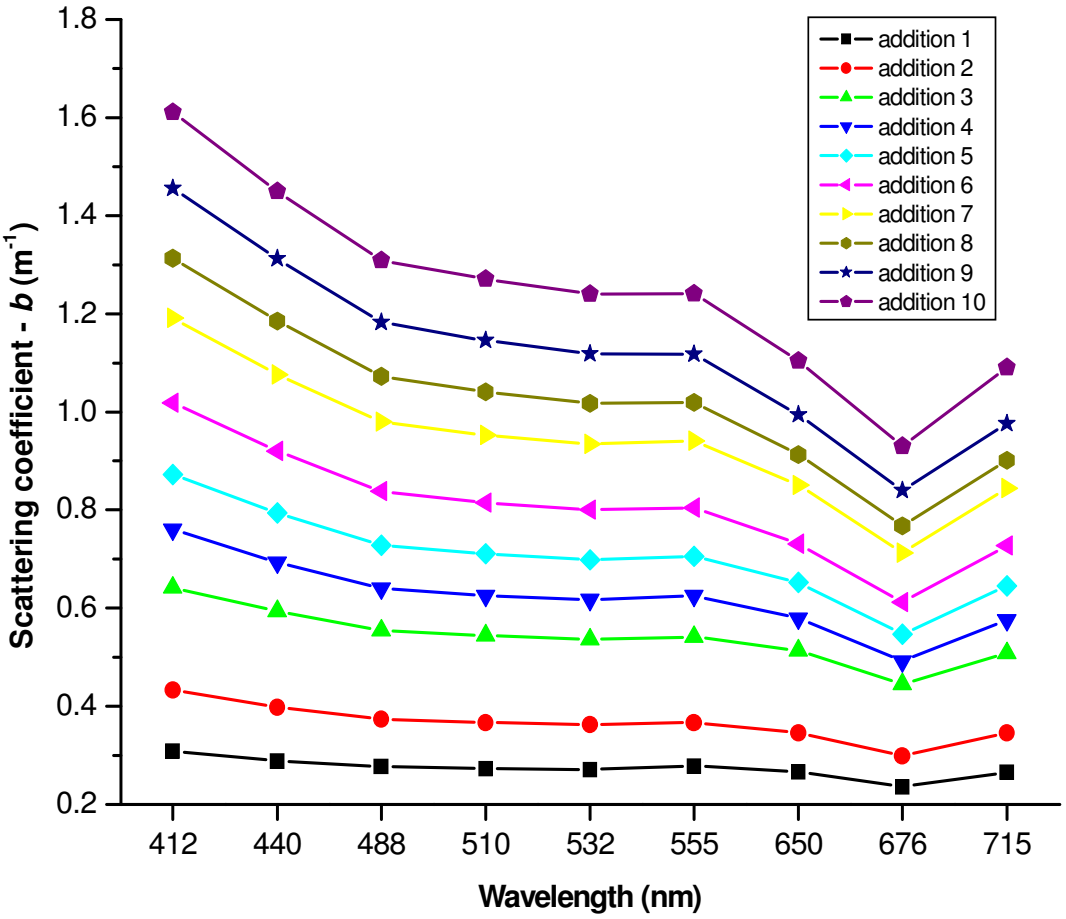

Figure 23. Spectral scattering coefficients [*b* (λ)] for the ten-step addition sequence of *C. polykrikoides* cultures measured with the ac-9. Values represent the median of the measurements recorded during periods of five minutes after the baseline correction.

2.3.2.3.5 Spectral backscattering coefficients

Backscattering coefficients for filtered seawater, which was considered the baseline, showed higher values in the shorter wavelengths with a decreasing trend towards longer wavelengths (Figure 24). This spectral pattern is in accordance with the theoretical values for pure seawater (Figure 24) reported in the literature (Morel, 1974; Vaillancourt et al., 2004). However, backscattering by filtered seawater was enhanced at all wavelengths up to twice the theoretical values. Since it was not possible to remove all particles in the filtered seawater, due to a nominal filter cut-off equal to 0.2 µm, the baseline backscattering values represent the combined effects of pure seawater, small particles, and the possible contributions from the cylinder's walls and bottom. These factors may thus explain the enhanced backscattering.

The backscattering curves corresponding to all ten *C. polykrikoides* culture additions (after baseline subtraction) are presented in Figure 25. Backscattering showed a progressive increment at all wavelengths with an increase in chlorophyll *a* concentration and cell abundance. The backscattering values were always higher in the blue and yellow-orange spectral regions, with maxima occurring at 442 and 589 nm, except for addition 1 where the maxima occurred at 589 and 620 nm. The strengthening of these spectral backscattering features (compared with the other wavelengths) with an increase in chlorophyll *a* concentration and cell abundance was apparent. Minimum backscattering values were consistently located at 470 and 675 nm excluding addition 1, where minima were found at 470 and 510 nm.

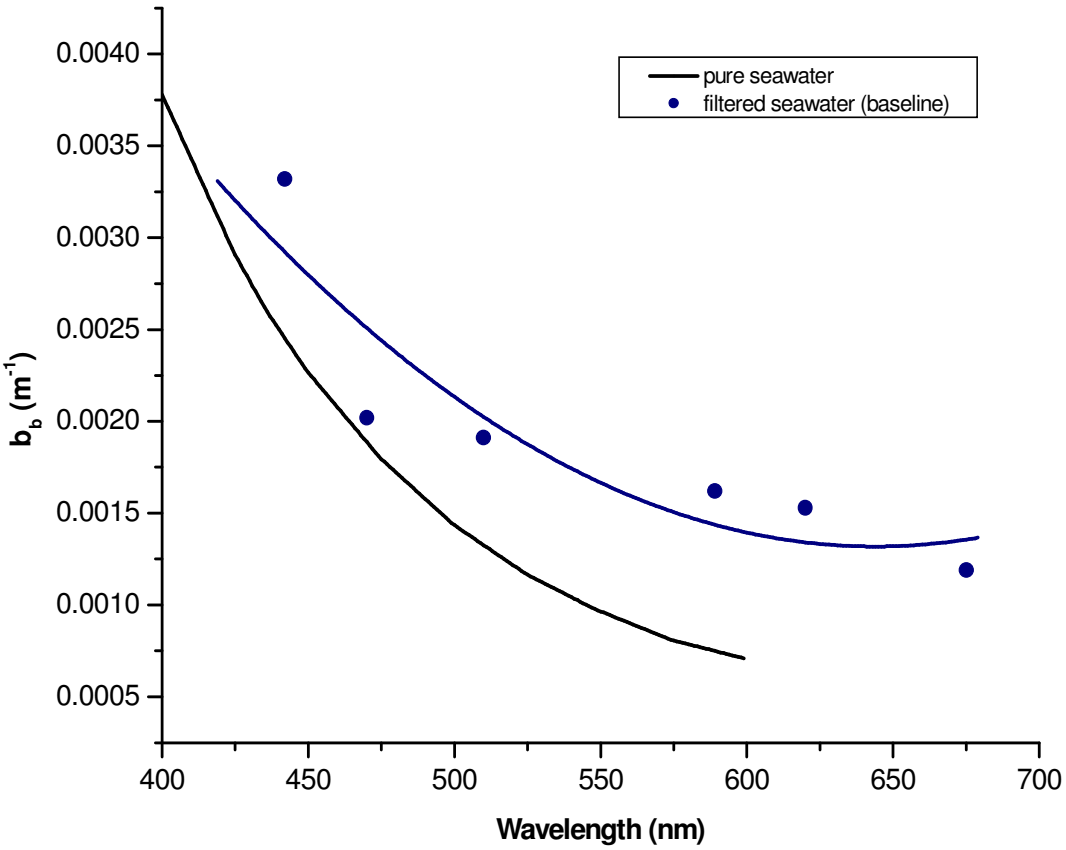

Figure 24. Backscattering (b_b) spectra of 0.2 µm filtered seawater measured with the HS6. Values represent the median of a five-minute data set collected prior to the addition of the *C. polykrikoides* cultures. The black line indicates b_b for pure seawater calculated as one-half the published values for the total scattering coefficient by Morel (1974). The blue line shows the polynomial fit of the filtered seawater b_b measurements.

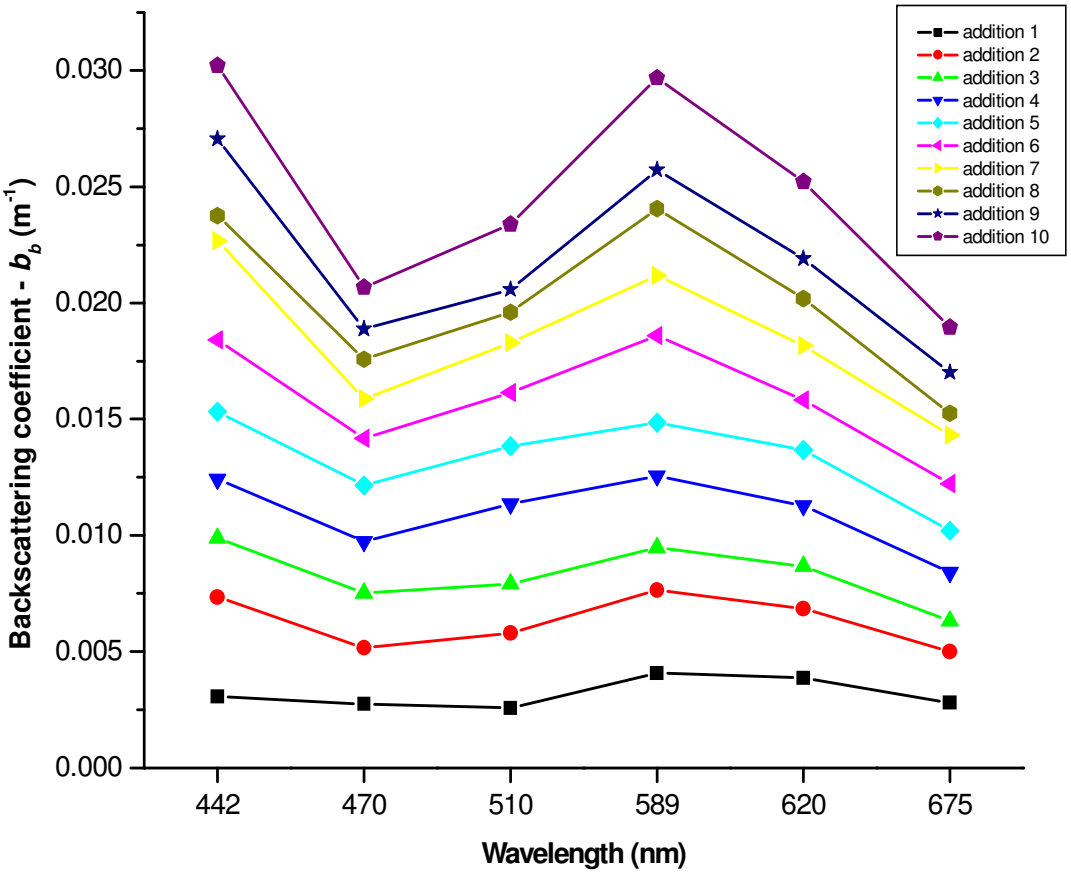

Figure 25. Spectral backscattering coefficients [$b_b(\lambda)$] for the ten-step addition sequence of *C. polykrikoides* cultures measured with the HS6. Values represent the median of measurements recorded during periods of five minutes after the baseline correction.

2.3.3 Apparent and inherent optical properties of natural communities

2.3.3.1 Monthly Samplings

2.3.3.1.1 Spatial and temporal variations of remote sensing reflectance [$R_{rs}(\lambda)$] spectra

Average $R_{rs}(\lambda)$ spectra measured at the six stations studied in Bahía Fosforescente from May 2002 to July 2003 (Figure 26) showed great similarity in their spectral shape, with variability being mostly related to the magnitude of the curves and of the spectral features. The following spectral pattern was common to all stations: $R_{rs}(\lambda)$ increased monotonously from 400 to approximately 570 nm, and then it started decreasing down to 750 nm, except for the occurrence of a shoulder at ~646 nm, and a secondary peak (or shoulder, depending on the station) at ~690 nm. This spectral pattern is indicative of typical coastal waters with high concentrations of chlorophyll, detritus and CDOM. These seawater constituents strongly absorb blue light (~400–500 nm) (detritus, like CDOM, exhibits exponentially decreasing absorption with increasing wavelength), causing low $R_{rs}(\lambda)$ in this spectral region. In contrast, pigment, detritus and CDOM absorption at the green wavelengths (~500-600 nm) is minimal; therefore, the relative contribution of particulate backscattering to $R_{rs}(\lambda)$ is much higher in this spectral range, resulting in high $R_{rs}(\lambda)$ (with a maximum around 570 nm). Beyond 600 nm (and up to 700 nm - red spectral region), aside from the red/NIR peak at ~690 nm due to chlorophyll *a* fluorescence and/or cell scattering, $R_{rs}(\lambda)$ remain low because of the absorption of chlorophyll and water.

Spatial variability among the $R_{rs}(\lambda)$ spectra was primarily due to the complex and variable water composition, and physical characteristics of the study area. Lower $R_{rs}(\lambda)$ values were observed for stations 1, 2 and 5 throughout most visible wavelengths. These three stations were located within the western- and eastern-most inlets (arms) of the bay,

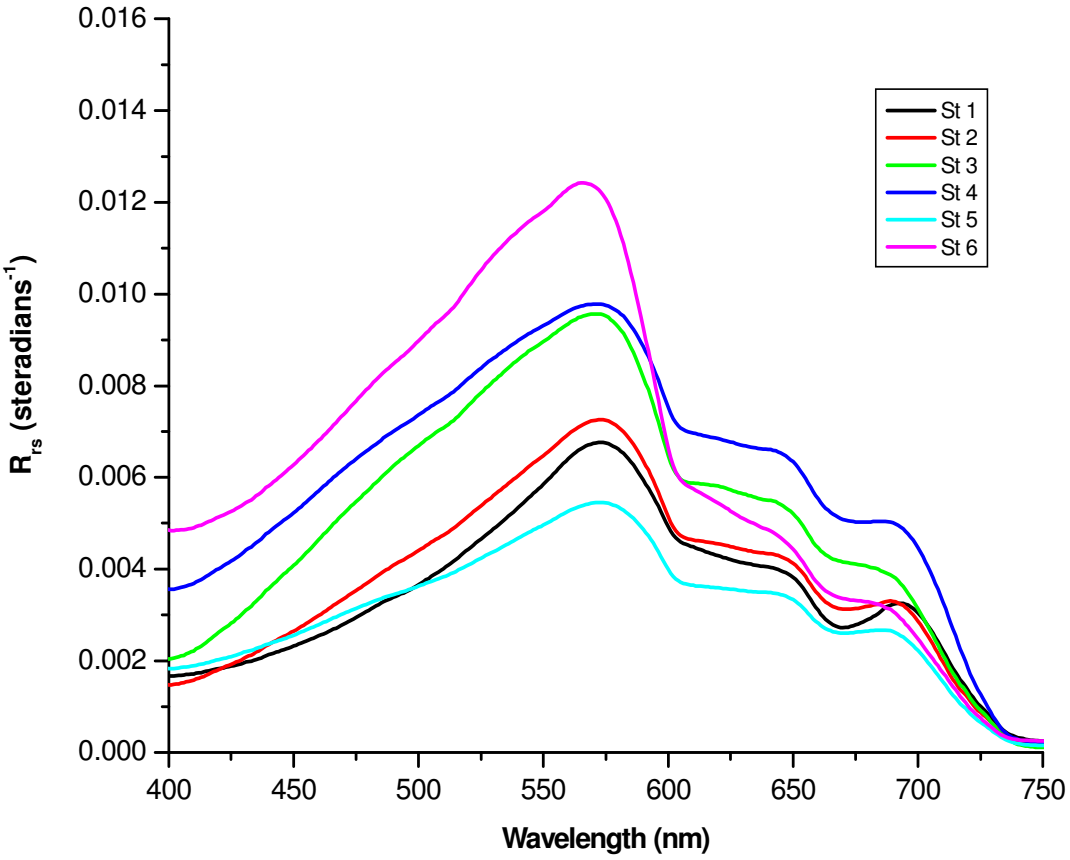

Figure 26. Average R_{rs} (λ) spectra measured at the six stations studied in Bahía Fosforescente from May 2002 to July 2003.

in relatively secluded areas that together with the prevailing wind and circulation patterns promote the accumulation of phytoplankton cells, detritus and CDOM, mainly contributed by the surrounding mangroves. Besides, because of their shallow depths (1-1.5 m) these stations are highly influenced by sediment resuspension. Consequently, these waters look darker (i.e. have lower R_{rs} (λ) values) than the other stations. In the particular case of station 1, it also exhibited the most distinct red/NIR peak on account of the phytoplankton blooms frequently observed in this area (see Chapter 1).

Highest R_{rs} (λ) values were observed for station 6 from 400 to ~600 nm, although values along the red spectral region were intermediate between those of the other stations (and more important, were proportionally lower relative to the blue and green spectral regions compared to the other spectra). Given its location near the center of the main bay area, this station is the deepest (~4 m), the most exposed to wind mixing and the less-proximate to the surrounding mangroves. Therefore, it is not usually as affected as the other stations by the accumulation of detritus and CDOM or by sediment resuspension. This results in waters of higher transparency (i.e. with higher R_{rs} (λ) values along the blue and green wavelengths and comparatively lower red R_{rs} (λ) values) that often appear blue-green or greenish in color as a function of phytoplankton cell density.

Stations 3 and 4, on the other hand, showed intermediate R_{rs} (λ) values between those of the other stations, except at the red wavelengths where R_{rs} (λ) values were the highest. This presumably responds to the fact that, even though these stations were located within the western and middle inlets of the bay, their location is not as isolated as that of stations 1, 2 and 5, so there is not as much accumulation of phytoplankton cells, CDOM, detritus and sediments. It is important to mention that station 4 was located in a very shallow area (~0.6 m), where the bottom could be seen from the boat during most samplings. Therefore, the

relatively high R_{rs} (λ) values observed for this station along the red spectral region might have been produced by bottom reflectance, given that bottom sediments strongly reflect red light.

The complete set of R_{rs} (λ) spectra collected at the six sampling stations from May 2002 to July 2003 (excluding those spectra collected under overcast conditions) is presented in Figure 27. All stations exhibited variability among their respective R_{rs} (λ) spectra, primarily associated with magnitude. Nevertheless, slight variations in spectral shape were also evident for some stations. This temporal variability is directly related to the numerous and largely uncorrelated constituents suspended or dissolved in the seawater, whose relative concentration change according to different biological (e.g. bloom formation, degradation) and physical processes (e.g. resuspension, dilution).

The stations that showed greater temporal variability were stations 1, 2 and 5. Stations 1 and 2 were characterized by the episodic occurrence of phytoplankton blooms predominantly constituted by *C. polykrikoides* (and occasionally by the dinoflagellate *Akashiwo sanguinea* - formerly *Gymnodinium sanguineum*), which imparted a striking brownish-red water discoloration (see Chapter 1). It is these extreme fluctuations in cell density (i.e. bloom versus no bloom conditions) rather than variations in species composition, the dominant species within the phytoplankton community, or in the relative concentrations of the other seawater constituents, that seems mainly responsible for the observed variability in these two stations. Similarly, variability in station 5 appears to be mostly linked to fluctuations in phytoplankton cell density, although no outstanding blooms were observed there during the samplings.

Stations 3, 4 and 6 demonstrated much less temporal variability among their individual R_{rs} (λ) spectra. Each of these stations showed R_{rs} (λ) spectra with rather similar

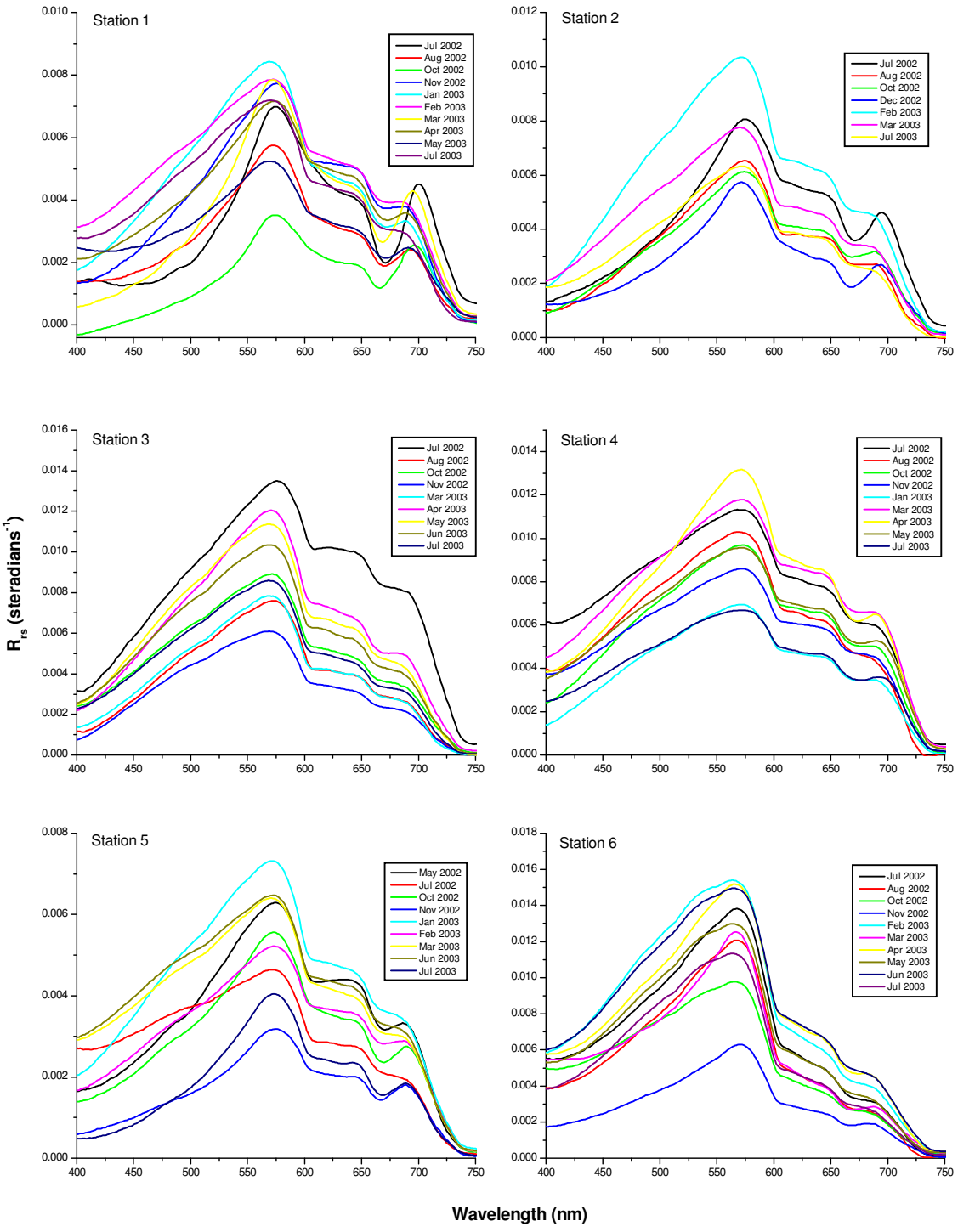

Figure 27. Complete set of R_{rs} (λ) spectra measured at the six stations studied in Bahía Fosforescente from May 2002 to July 2003. For each station, only those spectra collected under low cloud cover or clear sky conditions are presented.

spectral shapes; hence, variability was almost entirely related to magnitude. This suggests a certain level of stability regarding the relative concentrations of the different seawater constituents in these stations compared to the others.

2.3.3.1.2 Comparison among R_{rs} (λ) spectra of *C. polykrikoides*, *A. sanguinea* and *Ceratium furca* var. *hircus-Pyrodinium bahamense* blooms

As an initial effort to evaluate whether *C. polykrikoides* may be differentiated from other bloom-forming dinoflagellate species in Bahía Fosforescente based on R_{rs} (λ) data, spectra representative of blooms of *C. polykrikoides*, *A. sanguinea*, and *Ceratium furca* var. *hircus-Pyrodinium bahamense*, corresponding to similar chlorophyll *a* concentrations (11.81, 8.5 and 11.5 µg L^{-1}, respectively), were compared. Even though *A. sanguinea* is not a regularly occurring dinoflagellate species within this bay, bloom episodes dominated by this species were observed along the western-most inlet of the bay (in the exact same location where *C. polykrikoides* blooms occur) during December 2002 and April 2003. These blooms were extremely similar visually to those of *C. polykrikoides* (also giving the water a remarkable brownish-red color), thus likely to be erroneously qualified as *C. polykrikoides* blooms. *Ceratium furca* var. *hircus* and *P. bahamense*, on the other hand, are both widely distributed species throughout the bay that were often found co-occurring in high concentrations or bloom conditions, particularly at station 6.

The R_{rs} (λ) spectra of *C. polykrikoides* and *A. sanguinea* exhibited a great similarity, with no potential discriminating features being apparent (Figure 28). The small differences observed between them (including lower reflectance values in the blue spectral region and higher reflectance values along the green and red wavelengths for *C. polykrikoides*, as well as a more prominent red/NIR reflectance peak that was slightly shifted towards longer wavelengths) appear to be mostly related to the slightly higher chlorophyll *a* concentration

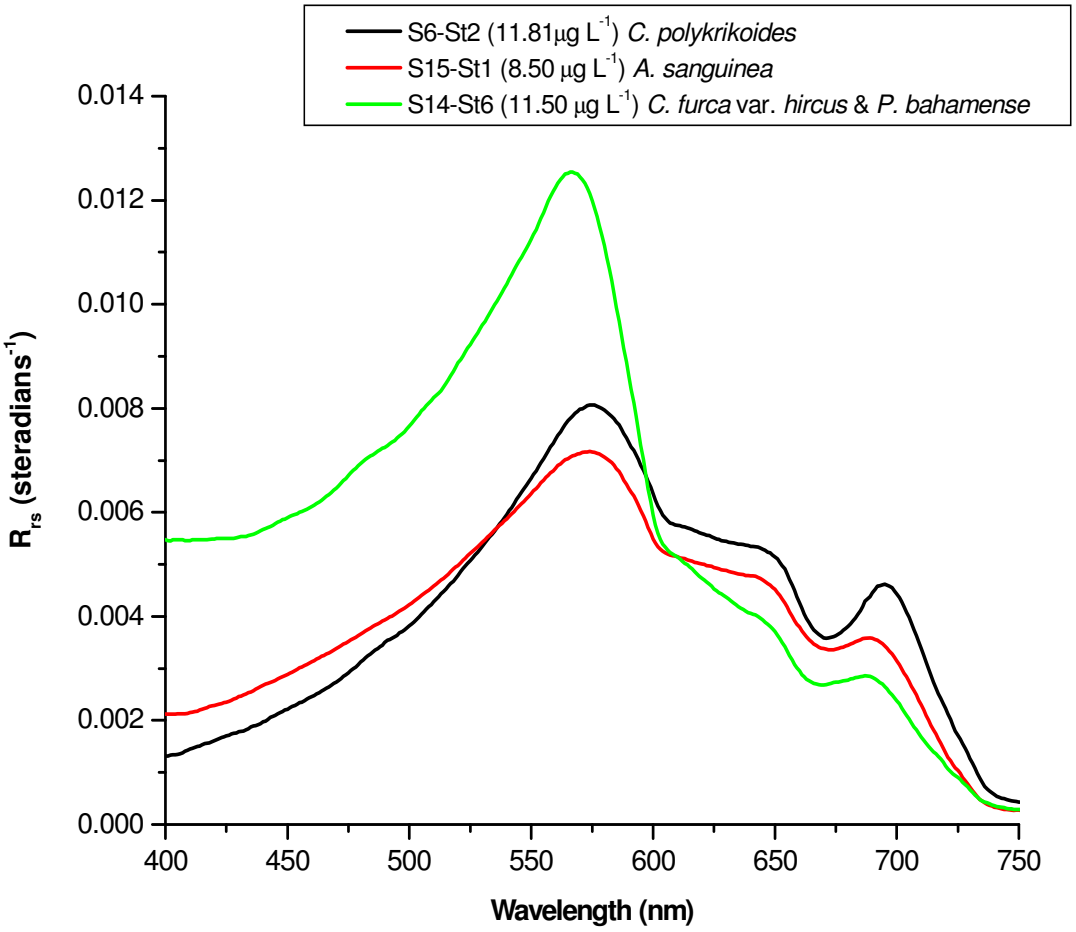

Figure 28. $R_{rs}(\lambda)$ spectra representative of blooms of *C. polykrikoides*, *A. sanguinea*, and *C. furca* var. *hircus-P. bahamense* corresponding to similar chlorophyll *a* concentrations, collected in Bahía Fosforescente during the monthly samplings period.

(and almost certainly, higher phytoplankton cell abundance) associated with the bloom of *C. polykrikoides*, rather than to species-specific features. Also, variations in the detritus, CDOM and sediment content of the seawater during these two blooms may have contributed to these differences.

Conversely, the spectrum of *C. furca* var. *hircus* and *P. bahamense* showed noticeable differences with the former spectra. The R_{rs} (λ) values for this bloom were not only higher throughout the blue and green spectral regions, but were also proportionately much higher along the blue and green wavelengths than in the red, compared with the *C. polykrikoides* and *A. sanguinea* spectra. This was probably due to a lower concentration of sediments, detritus and CDOM in the bloom area, resulting in waters of higher transparency despite their high chlorophyll content, but also suggested species-specific optical features.

2.3.3.1.3 Derivative analysis of the R_{rs} (λ) spectra of *C. polykrikoides*, *A. sanguinea* and *C. furca* var. *hircus-P. bahamense* blooms

Analysis of the second-derivatives of the R_{rs} (λ) spectra of the blooms of *C. polykrikoides*, *A. sanguinea*, and *C. furca* var. *hircus-P. bahamense* revealed no significant differences among them such as to make possible an effective discrimination between these species (Figure 29). Absorption features resolved by the second-derivatives were basically the same for the three spectra and corresponded to the typical dinoflagellate pigments including chlorophyll *a*, chlorophyll c_2 (or its combination with carotenoid pigments) and a mixture of carotenoids (consisting of peridinin, diadinoxanthin, diatoxanthin, dinoxanthin and β,β carotene). This implied that pigment absorption do not explain the differences observed among the R_{rs} (λ) spectra and, most certainly, do not represent an adequate optical property to differentiate *C. polykrikoides* from other dinoflagellate species within this bay.

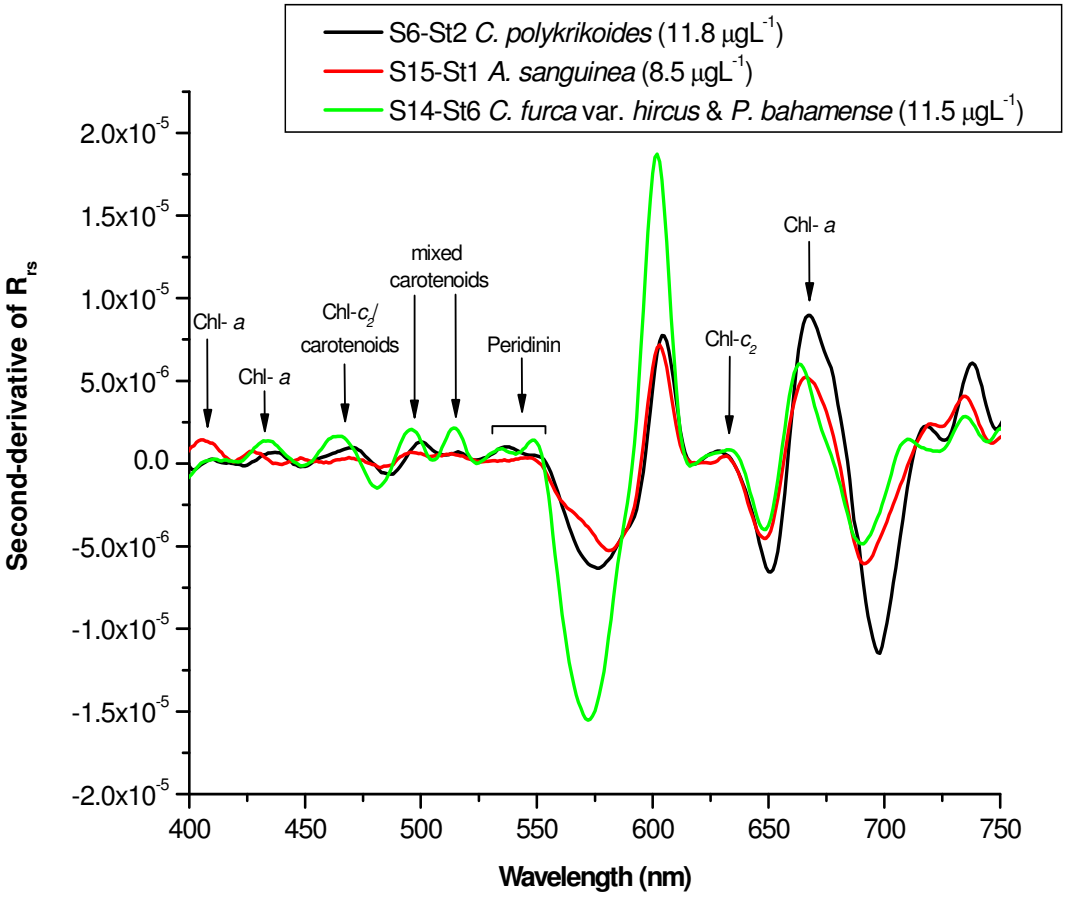

Figure 29. Second-derivative plots of the R_{rs} (λ) spectra of *C. polykrikoides*, *A. sanguinea* and *C. furca* var. *hircus-P. bahamense* blooms. Absorption features associated with the different dinoflagellate pigments are indicated.

2.3.3.2 Special samplings during a bloom episode of *C. polykrikoides*

Based on the results of the previews two sections, it was evident that a comprehensive knowledge about the IOP's and the different seawater constituents (CDOM, TSS, ISS, Chl *a* and cell abundance) associated with the dinoflagellate blooms observed in Bahía Fosforescente would be imperative to better understand variations among their R_{rs} (λ) spectra, and to be able to elucidate if it is feasible to discriminate *C. polykrikoides* from the other bloom-forming species. With that in mind, two special samplings during a bloom of *C. polykrikoides* included measurements of all the above-mentioned parameters. Apart from the two stations sampled within the extent of the bloom area, a reference station located near the center of the bay (corresponding to station 6 in the monthly samplings) was also sampled. The location of this reference station was selected based of the fact that *C. polykrikoides* was rarely found in this area during the monthly samplings (and when present, it was only found in background concentrations- as previously shown in Chapter 1). Instead, high concentrations and occasionally blooms of several dinoflagellate species widely distributed throughout the bay (predominantly *P. bahamense* and *C. furca* var. *hircus*, but also including other *Ceratium*, *Prorocentrum*, *Dinophysis* and *Protoperidinium* species) prevailed in that station. A summary of the seawater constituents measured as part of these samplings is presented in Table 10. Note that this was the most intense bloom of *C. polykrikoides* ever observed in Bahía Fosforescente during the study period, representing fundamentally a monoculture of this species. The reference station, on the other hand, represented a mixed assemblage mainly conformed by dinoflagellate species, but also including a minor component of diatoms.

Table 10. Summary of bio-geochemical parameters measured at Bahía Fosforescente during the samplings of May 16 and 18, 2007.

Date	Station	[Chl *a*] (µg L^{-1})	Cell abundance (cells L^{-1})					CDOM ($a_{CDOM}(412)$) (m^{-1})	TSS (mg L^{-1})	ISS (mg L^{-1})
May 16, 2007			*C. polykrikoides*	*Ceratium*	*P. bahamense*	*Protoperidinium*	*Dinophysis caudata*			
	BL-1	65.74	4,309,667					1.15	114	74
	BL-2	45.13	3,413,600					0.95	138	88
	Reference	5.62	1,354	26,116	7,733	969	107	0.48	47	36
May 18, 2007										
	BL-1	34.14	609,911					0.92	102	62
	BL-2	48.72	3,880,267					0.75	97	66
	Reference	2.93	1,850	4,340	7,793	470	62	0.56	40	29

2.3.3.2.1 Remote sensing reflectance [R_{rs} (λ)] spectra

The R_{rs} (λ) spectra collected during these two samplings (Figure 30) showed the same overall tendency, with the two stations located within the *C. polykrikoides* bloom area exhibiting curves with nearly identical spectral shapes and very closely related magnitudes. On the other hand, they were considerably different from those of the reference station. The R_{rs} (λ) values inside the bloom area were, in general, much lower than in the reference station, except for the longer visible and NIR wavelengths where bloom reflectances were higher due to a prominent peak. These differences in R_{rs} (λ) magnitude corresponded to a substantial disparity in the concentration of optically active constituents, given that the bloom stations exhibited extremely high chlorophyll *a* values and dinoflagellate cell abundances (34.14-65.74 μg L^{-1} and 609,911-4,309,667 cells L^{-1}, respectively) compared to the reference station (2.93 and 5.62 μg L^{-1}, and 14,515 and 36,279 cells L^{-1}, respectively), as well as a greater content of CDOM, TSS and ISS (up to ~3 times higher).

Noticeable differences in spectral shape were also observed. The *C. polykrikoides* bloom spectra were characterized by a strong depression in R_{rs} (λ) between 400 and 500 nm, because of the strong influence of absorption by phytoplankton pigments, detritus and CDOM, and by a well-defined red/NIR peak due to the exceedingly high accumulation of phytoplankton cells in this area. They also showed a green maximum positioned at ~573 nm, followed by a gradual decrease down to a pronounced trough around 668 nm, as a result of the high chlorophyll *a* content. On the contrary, the reference station spectra revealed a less flattened spectral shape from 400 to 500 nm, clearly indicating a smaller contribution by CDOM, detritus and pigment absorption, as well as an inconspicuous and slightly shifted towards shorter wavelengths red/NIR peak (that seemed more like a shoulder) due to the comparatively much lower concentrations

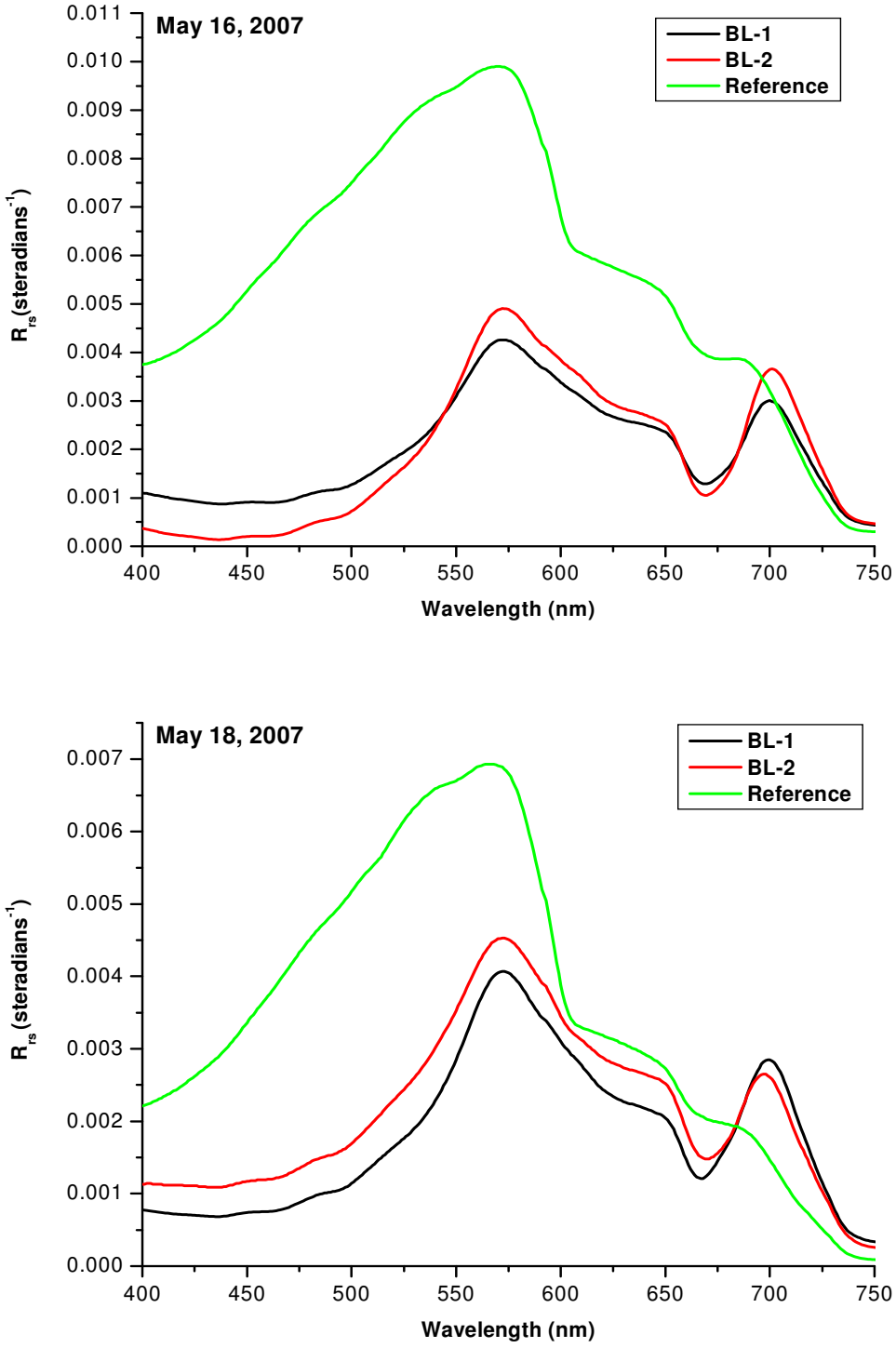

Figure 30. R_{rs} (λ) spectra measured at Bahía Fosforescente on May 16 and 18, 2007 during a bloom of *C. polykrikoides*. Data was collected at two stations located within the extent of bloom area (BL-1 and BL-2) and at a reference station located in the center of the bay (Reference).

of phytoplankton cells and chlorophyll *a* in this area. The upward spectral shift of the NIR peak with increased chlorophyll *a* has been widely observed and is explained by an upward shift in the position of the minimum combined absorption by pigments and water with increased chlorophyll *a* concentrations (Gitelson, 1992; Gitelson et al., 1999). The green maximum appeared also shifted to ~568 nm and was followed by an abrupt decrease in R_{rs} (λ) probably related to a lower backscattering and/or stronger water absorption along this spectral region. It could also be due to the much lower concentration of dinoflagellate pigments in this station. The dinoflagellate carotenoid pigment peridinin has significant activity in the mid-500 nm region and suppresses the green peak magnitude when present in high concentrations (Schalles, 2008). A much less pronounced chlorophyll *a* trough at ~668 nm was also apparent.

2.3.3.2.2 Derivative analysis of R_{rs} (λ) spectra

Even though certain differences were detected between the R_{rs} (λ) spectra of the bloom of *C. polykrikoides* and those of the reference station, no specific features or patterns that could be considered diagnostic of the presence of *C. polykrikoides* or of the dominant dinoflagellates in the reference station (i.e. *P. bahamense* and *Ceratium*) were evident. Consequently, second-derivatives of the average spectra for the *C. polykrikoides* bloom and reference stations were computed (Figure 31) to explore potential discriminating features that could have been masked in the R_{rs} (λ) spectra. The analysis resolved effectively absorption features attributable to chlorophyll *a*, chlorophyll c_2, peridinin and the combination of carotenoid pigments, and revealed differences between the two spectra around the range of 505-550 nm. In this spectral region, the second-derivatives showed a broad peak centered at ~540 nm primarily associated with peridinin for the *C. polykrikoides* bloom spectrum, but instead resolved two smaller peaks located at 513 and 550 nm for the spectrum of the reference station. These differences may be

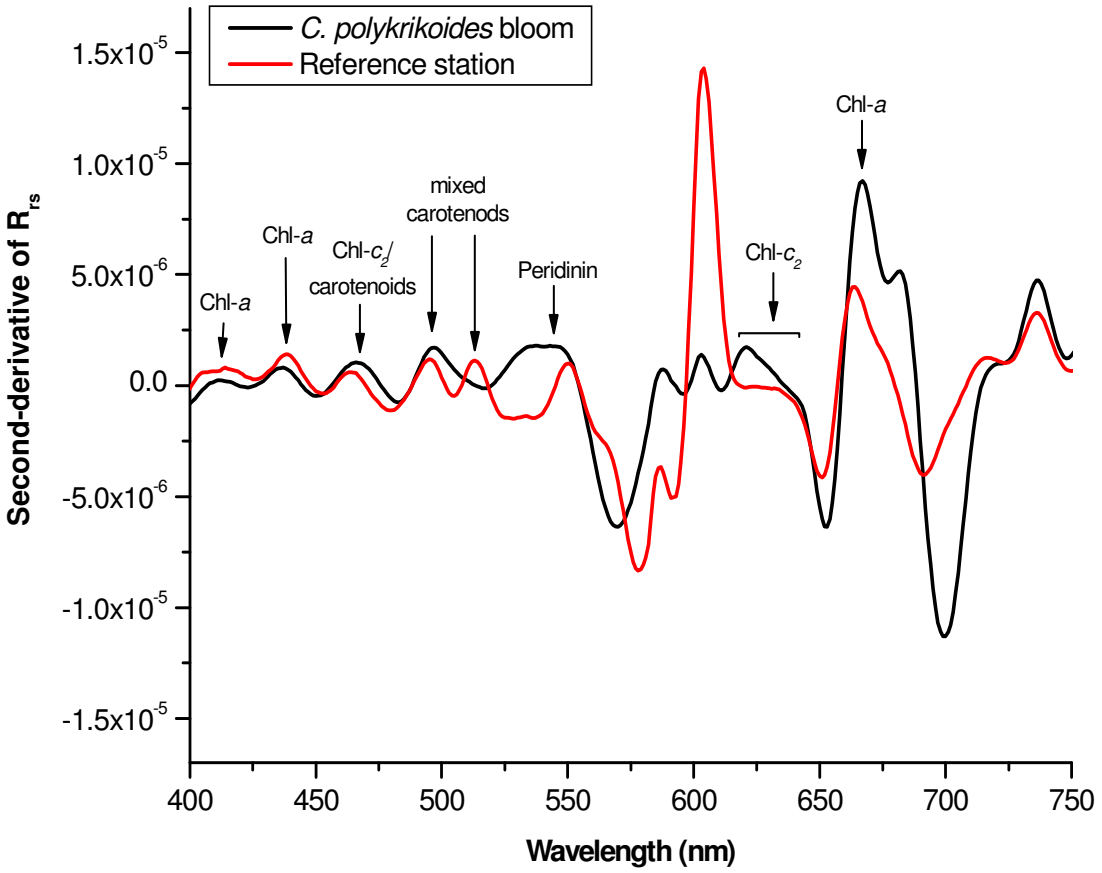

Figure 31. Second-derivative plots of the average R_{rs} (λ) spectra for the *C. polykrikoides* bloom and reference stations. Absorption features associated with the different dinoflagellate pigments are indicated.

explained by the extreme variation in phytoplankton pigments concentration between the two areas, rather than by unique optical features. Apparently, the high concentration of pigments associated with the bloom of *C. polykrikoides* allowed a robust separation of the peridinin absorption signal, whereas for the reference station, due to its much lower pigment content (and correspondingly weaker signals), the separation was more inefficient resulting in two separate peaks. Note that these two peaks were also observed, in very similar positions, in the second-derivatives of the R_{rs} (λ) spectra corresponding to the blooms of *C. polykrikoides* and *C. furca* var. *hircus-P. bahamense* presented in section 2.3.3.1.3 and have also been reported by several authors (see Table 7).

2.3.3.2.3 Spectral absorption coefficients

The absorption coefficients measured at the *C. polykrikoides* bloom stations were overall higher than those of the reference station (Figure 32), agreeing with the distribution of the strongly absorbing constituents between these two areas. Absorption coefficient values for the reference station incremented at all wavelengths with an increase in cell abundance (and corresponding pigment concentrations), whereas for the bloom area such a direct relationship was not observed, particularly for the three highest *C. polykrikoides* abundances and pigment concentrations. These inconsistencies may be related to the difficulties imposed by the patchy nature of *C. polykrikoides* blooms, as this species tends to form clumps or strips of cells embedded in a mucilaginous secretion, inevitably introducing great variability into the sampling data. For all stations, maximum absorption values occurred at 412 nm due to the strong influence of CDOM absorption, with a secondary chlorophyll *a* maximum at 676 nm. An inverse relationship with wavelength was observed for wavelengths shorter than 650 nm. Also, an increment in the magnitude of the absorption coefficients for wavelengths lower than

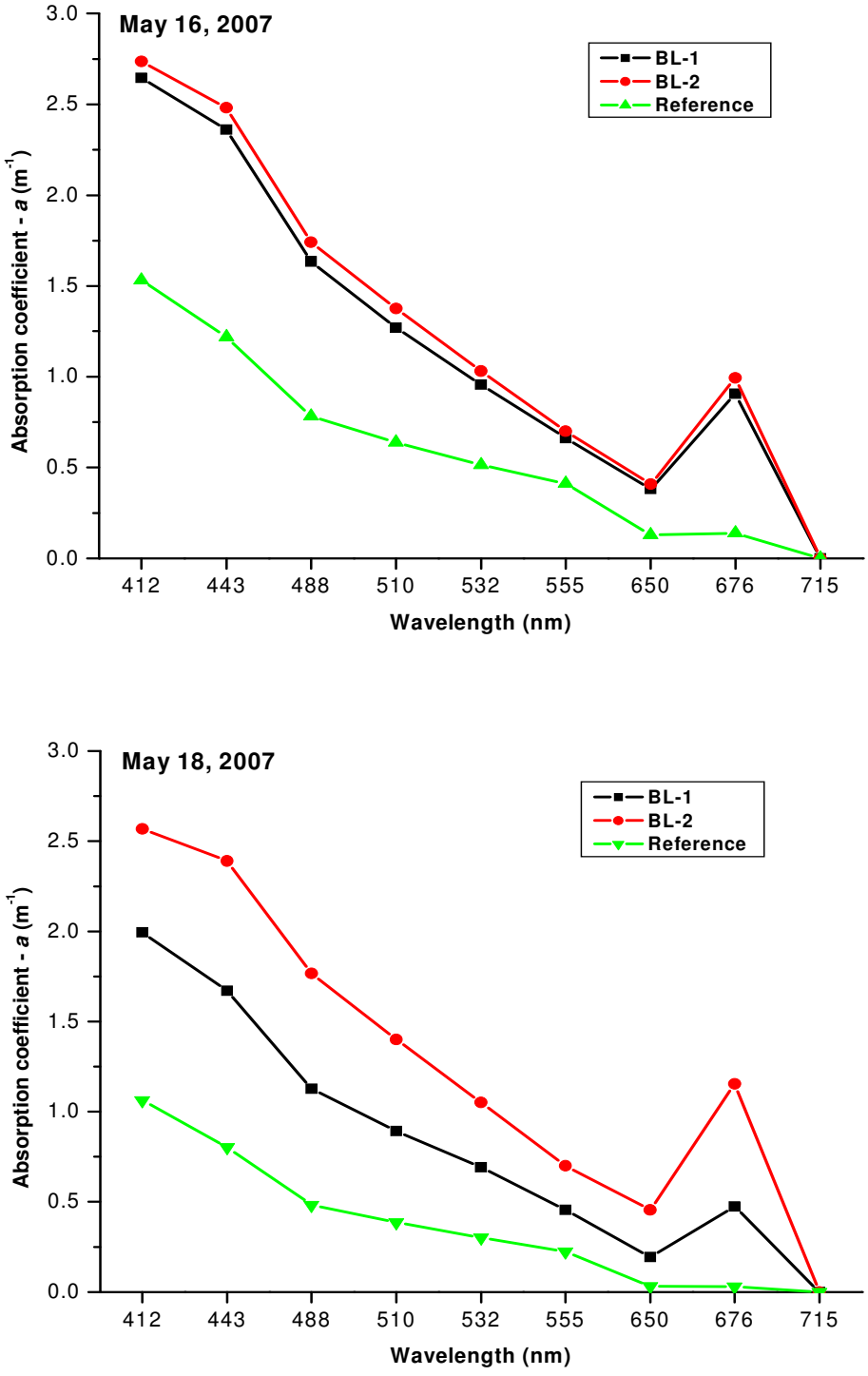

Figure 32. Spectral absorption coefficients [*a* (λ)] measured with the ac-9 at the *C. polykrikoides* bloom and reference stations. Values represent the median of the measurements recorded during periods of five minutes after removal of noisy data and the baseline correction.

555 nm and at 676 nm (regions of strong pigment and/or CDOM and detritus absorption), relative to 555 and 650 nm (regions of lower absorption), was apparent for the bloom stations compared to the reference station in response to their higher content of pigments, TSS and CDOM.

2.3.3.2.4 Spectral attenuation coefficients

Cochlodinium polykrikoides bloom stations showed much higher spectral attenuation coefficients than the reference station (Figure 33) due to a higher absorption and/or scattering by phytoplankton cells, pigments, CDOM and ISS (sediments). The attenuation coefficient values for the bloom area followed the same trend of the absorption coefficients, where an increment in the total content of optically active constituents in the seawater increased light attenuation at all wavelengths, except for the areas with the highest concentrations of these constituents. Absorption and attenuation measurements were taken simultaneously with the ac-9 and therefore both corresponded to the same water sample. Hence, these noticeable discrepancies are directly related to that observed for the absorption coefficients and presumably respond to the sampling difficulties explained in the previous section. For all stations, attenuation values were higher in the blue wavelengths and decreased with increasing wavelength in a near-monotonous fashion, with no prominent spectral features being apparent.

2.3.3.2.5 Spectral scattering coefficients

Spectral scattering coefficients (Figure 34) showed considerably higher values (2-75 times higher, depending on the spectral region and station) compared to that of absorption, contributing substantially more to light attenuation in these waters. Scattering coefficient values for the *C. polykrikoides* bloom stations were, in general, much higher than those of the reference station as a result of their higher particle loads. In addition, they varied with increasing

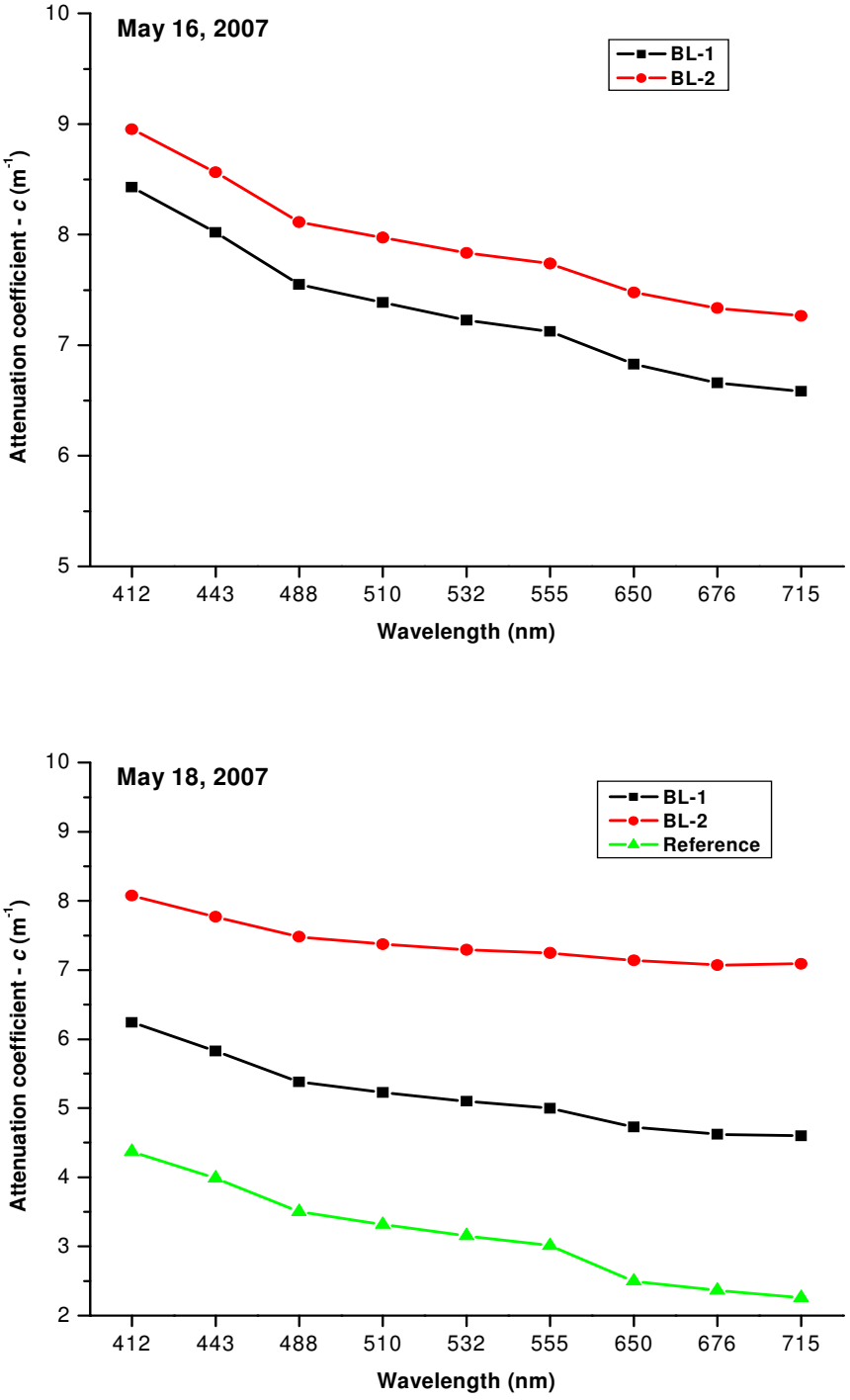

Figure 33. Spectral attenuation coefficients [c (λ)] measured with the ac-9 at the *C. polykrikoides* bloom and reference stations. Values represent the median of the measurements recorded during periods of five minutes after removal of noisy data and the baseline correction. Data for the reference station corresponding to the May 16 sampling are not included due to instrumental difficulties experienced during data collection.

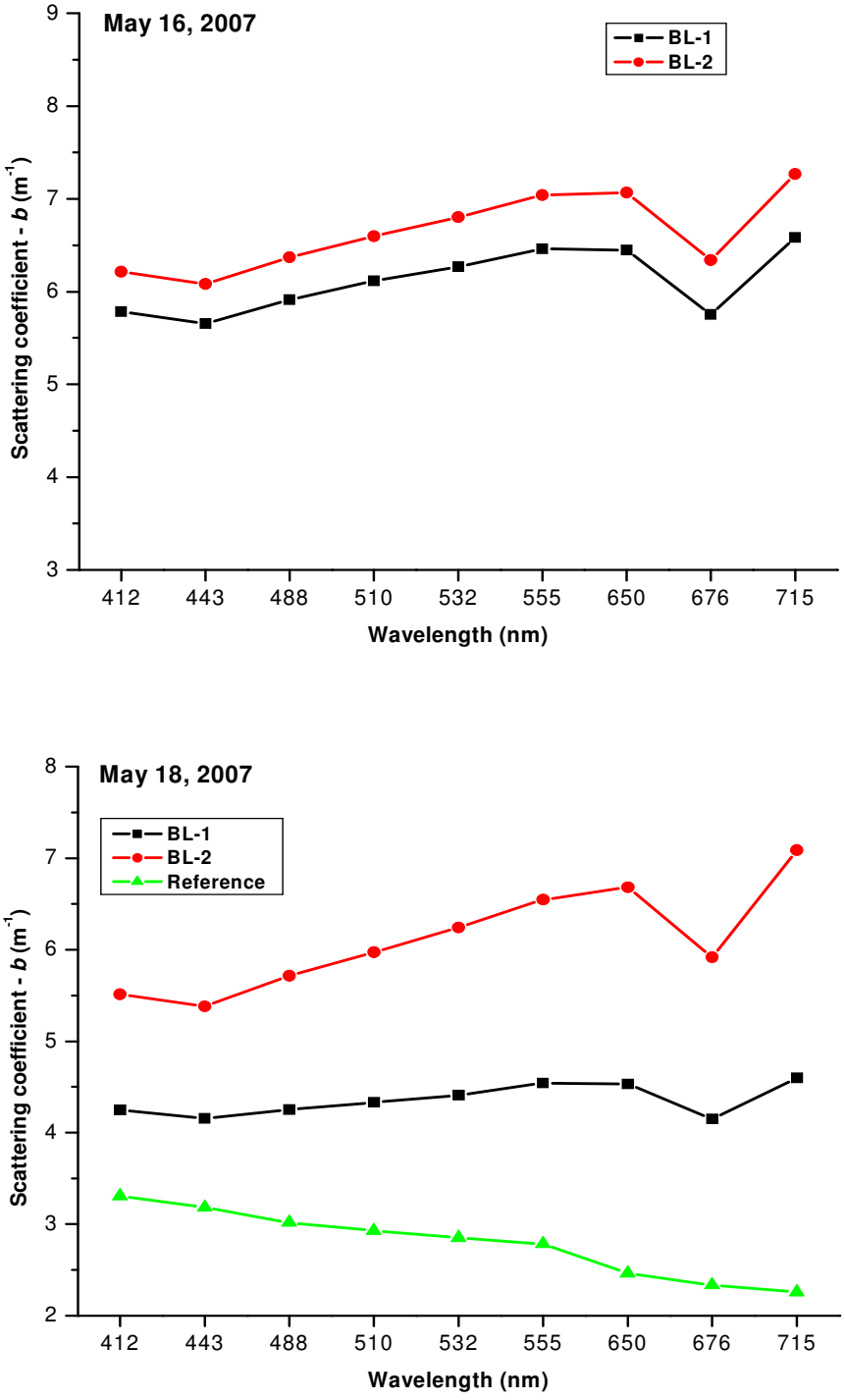

Figure 34. Spectral scattering coefficients [b (λ)] measured with the ac-9 at the *C. polykrikoides* bloom and reference stations. Values represent the median of the measurements recorded during periods of five minutes after removal of noisy data and the baseline correction. Data for the reference station corresponding to the May 16 sampling are not included due to instrumental difficulties experienced during data collection.

concentrations of particulate suspended matter (or TSS) in the exact same fashion as the absorption and attenuation values, since they were obtained as the difference between these two optical properties (scattering = attenuation – absorption). The reference station presented higher scattering values in the shorter blue wavelengths and exhibited a decreasing tendency towards longer wavelengths. The *C. polykrikoides* bloom stations revealed an opposite spectral pattern, with decreasing scattering values towards shorter wavelengths. This pattern responds to their higher absorption by phytoplankton pigments and CDOM, which strongly reduce the blue light available for scattering, and to their higher content of ISS, which strongly scatter red light. Two scattering minima associated with the chlorophyll *a* absorption maxima were observed at 443 and 676 nm.

2.3.3.2.6 Spectral backscattering coefficients

Backscattering coefficients measured at the three sampling stations (Figure 35) were considerably low compared to the scattering coefficients, representing roughly 3% or less of the total scattering values (based on the values of the matching wavelengths between the HS6 and ac-9, i.e. 442/443, 510 and 675/676 nm). Backscattering coefficients corresponding to the first sampling (May 16) showed higher values for the reference station than for the bloom of *C. polykrikoides*, whereas for the second sampling (May 18) their values were very much closer. This was probably due to the lower abundance of phytoplankton cells and concentration of ISS at the reference station during the second sampling, thus resulting in proportionately lower backscattering values. Although an increment in backscattering magnitude with an increase in *C. polykrikoides* abundance at wavelengths longer than 470 nm was observed for the bloom stations during the first sampling, this pattern was not sustained when the data of both samplings were considered together. This was primarily related to the fact that the backscattering coefficients

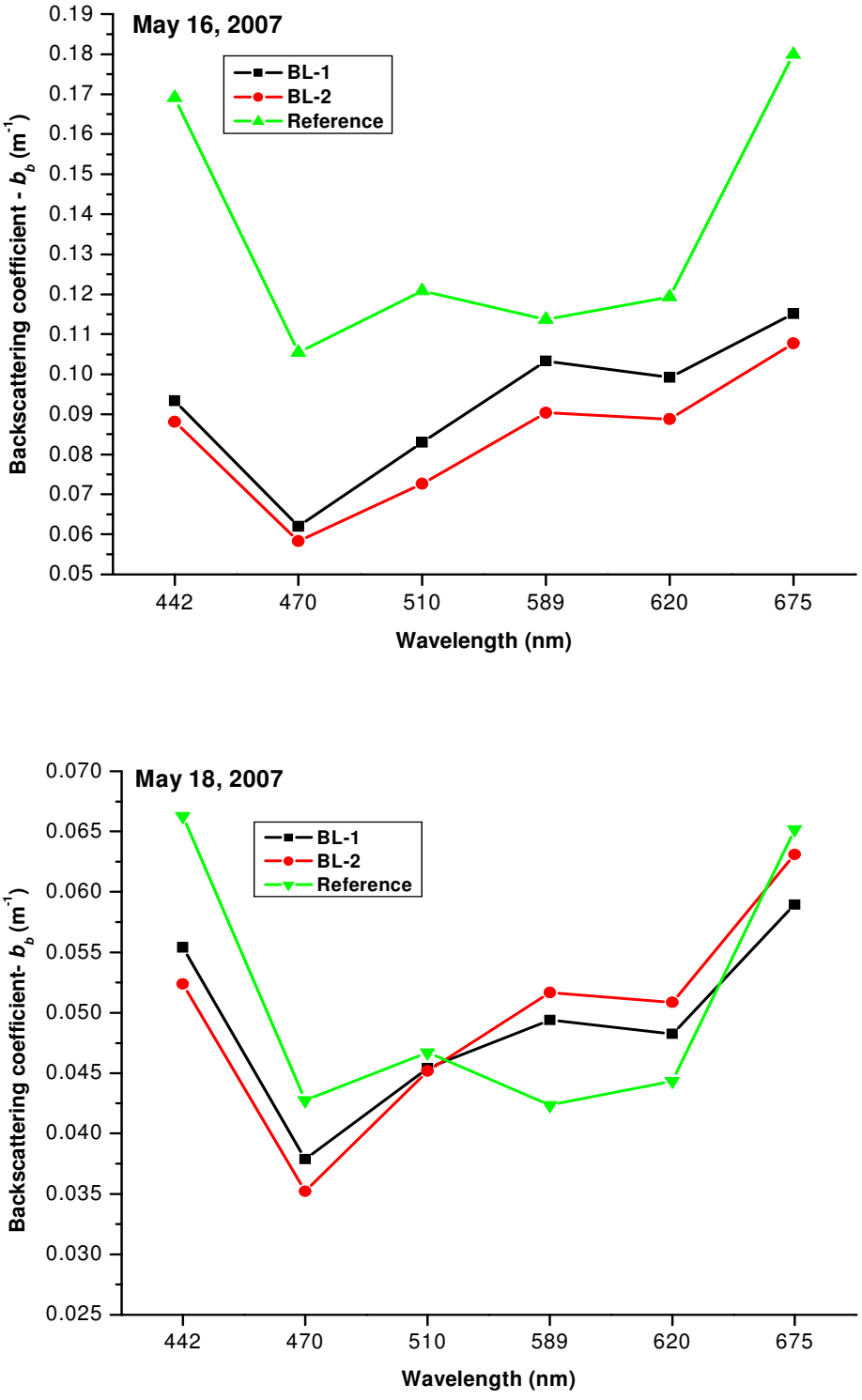

Figure 35. Spectral backscattering coefficients [$b_b(\lambda)$] measured with the HS6 at the *C. polykrikoides* bloom and reference stations. Values represent the median of the measurements recorded during periods of five minutes after removal of noisy data and the baseline correction.

measured at the bloom stations during the second sampling were, in general, lower than those of the first sampling, independently of *C. polykrikoides* abundance, most likely because of the great variability encountered within the blooms of this species (due to its clumping tendency). Maximum values for the reference station were observed at 442 and 675 nm, and minimum values at 470 and 589 nm. The *C. polykrikoides* bloom stations exhibited higher backscattering values in the shorter blue and from yellow to red wavelengths, with maxima at 442, 589 and 675 nm and a pronounced minimum at 470 nm. The main difference in the spectral shape of backscattering between these two areas consisted in the occurrence of proportionately higher values in the yellow and yellow-orange spectral regions (relative to the other wavelengths) for the bloom of *C. polykrikoides*, which seem to explain the bright brownish-red discoloration typically associated with the blooms of this species.

2.3.3.3 Quantitative analysis of $R_{rs}(\lambda)$ data

In order to explore whether it is possible to quantify blooms of *C. polykrikoides* from *in situ* hyperspectral R_{rs} data, different techniques and/or algorithms (listed in Table 11) were tested on a set of ten bloom spectra, and on their corresponding second-derivatives, collected in Bahía Fosforescente during the study period. Criteria for the selection of the bloom spectra included that *C. polykrikoides* was the absolute dominant species and that the spectra were measured under clear sky conditions. A significant relationship ($r^2 = 0.71$; $p = 0.002$) between *C. polykrikoides* cell abundance and chlorophyll *a* concentration was obtained for the bloom episodes chosen (Figure 36), thus suggesting the potential of remote sensing chlorophyll-based algorithms for estimations of *C. polykrikoides* cell abundance (both Case1 and Case 2 waters algorithms were tested).

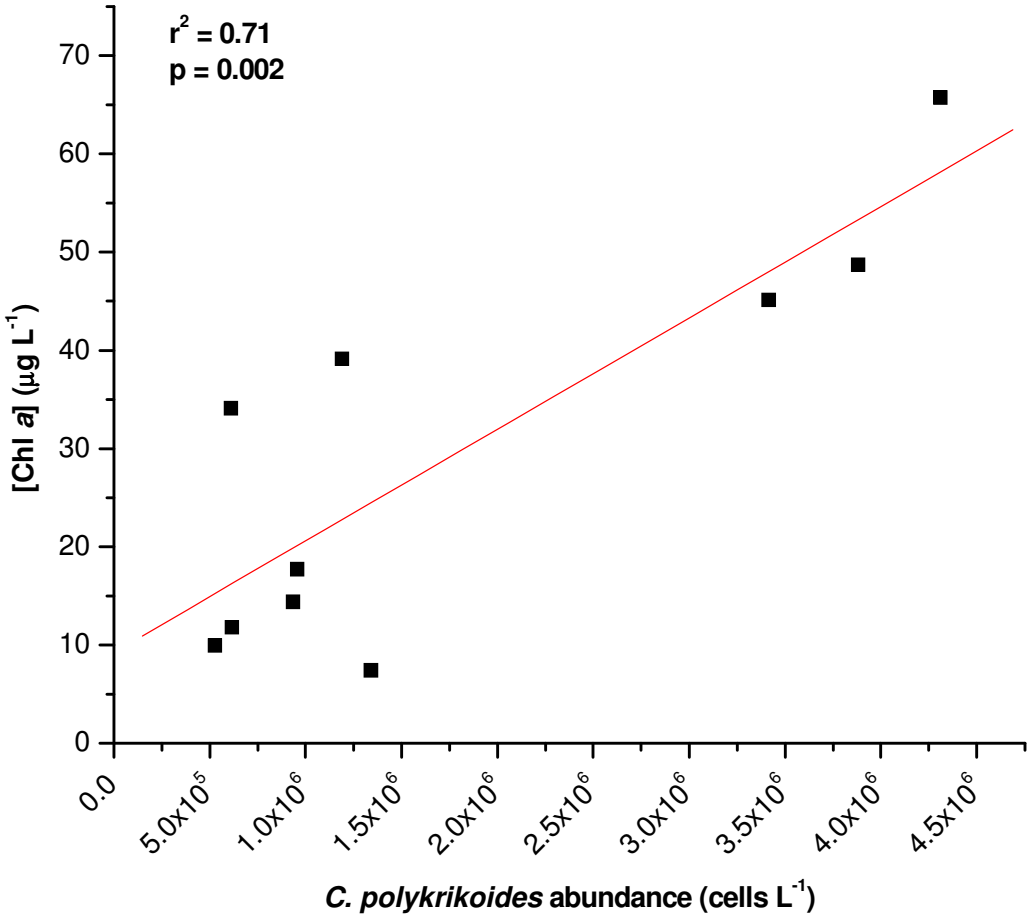

Figure 36. Relationship between *C. polykrikoides* cell abundance and chlorophyll *a* concentration corresponding to the data set used for the quantitative analysis for estimations of *C. polykrikoides* abundance based on *in situ* hyperspectral R_{rs} data.

Traditional R_{rs} (λ) blue to green ratios showed no relationship (i.e. 443/555) or relatively weak relationships (i.e. 490/555 and 510/555) with *C. polykrikoides* cell abundance (Table 11). In contrast, other two-band ratios involving the green and red/NIR spectral regions such as R_{rs}~700/R_{rs}~670, R_{rs}709/ R_{rs}510, R_{rs}670/ R_{rs}555 and R_{rs}~670/ R_{rs}~570 were strongly related to *C. polykrikoides* cell abundance (Figure 37, Table 11). Second-order, non-linear equations (polynomial fit) best described these relationships. Another algorithm that revealed a strong relationship with cell abundance involved the calculation of the depth of the red trough feature at ~670 nm, below a reference line between ~650 and ~750 nm, normalized as a ratio with the average of R_{rs} (λ) values for 440 and 550 nm (Figure 37, Table 11). Once again, a second-order, non-linear equation best described this relationship. Interestingly, the NIR peak magnitude (calculated as the height at ~700 nm, above a baseline between ~670 and ~750 nm) exhibited no relationship with cell abundance, despite being directly attributed to cell scattering processes. Likewise, none of the algorithms applied to the second-derivatives data showed significant relationships with *C. polykrikoides* cell abundance.

Table 11. A comparison of the relationships between various semi-empirical algorithms and *C. polykrikoides* cell abundance for the R_{rs} (λ) data set (n = 10) collected in Bahía Fosforescente during blooms of *C. polykrikoides* from July 2002 to May 2007. Algorithms in bold showed best relationships. [1] Algorithm taken from Schalles (2008). [2] Algorithm taken from Lubac et al. (2005).

Algorithm	Equation	r^2; significant (s)/not significant (ns); p value
R_{rs} spectra data		
NIR peak magnitude [1]	Y = 6E+08x + 20326	r^2 = 0.32; ns
R_{rs}~700/R_{rs}~670 (R_{rs} NIR max/R_{rs} red min) [1]	y = 889848x – 463082 y = 679477x^2 - 2E+06x + 2E+06	r^2 = 0.66; s; p = 0.004 r^2 = 0.87; s; p = 0.001
(ave R_{rs}650+Rrs 700)-R_{rs} 675 [1]	y = 1E+08x + 746763	r^2 = 0.02; ns
((ave R_{rs}650+ R_{rs} 700)- R_{rs} 675)/550 [1]	y = 2E+06x – 617462 y = 6E+06x^2 - 1E+07x + 6E+06	r^2 = 0.48; s; p = 0.03 r^2 = 0.80; s; p = 0.004
((ave R_{rs} 650+ R_{rs} 700)- R_{rs} 675)/(ave R_{rs} 550+ R_{rs} 440) [1]	y = 2E+06x – 359995 y = 5E+06x^2 - 7E+06x + 3E+06	r^2 = 0.53; s; p = 0.02 r^2 = 0.86; s; p = 0.001
R_{rs} 709/ R_{rs} 510 [2]	y = 821308x + 219127 y = 546431x^2 - 919333x + 1E+06	r^2 = 0.67; s; p = 0.004 r^2 = 0.88; s; p = 0.001
R_{rs} 443/ R_{rs} 555	y = -3E+06x + 2E+06	r^2 = 0.20; ns
R_{rs} 490/ R_{rs} 555	y = -4E+06x + 3E+06	r^2 = 0.46; s; p = 0.03
R_{rs} 510/ R_{rs} 555	y = -5E+06x + 4E+06	r^2 = 0.48; s; p = 0.02
R_{rs} 670/ R_{rs} 555 [2]	y = -1E+07x + 6E+06 y = 1E+08x^2 - 9E+07x + 2E+07	r^2 = 0.64; s; p = 0.005 r^2 = 0.88; s; p = 0.001
R_{rs}~670/ R_{rs}~570 (R_{rs} red min/R_{rs} green max)	y = -1E+07x + 5E+06 y = 8E+07x^2 - 7E+07x + 1E+07	r^2 = 0.61; s; p = 0.01 r^2 = 0.86; s; p = 0.001
R_{rs}~700/ R_{rs}~570 (R_{rs} NIR max/R_{rs} green max)	y = 4E+06x - 859128	r^2 = 0.28; ns
Second-derivatives of R_{rs} spectra data		
NIR peak magnitude [1]	y = -3E+10x + 777534	r^2 = 0.04; ns
NIR peak values (~700)	y = -6E+10x + 497727	r^2 = 0.10; ns
~700/~670 (NIR max/red min) [1]	y = -3E+06x - 2E+06	r^2 = 0.19; ns
~670/~570 (red min/green max)	y = 123003x + 1E+06	r^2 = 0.08; ns

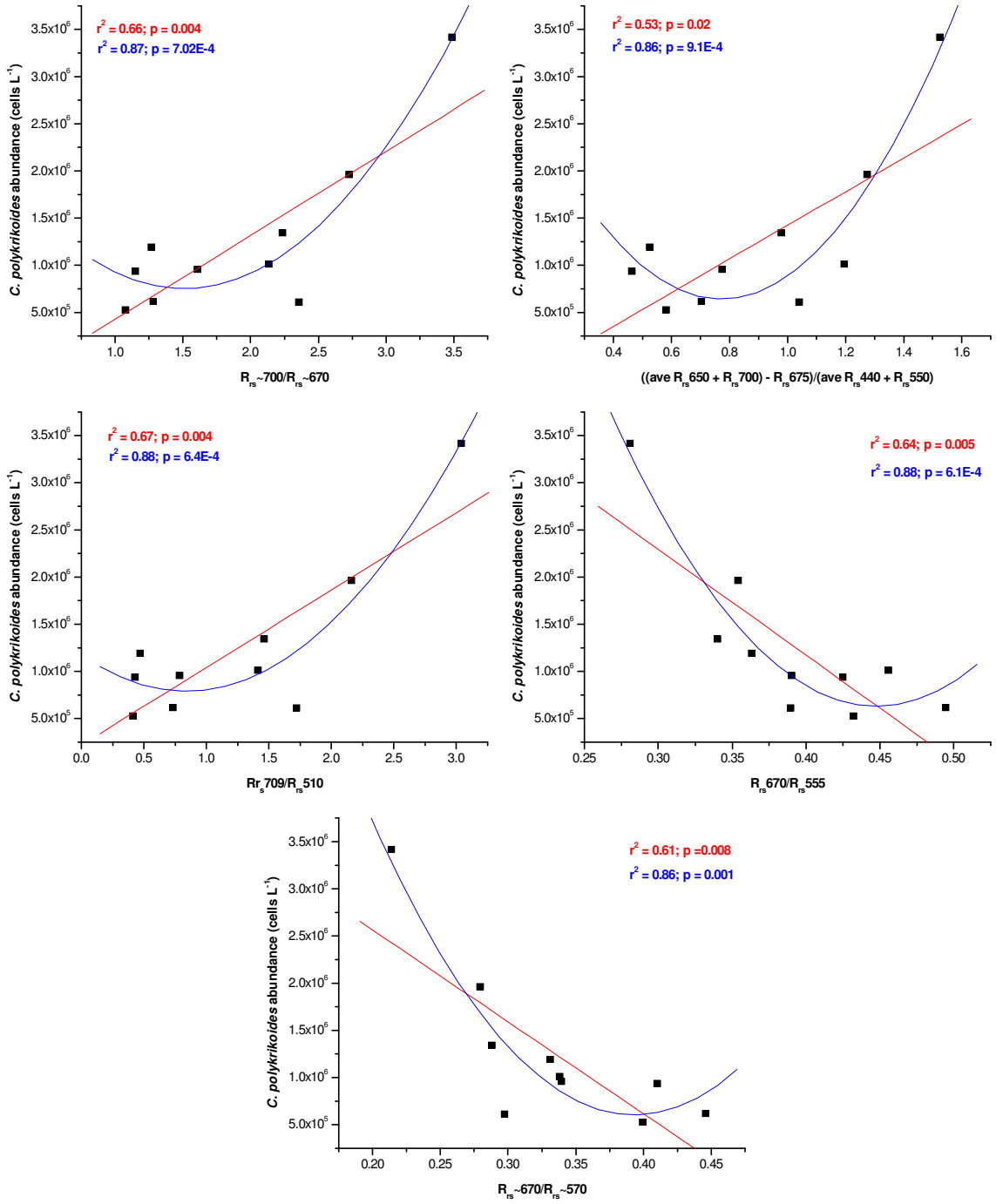

Figure 37. Comparison of algorithms that showed the best relationships for estimations of *C. polykrikoides* cell abundance based on *in situ* hyperspectral R_{rs} data. The red line represents the linear fit of the data and the blue line represents the second-order polynomial fit of the data.

2.4 Discussion

Optical properties of *C. polykrikoides*

The AOP's (R_{rs}) and IOP's (*a*, *c*, *b* and b_b) of the dinoflagellate *C. polykrikoides* were characterized based on pure cultures measurements. These experiments were intended to provide essential information to interpret accurately the variations in ocean color associated with the blooms of this species in natural waters. This information was also fundamental to understand the extent of our capabilities to discriminate and quantify the blooms of this species in Bahía Fosforescente from *in situ* hyperspectral R_{rs} data.

The R_{rs} (λ) spectra of *C. polykrikoides* exhibited the characteristic spectral shape of chlorophyll *c*-containing microalgae, with reduced reflectances along spectral regions of strong pigment absorption, and well-defined green (570 nm) and red/NIR peaks centered in areas of minimum pigment absorption, where backscattering processes prevail. The apparent intensification of these spectral features as a function of increasing cell abundance and chlorophyll *a* clearly demonstrated the influential role of pigment absorption and cell scattering processes in controlling the shape and magnitude of R_{rs} (λ) spectra. Another important observation was the increment in R_{rs} at all wavelengths with an increase in cell abundance and chlorophyll *a*. This trend differs from the conceptual model of microalgae reflectance, based on which it would be expected that an increment in cell density accompanied by increased pigment absorption would result in strongly reduced blue reflectances, whereas scattering would outcompete absorption in the green peak region (and the red/NIR peak region), resulting in increasing R_{rs} (λ) values (Gitelson et al., 1995 and references therein; Schalles, 2008). The observed trend coincides with the findings of Gitelson et al. (1995) for the cyanobacterium

Spirulina platensis and of Gitelson et al. (1999) for the cyanobacterium *Anabaena* sp. and the diatom *Navicula minima* var. *atomoides*, and was presumably related to the remarkably strong scattering caused by the microalgal cells at such high densities, which seemed to be much more effective than absorption in governing the R_{rs} magnitude overall.

An interesting finding was the shift of the green peak towards higher reflectance values relative to the red/NIR peak with increasing cell abundance (and corresponding chlorophyll *a* concentrations). Since both peaks are located in spectral regions of weak or minimum pigment absorption that are limited on both sides either by pigment or water absorption features, they were likely to respond in a similar fashion to an increase in cell density (and chlorophyll *a*). Alternatively, the red/NIR peak would have been expected to reach higher values compared to the green peak (the opposite of what was observed), given the strong absorption of peridinin (whose *in vivo* absorption maximum is centered at ~520 nm) which has been reported to suppress significantly the green reflectance peak (Gitelson et al., 1999). These results suggest that the influence of cell backscattering on R_{rs} was increasingly stronger at 570 nm compared to the red/NIR peak, as cell densities incremented.

In order to assess the viability of hyperspectral R_{rs} data for quantitative estimations of *C. polykrikoides* cell abundance, different techniques were tested. The positive correlation found between the magnitude of the red/NIR peak and cell density/chlorophyll *a* strongly implied its potential use as an indicator of cell abundance and/or chlorophyll *a* concentration, as proposed by Gitelson (1992). Likewise, second-derivative analysis of the R_{rs} (λ) spectra proved feasible for quantitative approximations of cell abundance and chlorophyll *a*, based on the values of the derivative features associated with chlorophyll *a* absorption and/or to the red/NIR peak deconvolved by the analysis. The second-derivative analysis also proved effective to resolve

absorption features related to chlorophyll *a*, chlorophyll c_2 and peridinin, but it was unable to separate the highly overlapped absorption signals of most carotenoid pigments.

The light absorption characteristics of phytoplankton are fundamentally determined by their pigment composition. Hence, the spectral shape of the *in vivo* absorption measured for *C. polykrikoides* (which fitted almost perfectly with the extracted pigment absorption spectrum, a_{ph}, measured for this species) mostly obeyed to well known pigment absorption features. For instance, the absorption maxima observed at 440 and 676 nm correspond to the blue and red absorption maxima of chlorophyll *a*, whereas the intermediate absorption values occurring at 488, 510 and 532 nm are indicative of absorption by accessory pigments, particularly carotenoids, whose absorption range is centered in the blue-green spectral region. In contrast, the lower absorption values found at 555 and 650 nm, and at 715 nm coincide with spectral regions characterized by weak or undetectable pigment absorption. The maximum observed at 412 nm, on the other hand, is primarily explained by the high CDOM content in the cultures (mainly resulting from the metabolism and decomposition of *C. polykrikoides* cells), although it may also indicate the presence of phaeopigments (chlorophyll *a* degradation products) which exhibit maximum absorption around 410 nm (Jeffrey et al., 1997; Astoreca et al., 2005). An increase in cell abundance (and pigment content) produced, as expected, a noticeable increment in pigment absorption at all visible wavelengths that was consistent with the trend observed in the R_{rs} (λ) curves (i.e. the intensification of the spectral features directly related to pigment absorption, as cell density increased).

Because light attenuation results from the combined contributions of absorption and scattering processes, the observed trend of increasing light attenuation towards the shorter wavelengths was the outcome of the interaction between the strong pigment and CDOM

absorption in the blue wavelengths and the particular scattering properties of *C. polykrikoides*, which were also found to be inversely proportional to wavelength within the visible spectral region. (Scattering values at 715 nm were higher than the minimum values at the visible wavelengths, because chlorophyll *a* absorption decreases sharply beyond 700 nm and cell scattering prevails in this spectral region.) However, by comparing the magnitude of the absorption, attenuation and scattering coefficient values, it was evident that cell scattering contributed significantly more (from ~5 to 25 times more depending on wavelength) to the attenuation of light than pigment absorption. The spectral shape of scattering was in partial conformity with the anomalous dispersion theory, which predicts that variations in scattering will occur within spectral regions with sharp variations in absorption like, for example, on the limits of absorption peaks (Vaillancourt et al., 2004 and references therein). These theoretical predictions (i.e. the occurrence of scattering depressions within the strong blue and red pigment absorption peaks) have been previously shown in scattering spectra measured for culture samples of various harmful algal species (Mc-Leroy Etheridge and Roesler, 1998) and in spectral scattering simulations of different phytoplankton species based on reverse IOP modeling methods (Stramski et al., 2001). In the particular case of *C. polykrikoides*, however, even though the blue and red (440 and 676 nm, respectively) scattering depressions were apparent, scattering values along the blue-green and green spectral regions (488, 510, 532 and 555 nm) were much lower than at 440 nm, thus diverging from the expected theoretical spectral pattern. Although there is no precise explanation for this scattering pattern, it could be related to the copious secretions of mucopolysaccharides substances associated with high concentrations of *C. polykrikoides* cells, which may influence the scattering properties of this species. The enhancement in light attenuation and scattering that resulted from an increase in cell abundance

was predictable, on account of their strong absorption and scattering properties. More importantly, the substantially higher scattering values consistently observed at all wavelengths relative to the absorption values (independently of cell abundance) were in full agreement with the observed increment in magnitude of the R_{rs} (λ) spectra with an increase in cell abundance.

Backscattering coefficient values represented a small fraction (~2%, based on the matching wavelengths between the HS6 and the ac-9, i.e. 440/442, 510 and 675/676 nm) of the total scattering, as expected from theory (Boss et al., 2004). *Cochlodinium polykrikoides* is an ineffective backscatterer because it is large compared to the wavelengths of light and has a low refractive index relative to water. Even though the refraction index of *C. polykrikoides* was not determined during this study, it is well known that phytoplankton species lacking a hard mineral exoskeleton normally have refraction indices around 1.04-1.05 (Stramski et al., 2004). In spectral terms, the effect of absorption on backscattering was evident (as predicted from the theory of anomalous scattering), with minima occurring at 470 and 670 nm, regions of strong pigment absorption. Nevertheless, similar to the scattering curves, the blue backscattering minimum did not take place at 440 nm where the blue pigment absorption maximum typically occurs. Backscattering is strongly related to the size, shape, refraction index, growth phase and internal structure of the cells (Mc-Leroy Etheridge and Roesler, 1998; Boss et al., 2004; Stramski et al., 2004). Therefore, the spectral pattern of backscattering of *C. polykrikoides* is a complex function of the intricate influences of pigment absorption, the specific properties of this species cells and the mucopolysaccharide secretions in which these cells are usually embedded. These results are supported by Ahn et al. (1992) and Stramski et al. (2001), which demonstrated that phytoplankton species with different cellular properties exhibit dissimilar backscattering spectral shapes, with more or less pronounced features within the major absorbing bands of pigments.

The strong backscattering signals exhibited by *C. polykrikoides* at 589 and 620 nm are mostly responsible for the brownish-red discolorations typically associated with the blooms of this species. As *C. polykrikoides* cell concentrations increase, more blue/green light is absorbed and more yellow/red light is backscattered out of the water. Therefore, red color receptors in the human eye are preferentially stimulated over the blue and green receptors, thus resulting in perceivably brownish-red waters (Dierssen et al., 2006). The noticeable increment in backscattering observed at all wavelengths with increasing cell abundance, clearly explains the overall increment in reflectance magnitude that resulted from an increase in cell abundance.

This study makes an important contribution to the scarce available information regarding the optical properties of *C. polykrikoides*. However, it is most certainly not without limitations. During these experiments, a limited range of chlorophyll *a* concentrations and cell abundances were attained, due to difficulties associated with culturing *C. polykrikoides*. This species was extremely difficult to grow in the laboratory to high cell densities. It would be necessary to evaluate a much wider range of cell abundances and corresponding chlorophyll *a* concentrations, in order to gain a better idea on how the optical properties presented here vary at such extremely high cell abundances and chlorophyll *a* concentrations typically found during natural blooms of *C. polykrikoides*. Additionally, potential changes in the optical properties associated with variations in the physiological status of the cells must be evaluated. Previous research has demonstrated substantial variations in the absorption and scattering properties of harmful algae, at different light regimes and growth phases (Johnsen and Sakshaug, 1993; Mc-Leroy Etheridge and Roesler, 1998).

The use of a small container in mesocosm experiments to measure the optical properties of *C. polykrikoides*

This study demonstrates the use of a ~100 L mesocosm tank to characterize the optical properties of monospecific microalgal cultures in the laboratory and outdoors. Previous studies with similar aims (e.g. Gitelson et al., 1995; Rundquist et al., 1995; Gitelson et al., 1999) have used, preferentially, tanks or containers of considerably larger dimensions in order to reduce as much as possible spurious sidewall and bottom signals that may contaminate the optical measurements (i.e. to achieve optically deep-water conditions). Black-colored tank interiors have been also commonly used for these purposes (Rundquist et al., 1995; Gitelson et al., 1999; Vaillancourt et al., 2004), since the reflectance of black surfaces is minimal, particularly if they are flat-black. In this study, however, the use of a container of large dimensions was not a viable option because of the limited culture volumes available. The densest and brightest cultures of *C. polykrikoides*, as needed for the optical measurements, were attained when grown to 1 L volumes in Fernbach flasks. Higher volume cultures were simply unattainable, as this species was extremely sensitive to aeration.

The obtained results indicate that, despite its small size, the contribution of the tank's sidewalls and bottom to the optical measurements was minimal. Several characteristics of the set-up used to perform the optical measurements compensated for the reduced dimensions of the tank, making it appropriate for this study. They were: the flat-black painted interior, the 45º angle bottom used for the $R_{rs}(\lambda)$ measurements (which helped reduce spurious bottom contribution by deflecting any bottom signals at right angles, or away, from the look angle of the spectroradiometer sensor) and the mechanical pump-driven system that kept the cells homogenously distributed in the water column. Other precautions taken specifically during the

backscattering measurements, such as to cover the set-up with black fabric (to prevent extraneous light from entering the cylinder) and to determine the depth where the backscattering contribution from the bottom was minimal prior to taking the measurements, contributed enormously to minimize potential contamination of the optical data from external and internal sources.

Feasibility of hyperspectral R_{rs} data for the discrimination and quantification of *C. polykrikoides* blooms in Bahía Fosforescente

The R_{rs} (λ) spectra measured in Bahía Fosforescente between May 2002 and July 2003, and during May 2007, revealed the same general spectral pattern indicative of coastal waters with a high content of pigments, CDOM, detritus and sediments. Differences among the spectra mainly consisted of variations in the magnitude of the curves and of the spectral features and were very much less related to spectral shape. These differences responded primarily to variations in the relative concentrations of the various optically active seawater constituents. In fact, the most dramatic deviations were observed in spectra corresponding to high concentrations or blooms of dinoflagellates, which were characterized by strongly suppressed reflectances along the blue spectral region and a conspicuous red/NIR peak near 700 nm. This clearly indicates that the occurrence of microalgal blooms in Bahía Fosforescente can be detected from hyperspectral R_{rs} measurements.

A comparison among R_{rs} (λ) spectra representative of blooms of *C. polykrikoides*, *A. sanguinea* and *C. furca* var. *hircus-P. bahamense* with similar chlorophyll *a* concentrations, demonstrated strong similarities between them, particularly between those of *C. polykrikoides* and *A. sanguinea*. Indeed, the blooms of these two species were extremely difficult to discern

visually, as they imparted the seawater the same brownish-red discoloration (plus occurred in the same area). This suggested similar optical properties between these species. Unfortunately, it could not be confirmed because the IOP's of *A. sanguinea* were not measured during this study. Nevertheless, certain assumptions can be made based on theory and previous research. Given that dinoflagellates have, in general, the same pigment composition, their spectral absorption signatures are practically identical, even in the few species with unique pigments (Millie et al., 1997). Therefore, it is safe to assume that the absorption properties of *C. polykrikoides* and *A. sanguinea* should vary little. This was, to some extent, demonstrated in the second-derivatives of the R_{rs} (λ) spectra, seeing as the analysis resolved basically the same absorption features for the two species. Their backscattering properties are also likely to be similar, since they are both unarmored (athecate) species, with oval-like shapes and comparable effective sizes. Even though the cells of *A. sanguinea* may be about two times larger (40-80 µm) than those of *C. polykrikoides* (30-40 µm) individually (Steidinger and Tangen, 1997), *C. polykrikoides* was mostly observed forming chains of 2 or 4 cells, where cells were usually much smaller or compressed than the individual ones (proportionally to the number of cells in the chain), making its effective size closer to that of *A. sanguinea*. Based on these assumptions and on their measured R_{rs} (λ) spectra, it is hypothesized that it would be very unlikely to differentiate optically the blooms of *C. polykrikoides* from the ones of *A. sanguinea*, or of any other dinoflagellate species with such similar cellular characteristics.

Differences between the R_{rs} (λ) spectra of *C. furca* var. *hircus-P. bahamense* and *C. polykrikoides* blooms were, on the other hand, more defined and consistent with the seawater colors perceived during their occurrence, which for the former bloom was somewhat greenish-brown. These differences were partly due to the comparatively lower CDOM and sediment

content typically associated with the area where the *C. furca* var. *hircus-P. bahamense* bloom occurred. But, because of the exceedingly high cell concentrations of both species observed (which should have dominated the optical signals), they were probably mainly attributable to species-specific optical properties. Since no significant differences in the absorption properties of *C. polykrikoides* and these two species are expected, nor were suggested from the derivative analysis, differences in their backscattering signals may be invoked. *Ceratium furca* var. *hircus* and *P. bahamense* are both armored (thecate) species with different shapes and sizes compared to *C. polykrikoides*. *Ceratium furca* var. *hircus* has an elongated body that varies from 128 to 149 µm in length, while *P. bahamense* is round in shape with a prominent antapical spine and ranges from 40 to 50 µm in size (Hernández-Becerril and Navarro, 1996; Badylak et al., 2004). Thus, differences in their backscattering properties are likely, especially for *C. furca* var. *hircus* given its much larger size and rather different shape. Although the abundance of *C. furca* var. *hircus* and *P. bahamense* cells during this bloom was not determined, qualitative analyses of water samples collected concurrently with the optical measurements indicated that *C. furca* var. *hircus* was, by far, the most abundant species. This was supported by the work of Soler (2006), who reported *C. furca* var. *hircus* and *P. bahamense* cell abundances of 830,199 and 303,053 cells L^{-1}, respectively, for that same station and week. Therefore, these two blooms must have had, in all probability, different scattering and backscattering properties such as to explain the observed differences between their $R_{rs}(\lambda)$ spectra.

Certainly, noticeable differences were apparent between the scattering and backscattering properties measured within the extent of a dense bloom of *C. polykrikoides* and in the center of the bay (the same area where the *C. furca* var. *hircus-P. bahamense* bloom occurred) during the two special samplings of May 2007. Although no blooms of *C. furca* var. *hircus* and *P.*

bahamense were found there in this occasion, a few *Ceratium* species (mainly *C. furca* var. *hircus*) and *P. bahamense* dominated the dinoflagellate community, especially during the first sampling when significant concentrations of *Ceratium* cells were observed. Consequently, these optical measurements are representative, to a large extent, of a phytoplankton community predominantly conformed by *C. furca* var. *hircus* and *P. bahamense*, comparable to that observed during the blooms of these two species. Backscattering coefficients exhibited substantial differences within the spectral range of 470-620 nm, where the bloom of *C. polykrikoides* presented a positive spectral slope (i.e. higher values towards the yellow-orange wavelengths), whereas the center of the bay showed a more flattened slope with slightly higher values in the green region. These dissimilarities in backscattering properties are in agreement and may, in fact, explain (that is, assuming that *C. furca* var. *hircus* and *P. bahamense* had truly influenced significantly the backscattering measurements) the observed differences between the R_{rs} (λ) spectra of the blooms of *C. polykrikoides* and *C. furca* var. *hircus-P. bahamense*, and the discolorations they impart to the seawater. Apparently, just like the backscattering properties of *C. polykrikoides* blooms induce a preferential stimulation of red color receptors in the human eye that makes us perceive the seawater brownish-red in color, the backscattering properties of *C. furca* var. *hircus-P. bahamense* blooms tend to stimulate equally the green and red light receptors (because of their flat backscattering signals along those wavelengths), and are thus perceived greenish-brown (Dierssen et al., 2006). The higher backscattering coefficient values observed at 675 nm for both areas, primarily due to the high concentration of suspended sediments (ISS) in these waters, had little impact in the perceived seawater color, as the human eye red color receptors are only slightly sensitive to wavelengths greater than 650 nm (Dierssen et al., 2006). Likewise, the strong backscattering signals at 442 nm, most likely due to seawater

and species-specific backscattering properties, had a minor impact in the seawater color because of the predominant influence of pigment (and CDOM) absorption in that spectral region during high cell accumulations. Therefore, the differentiation of the blooms of *C. polykrikoides* from the ones of *C. furca* var. *hircus* and *P. bahamense* (or any other bloom-forming dinoflagellate species exhibiting substantially different cellular characteristics compared to *C. polykrikoides*) in Bahía Fosforescente, based on *in situ* hyperspectral R_{rs} measurements, seems plausible.

In situ hyperspectral R_{rs} data also proved suitable for quantitative estimations of *C. polykrikoides* cell abundance under bloom conditions, through the application of chlorophyll-based semi-empirical algorithms. An inherent assumption in using these algorithms is that chlorophyll *a* varies in direct proportion with *C. polykrikoides* cell abundance during these blooms, which according to the limited data set available is, for the most part, correct. The algorithms that demonstrated to be more reliable to quantify *C. polykrikoides* in these Case 2 waters were those based on the chlorophyll *a* red absorption feature, the green peak and/or the red/NIR peak, given their location in spectral regions of low sensitivity to CDOM and detritus absorption and strong sensitivity to cell scattering (in the case of the green and red/NIR peaks). A remarkable exception was the magnitude of the red/NIR peak which showed a poor relationship with *C. polykrikoides* cell abundance, contrary to the tendency observed in the culture additions experiment and despite the fact that it is strongly influenced by cell scattering processes. This was presumably related to a combination of factors associated with the complex and variable optical nature of these waters including: the great variability that characterizes the blooms of this species as imposed by their highly patchy nature, the contribution of other phytoplankton cells to cell scattering in the red/NIR spectral region, variations in the concentration of ISS which have also been reported to play an important role in the magnitude of

this peak (Schalles, 2008 and references therein), and the variable illumination conditions encountered throughout the samplings. The poor potential exhibited by the second-derivatives of the R_{rs} (λ) spectra to quantify these blooms (as opposed to what the pure cultures data suggested) may have also been related to these same factors, since the magnitude of the derivative peaks and troughs corresponding to the spectral features in which these algorithms are based, did not necessarily correspond to chlorophyll *a* concentration or *C. polykrikoides* cell density. Instead, they were more related to the rate of change in spectral slope of these features in the original R_{rs} (λ) curves, which was affected by these factors in the first place.

More studies are still needed before it can be concluded with certainty if *C. polykrikoides* blooms can or cannot be optically differentiated from those of other bloom-forming dinoflagellate species in Bahía Fosforescente and to determine the most appropriate algorithm for their quantification. Future research must include an extensive data set consisting of simultaneous measurements of AOP's and IOP's, together with a quantitative assessment of the different optically active seawater constituents during the occurrence of blooms of *C. polykrikoides* and of the other few bloom-forming species within this bay. If significant differences are detected between the R_{rs} (λ) spectra of *C. polykrikoides* blooms and those of other species that can be irrefutably attributed to species-specific IOP's, then the development of an algorithm to discriminate *C. polykrikoides* blooms from R_{rs} (λ) data should be relatively straightforward. If, on the contrary, the AOP's and IOP's of a particular bloom-forming species and those of *C. polykrikoides* are so similar that their blooms are impossible to tell apart (as is probably the case for *A. sanguinea*), then a discrimination method based on optical measurements would be very unlikely. Nevertheless, even in those cases the use of hyperspectral R_{rs} data could be very useful. For instance, given that *C. polykrikoides* is known to

be the most common bloom-forming species in the western-most inlet of the bay, the observation of a reddish water discoloration in this particular area, accompanied by a R_{rs} (λ) spectrum revealing typical high-chlorophyll spectral features, should be sufficient to suspect a bloom of this dinoflagellate. Then, if microscopic cell examinations confirm *C. polykrikoides* as the responsible species, R_{rs} (λ) data could be used to follow the progress of the bloom by means of a quantitative algorithm.

2.5 Conclusions

- This study provides the first comprehensive characterization of the optical properties of the dinoflagellate *Cochlodinium polykrikoides*. The apparent and inherent optical properties of this organism were determined based on pure culture measurements.

- The intensification of R_{rs} spectral features, as a function of increasing *C. polykrikoides* abundance and pigment concentration, clearly demonstrated the influential role of pigment absorption and cell scattering processes in controlling the shape and magnitude of R_{rs} (λ) spectra.

- *Cochlodinium polykrikoides* exhibited the typical pigment profile and absorption characteristics of the majority of dinoflagellates. This confirms, as expected, that the exclusive use of spectral absorption properties could not be used to discriminate this organism.

- The strong backscattering signals exhibited by *C. polykrikoides* at 589 and 620 nm accounts for the striking brownish-red discoloration associated with the blooms of this species.

- The results of the optical experiments for determinations of the inherent and apparent optical properties proved that the mesocosm tank set-up used was adequate for these purposes.

- Second-derivatives of the R_{rs} (λ) spectra proved feasible for quantitative approximations of *C. polykrikoides* abundance under pure culture conditions, but not under natural bloom conditions.

- The R_{rs} (λ) spectra collected at Bahía Fosforescente throughout the study period shared the same general spectral pattern characteristic of optically complex coastal waters. However, substantial deviations in the spectra corresponding to dense accumulations or blooms of dinoflagellates clearly indicated that the occurrence of these blooms in Bahía Fosforescente can be detected from hyperspectral R_{rs} data.

- Based on the measured R_{rs} (λ) spectra, it would be unlikely to differentiate optically the blooms of *C. polykrikoides* from those of *A. sanguinea* or of any other dinoflagellate species with such similar cellular characteristics.

- The differentiation of the blooms of *C. polykrikoides* from those of *C. furca var. hircus-P. bahamense* (or any other bloom-forming dinoflagellate species exhibiting substantially different cellular characteristics) in Bahía Fosforescente, based on *in situ* hyperspectral R_{rs} measurements, seems plausible.

- *In situ* hyperspectral R_{rs} data also proved suitable for quantitative estimations of *C. polykrikoides* abundance under bloom conditions, through the application of chlorophyll-based semi-empirical algorithms.

Literature Cited

Aguirre-Gomez, R., A. R. Weeks and S. R. Boxall. 2001. The identification of phytoplankton pigments from absorption spectra. Int. J. Remote Sensing. 22(2&3): 315-338.

Ahn, Y. H., A. Bricaud and A. Morel. 1992. Light backscattering efficiency and related properties of some phytoplankters. Deep-Sea Res. 39(11/12): 1835-1855.

Ahn, Y. H. and P. Shanmugam. 2006. Detecting the red tide algal blooms from satellite ocean color observations in optically complex Northeast-Asia coastal waters. Remote Sens. Environ. 103: 419-437.

Ahn, Y. H., P. Shanmugam, J. H. Ryu and J. C. Jeong. 2006. Satellite detection of harmful algal bloom occurrences in Korean waters. Harmful Algae. 5(2): 213-231.

Alvain, S., C. Moulin, Y. Dandonneau and F. M. Bréon. 2005. Remote sensing of phytoplankton groups in case 1 waters from global Sea WiFS imagery. Deep-Sea Res. I. 52(11): 1989-2004.

Anderson, D. M. 1994. Red Tides. Scientific American. 271: 52-58.

Anderson, D. M. 1995. Toxic red tides and harmful algal blooms: A practical challenge in coastal oceanography. Rev. Geophys. 33 (suppl.): 1189-1200.

Anderson, D. M. and D. Wall. 1978. Potential importance of benthic cysts of *Gonyaulax tamarensis* and *G. excavata* in initiating toxic dinoflagellate blooms. J. Phycol. 14: 224-234.

Anton, A., P. L. Teoh, S. R. Mohd-Shaleh and N. Mohammad-Noor. 2008. First occurrence of *Cochlodinium* blooms in Sabah, Malaysia. Harmful Algae. 7: 331-336.

Astoreca, R., V. Rousseau, K. Ruddick, B. Van Mol, J. Y. Parent and C. Lancelot. 2005. Optical properties of algal blooms in an eutrophicated coastal area and its relevance to remote sensing, 5885: 245-255. *In* R. J. Frouin, M. Babin, S. Sathyendranath [eds.], Remote sensing of the coastal oceanic environment. Proc. SPIE.

Azanza, R. V., L. T. David, R. T. Borja, I. U. Baula and Y. Fukuyo. 2008. An extensive *Cochlodinium* bloom along the western coast of Palawan, Phillipines. Harmful Algae. 7: 324-330.

Badylak, S., K. Kelley and E. J. Phlips. 2004. A description of *Pyrodinium bahamense* (Dinophyceae) from the Indian River Lagoon, Florida, USA. Phycologia. 43(6): 653-657.

Bidigare, R. R., J. H. Morrow and D. A. Kiefer. 1988. Derivative analysis of spectral absorption by phytoplankton pigments. SPIE Ocean Optics IX. 925: 101-104.

Bidigare, R. R. 1989. Derivative analysis of spectral absorption by photosynthetic pigments in the western Sargasso Sea. J. Mar. Res. 47: 323-341.

Bidigare, R. R., M. E. Ondrusek, J. H. Morrow and D. A. Kiefer. 1990. *In vivo* absorption properties of algal pigments. SPIE Ocean Optics X. 1302: 290-302.

Boss, E., D. Stramski, T. Bergmann, W. S. Pegau and M. Lewis. 2004. Why should we measure the optical backscattering coefficient? Oceanography. 17(2): 44-49.

Braman, R. S. and S. A. Hendrix. 1989. Nanogram nitrite and nitrate determination in environmental and biological materials by Vanadium [III] reduction with chemiluminescence detection. Anal. Chem. 61: 2715-2718.

Burkholder, P. R. and L. M. Burkholder. 1958. Studies on B vitamins in relation to productivity of the Bahía Fosforescente, Puerto Rico. Bull. Mar. Sci. Gulf & Carib. 8(3): 201-223.

Burkholder, P. R., L. M. Burkholder and L. R. Almodovar. 1967. Carbon assimilation of marine flagellate blooms in neritic waters of southern Puerto Rico. Bull. Mar. Sci. 17(1): 1-15.

Butler, W. L. and D. W. Hopkins. 1970. Higher derivative analysis of complex absorption spectra. Photochem. Photobiol. 12: 439-450.

Cannizzaro, J. 2004. Detection and quantification of *Karenia brevis* blooms on the West Florida shelf from remotely sensed ocean color imagery. MS thesis. University of South Florida, St. Petersburg, FL. 71 p.

Cintrón, G. 1969. Seasonal fluctuations in a tropical bay. MS thesis. University of Puerto Rico, Mayagüez. 53p.

Cintrón, G., W. S. Maddux and P. R. Burkholder. 1970. Some consequences of brine pollution in the Bahía Fosforescente, Puerto Rico. Limnol. Oceanogr. 15(2): 246-249.

Coker, R. E. and J. G. González. 1960. Limnetic copepod populations of Bahía Fosforescente and adjacent waters, Puerto Rico. J. Elisha Mitchell Scient. Soc. 76: 8-28.

Craig, S. E., S. E. Lohrenz, Z. Lee, K. L. Mahoney, G. J. Kirkpatrick, O. M. Schofield and R. G. Steward. 2006. Use of hyperspectral remote sensing reflectance for detection and assessment of the harmful alga, *Karenia brevis*. Appl. Opt. 45(21): 5414-5425.

Cullen, J. J., A. M. Ciotti, R. F. Davis and M. R. Lewis. 1997. Optical detection and assessment of algal blooms. Limnol. Oceanogr. 42(5, part 2): 1223-1239.

Curtiss, C. C., G. W. Langlois, L. B. Busse, F. Mazzillo and M. W. Silver. 2008. The emergence of *Cochlodinium* along the California Coast (USA). Harmful Algae. 7: 337-346.

Del Castillo, C. E., P. G. Coble, J. M. Morell, J. M. López and J. E. Corredor. 1999. Analysis of the optical properties of the Orinoco River plume by absorption and fluorescence spectroscopy. Mar. Chem. 66: 35-51.

Demetriades-Shah, T. H., M. D. Steven and J. A. Clark. 1990. High resolution derivative spectra in remote sensing. Remote Sens. Environ. 33: 55-64.

Dierssen, H. M., R. M. Kudela, J. P. Ryan and R. C. Zimmerman. 2006. Red and black tides: quantitative analysis of water-leaving radiance and perceived color for phytoplankton, color dissolved organic matter, and suspended sediments. Limnol. Oceanogr. 51(6): 2646-2659.

Du, Q., D., Y. Huang and X. Wang. 1993. Toxic dinoflagellate red tide by a *Cochlodinium* sp. along the coast of Fujian, China, p. 235-238. *In* T.J. Smayda and Y. Shimizu [eds.], Toxic phytoplankton blooms in the sea. Proc. 5th Int. Conf. on Toxic Marine Phytoplankton. Elsevier.

Fraga, S., S. M. Gallagher and D. M. Anderson. 1989. Chain-forming dinoflagellates: an adaptation to red tides, p. 281-284. *In* T. Okaichi, D. Anderson, and T. Nemoto [eds.], Red Tides: Biology, Environmental Science and Toxicology. Elsevier, Amsterdam.

Gárate-Lizárraga, I., J. J. Bustillos-Guzmán, L. M. Morquecho and C. H. Lechuga-Deveze. 2000. First outbreak of *Cochlodinium polykrikoides* in the Gulf of California. Harmful Algae News. 21: 7.

Gárate-Lizárraga, I., D. J. López-Cortes, J. J. Bustillos-Guzmán and F. Hernández-Sandoval. 2004. Blooms of *Cochlodinium polykrikoides* (Gymnodiniaceae) in the Gulf of California, Mexico. Rev. Biol. Trop. 52(1): 51-58.

Garver, S. A., D. A. Siegel and B. G. Mitchell. 1994. Variability in near-surface particulate absorption spectra: What can a satellite ocean color imager see? Limnol. Oceangr. 39(6): 1349-1367.

Gitelson, A. 1992. The peak near 700 nm on radiance spectra of algae and water: relationships of its magnitude and position with chlorophyll concentration. Int. J. Remote Sensing. 13(17): 3367-3373.

Gitelson, A., S. Laorawat, G. P. Keydan and A. Vonshak. 1995. Optical properties of dense algal cultures outdoors and their application to remote estimation of biomass and pigment concentration in *Spirulina platensis* (Cyanobacteria). J. Phycol. 31: 828-834.

Gitelson, A., J. F. Schalles, D. C. Rundquist, F. R. Schiebe and Y. Z. Yacobi. 1999. Comparative reflectance properties of algal cultures with manipulated densities. J. Appl. Phycol. 11:345-354.

Gitelson, A., Y. A. Grits, D. Etzion, Z. Ning and A. Richmond. 2000. Optical properties of *Nannochloropsis* sp. and their application to remote estimation of cell mass. Biotechnol. Bioeng. 69(5): 516-525.

Guillard, R. R. L. and P. E. Hargraves. 1993. *Stichochrysis immobilis* is a diatom, not a chrysophyte. Phycologia. 32: 234-236.

Glibert, P. M., D. M. Anderson, P. Gentien, E. Granéli, and K. G. Sellner. 2005. The global, complex phenomena of harmful algal blooms. Oceanography. 18(2): 136-147.

Glynn, P. W. 1973. Ecology of a Caribbean coral reef. The *Porites* reef-flat biotope: Part 1. Meteorology and hydrography. Mar. Biol. 20: 297-318.

Gobler, C. J., D. L. Berry, O. R. Anderson, A. Burson, F. Koch, B. S. Rodgers, L., K. Moore, J. A. Goleski, B. Allam, P. Bowser, Y. Tang and R. Nuzzi. 2008. Characterization, dynamics, and ecological impacts of harmful *Cochlodinium polykrikoides* blooms on eastern Long Island, NY, USA. Harmful Algae. 7: 293-307.

González, J. G. 1965. Primary productivity of the neritic and offshore waters of western Puerto Rico. Final Report. U. S. Office of Naval Research, Contract #NONR-4318(00). 52 p.

Gordon, H. R. 1979. Diffusive reflectance of the ocean: the theory of its augmentation by chlorophyll-*a* fluorescence at 685 nm. Appl. Opt. 18: 1161-1166.

Hallegraeff, G. M. 1993. A review of harmful algal blooms and their apparent global increase. Phycologia. 32: 79-99.

Hannach, G. and A. C. Sigleo. 1998. Photoinduction of UV-absorbing compounds in six species of marine phytoplankton. Mar. Ecol. Prog. Ser. 174: 207-222.

Hernández-Becerril, D. U. and N. Navarro. 1996. Thecate dinoflagellates (Dinophyceae) from Bahía Fosforescente, Puerto Rico. Rev. Biol. Trop. 44(2): 465-475.

Ho, M. S. and P. L. Zubkoff. 1979. The effects of a *Cochlodinium heterolobatum* bloom on the survival and calcium uptake by larvae of the American oyster, *Crassostrea virginica*, p. 409-412. *In* F. J. R. Taylor and H.H. Seliger [eds.], Toxic dinoflagellate blooms. Elsevier, New York.

Hoepffner, N. and S. Sathyendranath. 1991. Effect of pigment composition on absorption properties of phytoplankton. Mar. Ecol. Prog. Ser. 73: 11-23.

Holmes, R. M., A. Aminot, R. Kérouel, B. A. Hooker and B. J. Peterson. 1999. A simple and precise method for measuring ammonium in marine and freshwater ecosystems. Can. J. Aquat. Sci. 56: 1801-1808.

Huguenin, R. L. and J. L. Jones. 1986. Intelligent information extraction from reflectance spectra: absoption band positions. J. Geophys. Res. 91: 9585-9598.

Jeffrey, S. W. and G. F. Humphrey. 1975. New spectrophotometric equations for determining chlorophylls *a*, *b*, c_1 and c_2 in higher plants, algae and natural phytoplankton. Biochem. Physiol. Pflanzen. 167: 191-194.

Jeffrey, S. W., R. F. C. Mantoura and T. Bjørnland. 1997. Data for the identification of 47 key phytoplankton pigments, p.449-559. *In* S. W. Jeffrey, R. F. C. Mantoura and S. W. Wright [eds.], Phytoplankton pigments in oceanography: guidelines to modern methods. Monographs on oceanographic methodology. UNESCO publishing, Paris.

Jeffrey, S. W. and M. Vesk. 1997. Introduction to marine phytoplankton and their pigment signatures, p.37-84. *In* S. W. Jeffrey, R. F. C. Mantoura and S. W. Wright [eds.], Phytoplankton pigments in oceanography: guidelines to modern methods. Monographs on oceanographic methodology. UNESCO publishing, Paris.

Jeong, H. J., Y. D. Yoo, J. S. Kim, T. H. Kim, J. H. Kim, N. S. Kang and W. Yih. 2004. Mixotrophy in the phototrophic harmful alga *Cochlodinium polykrikoides* (Dinophycean): Prey species, the effects of prey concentration, and grazing impact. J. Eukariot. Microbiol. 51(5): 563-569.

Johnsen, G. and E. Sakshaug. 1993. Bio-optical characteristics and photoadaptive responses in the toxic and bloom-forming dinoflagellates *Gyrodinium aureolum*, *Gymnodinium galatheanum*, and two strains of *Prorocentrum minimum*. J. Phycol. 29: 627-642.

Johnsen, G., N. B. Nelson, R. V. M. Jovine and B. B. Prézelin. 1994a. Chromoprotein- and pigment-dependent modeling of spectral light absorption in two dinoflagellates, *Prorocentrum minimum* and *Heterocapsa pygmaea*. Mar. Ecol. Prog. Ser. 114: 245-258.

Johnsen, G., O. Samset, L. Granskog and E. Sakshaug. 1994b. *In vivo* absorption characteristics in 10 classes of bloom-forming phytoplankton: taxonomic characteristics and responses to photoadaptation by means of discriminant and HPLC analysis. Mar. Ecol. Prog. Ser. 105: 149-157.

Jørgensen, B. B. and D. J. Des Marais. 1988. Optical properties of benthic photosynthetic communities: Fiber-optic studies of cyanobacterial mats. Limnol. Oceanogr. 33(1): 99-113.

Kim, H. G. 1998. *Cochlodinium polykrikoides* blooms in Korean coastal waters and their mitigation, p. 227-228. *In* B. Reguera et al. [eds.], Harmful Algae. Proc. 8th Int. Conf. Xunta de Galicia and Interngovernmental Oceanographic Commision of UNESCO.

Kim, C. S., S. G. Lee, C. K. Lee, H. G. Kim and J. Jung. 1999. Reactive oxygen species as causative agents in the ichthyotoxicity of the red tide dinoflagellate *Cochlodinium polykrikoides*. J. Plankton Res. 21(11): 2105-2115.

Kim, C. S., S. G. Lee, C. K. Lee and H. G. Kim. 2000. Biochemical responses of fish exposed to a harmful dinoflagellate *Cochlodinium polykrikoides*. J. Exp. Mar. Biol. Ecol. 254: 131-141.

Kim, C. H., H. J. Cho, J. B. Shin, C. H. Moon and K. Matsuoka. 2002. Regeneration from hyaline cysts of *Cochlodinium polykrikoides* (Gymnodiniales, Dinophyceae), a red tide organism along the Korean coast. Phycologia. 41(6): 667-669.

Kirkpatrick, G. J., D. F. Millie, M. A. Moline and O. Schofield. 2000. Optical discrimination of a phytoplankton species in natural mixed populations. Limnol. Oceanogr. 45(2): 467-471.

Kishino, M., N. Takahashi, N. Okami and S. Ikimura. 1985. Estimation of the spectral absorption coefficients of phytoplankton in the sea. Bull. Mar. Sci. 37: 634-642.

Louchard, E. M., R. P. Reid, C. F. Stephens, C. O. Davis, R. A. Leathers, T. V. Downes and R. Maffione. 2002. Derivative analysis of absorption features in hyperspectral remote sensing data of carbonate sediments. Optics Express. 10(26): 1573-1584.

Lubac, B., H. Loisel, A. Poteau and X. Meriaux. 2005. Challenges to identify phytoplankton species in coastal waters by remote sensing, 5885: 235-244. *In* R. J. Frouin, M. Babin, S. Sathyendranath [eds.], Remote sensing of the coastal oceanic environment. Proc. SPIE.

Maffione, R. A. and D. R. Dana. 1997. Instruments and methods for measuring the backward-scattering coefficient of ocean waters. Appl. Opt. 36(24): 6057-6067.

Margalef, R. and J. G. González. 1958. Densification of phytoplankton in the vicinity of a shallow coast subjected to intense evaporation. Proceedings of the 2nd meeting of the Association of Island Marine Laboratories. 1: 14-15.

Margalef, R. 1961. Hidrografía y fitoplancton de un área marina de la costa meridional de Puerto Rico. Inv. Pesq. 18: 33-96.

Marshall, H. G. 1995. Succession of dinoflagellate blooms in the Chesapeake Bay, USA, p. 615-620. *In* P. Lassus, G. Arzul, E. Erard-Le Denn, P. Gentien and M. Marcillou-Le Baut [eds.], Harmful Marine Algal Blooms. Lavoisier, Paris.

McLeroy-Etheridge, S. L. and C. S. Roesler. 1998. Are the inherent optical properties of phytoplankton responsible for the distinct ocean colors observed during harmful algal blooms? SPIE Ocean Optics XIV. 1: 109-116.

Millie, D. F., G. J. Kirkpatrick and B. T. Vinyard. 1995. Relating photosynthetic pigments and *in vivo* optical density spectra to irradiance for the Florida red-tide dinoflagellate *Gymnodinium breve*. Mar. Ecol. Prog. Ser. 120: 65-75.

Millie, D. F., O. M. Schofield, G. J. Kirkpatrick, G. Johnsen, P. A. Tester and B. T. Vinyard. 1997. Detection of harmful algal blooms using photopigments and absorption signatures: A case study of the Florida red tide dinoflagellate, *Gymnodinium breve*. Limnol. Oceanog. 42(5, part 2): 1240-1251.

Morel, A. 1974. Optical properties of pure water and pure seawater, p. 1-24. *In* N.G. J. E. Steeman-Nielsen [ed.], Optical aspects of oceanography. Academic.

Morel, A. and L. Prieur. 1977. Analysis of variations in ocean color. Limnol. Oceanogr. 22: 709-722.

Nuzzi, R. *Cochlodinium polykrikoides* in the Peconic Estuary. 2004. Harmful Algae News. 27: 10-11

Park, J. G., M. K. Jeong, J. A. Lee, K. J. Cho and O. S. Kwon. 2001. Diurnal vertical migration of *Cochlodinium polykrikoides* (Dinophyceae), during a red tide in coastal waters of Namhae Island, Korea. Phycologia. 40: 292-297.

Pegau, W. S., D. Gray and J. R. V. Zaneveld. 1997. Absorption and attenuation of visible and near-infrared light in water: dependence on temperature and salinity. Appl. Opt. 36(24): 6035-6046.

Pope, R. M. and E. S. Fry. 1997. Absorption spectrum (380-700 nm) of pure water. II. Integrating cavity measurements. Appl. Opt. 36(33): 8710-8723.

Reynolds, C. S. 2006. The ecology of phytoplankton. Cambridge University Press. Cambridge, UK. 535p.

Richardson, L. L. 1996. Remote sensing of algal bloom dynamics. BioScience. 46 (7): 492-501.

Roesler, C. S. 1998. Theoretical and experimental approaches to improve the accuracy of particulate absorption coefficients derived from the quantitative filtering technique. Limnol. Oceanogr. 43: 1649-1660.

Roesler, C. S. and S. L McLeroy-Etheridge. 1998. Remote detection of harmful algal blooms. SPIE Ocean Optics XIV. 1: 117-128.

Roesler, C. S., S. M. Etheridge, and G. C. Pitcher. 2004. Application of an ocean color algal taxa detection model to red tides in the Southern Benguela, p. 303-305. *In* K. A. Steidinger, J. H. Landsberg, C. R. Tomas and G. A. Vargo [eds.], Proceedings of the Xth International Conference on Harmful Algae. Florida Fish and Wildlife Conservation Commission and Intergovernmental Oceanographic Commission of UNESCO.

Rosales-Loessener, F., K. Matsuoka, Y. Fukuyo and E. H. Sanchez. 1996. Cysts of harmful dinoflagellates found from Pacific coastal waters of Guatemala, p. 192-195. *In* G. M. Hallegraeff, C. J. Bolch and R. J. Lewis [eds.], Harmful and Toxic Blooms. IOC UNESCO, Paris.

Rundquist, D. C., J. F. Schalles and J. S. Peake. 1995. The response of volume reflectance to manipulated algal concentrations above bright and dark bottoms at various depths in an experimental pool. Geocarto International. 10(4): 5-14.

San Juan, A. E. and J. G. González. 2000. Distribution of nutrients in the Phosphorescent Bay at La Parguera, on the southwest coast of Puerto Rico. Proceedings of the 51st annual Gulf and Caribbean Fisheries Institute. 1: 451-456.

Sannio, A., A. Luglie and N. Sechi. 1997. Potentially toxic dinoflagellates in Sardinia. Plant Biosyst. 131: 73-78.

Savitzky, A. and M. J. E. Golay. 1964. Smoothing and differentiation of data by simplified least squares procedures. Anal. Chem. 36: 1627-1639.

Schalles, J. F. 2008. Optical remote sensing techniques to estimate phytoplankton chlorophyll *a* concentrations in costal waters with varying suspended matter and CDOM concentrations, p. 27-79. *In* L. L. Richardson and E. F. LeDrew [eds.], Remote sensing of aquatic coastal ecosystem processes. Science and management applications. Springer.

Schofield, O., J. Grzymski, W. P. Bissett, G. J. Kirkpatrick, D. F. Millie, M. Moline and C. S. Roesler. 1999. Optical monitoring and forecasting systems for harmful algal blooms: possibility or pipe dream? 1999. J. Phycol. 35: 1477-1496.

Seixas, C. E. 1983. Algunas variaciones en la dinámica del fitoplancton en dos bahías del suroeste de Puerto Rico. MS thesis. University of Puerto Rico, Mayagüez. 92p.

Seixas, C. E. 1988. Patrones de distribución espacial y sucesión temporal en poblaciones de dinoflagelados de la Bahía Fosforescente, Puerto Rico. Ph.D. thesis. University of Puerto Rico, Mayagüez. 88p.

Seliger, H. H., J. H. Carpenter, M. Loftus, W. H. Biggley and W. D. McElroy. 1971. Bioluminescence and phytoplankton successions in Bahía Fosforescente, Puerto Rico. Limnol. Oceanogr. 16(4): 608-622.

Silva, E. S. 1967. *Cochlodinium heterolobatum* n. sp.: structure and some cytophysiological aspects. J. Protozool. 14: 745-754.

Smayda, T. J. 1970. Growth potential bioassay of water masses using diatom cultures: Phosphorescent Bay (Puerto Rico) and Caribbean waters. Helgoländer wiss. Meeresunters. 20: 172-194.

Smayda, T. J. 1990. Novel and nuisance phytoplankton blooms in the sea: Evidence for a global epidemic, p. 29-40. *In* E. Graneli et al. [eds.], Toxic marine phytoplankton. Elsevier.

Smayda, T. J. 1997. Harmful algal blooms: Their ecophysiology and general relevance to phytoplankton blooms in the sea. Limnol. Oceanogr. 42: 1137-1153.

Smayda, T. J. 2002. Turbulence, watermass stratification and harmful algal blooms: an alternative view and frontal zones as “pelagic seed banks”. Harmful Algae. 1: 95-112.

Soler, B. M. 2006. Comparación temporal y espacial de factores bióticos y abióticos en la Bahía Bioluminiscente en La Parguera y Puerto Mosquito en Vieques. MS thesis. University of Puerto Rico, Mayagüez. 94p.

Stæhr, P. A. and J. J. Cullen. 2003. Detection of *Karenia mikimotoi* by spectral absorption signatures. J. Plankton Res. 25(10): 1237-1249.

Steidinger, K. A. and K. Tangen. 1997. Dinoflagellates, p. 387-584. *In* C. Tomas [ed.], Identifying marine phytoplankton. Academic Press.

Stephens, F. C., E. M. Louchard, R. P. Reid and R. Maffione. 2003. Effects of microalgal communities on reflectance spectra of carbonate sediments in subtidal optically shallow marine environments. Limnol. Oceanogr. 48(1, part 2): 535-546.

Stramski, D., A. Bricaud and A. Morel. 2001. Modeling the inherent optical properties of the ocean based on the detailed composition of the planktonic community. Appl. Opt. 40(18): 2929-2945

Stramski, D. E. Boss, D. Bogucki and K. J. Voss. 2004. The role of seawater constituents in light backscattering in the ocean. Prog. Oceanogr. 61: 27-56.

Strickland, J. D. H. and T. R. Parsons. 1972. (2nd edition) A practical handbook of seawater analysis. Fish. Res. Bd. Canada Bull. 167: 311p.

Stumpf, R. P., M. E. Culver, P. A. Tester, M. Tomlinson, G. J. Kirkpatrick, B. A. Pederson, E. Truby, V. Ransibrahmanakul and M. Soracco. 2003. Monitoring *Karenia brevis* blooms in the Gulf of Mexico using satellite ocean color imagery and other data. Harmful Algae. 2(2): 147-160.

Subramaniam, A. and E. J. Carpenter. 1994. An empirically derived protocol for the detection of blooms of the marine cyanobacterium *Trichodesmium* using CZCS imagery. Int. J. Remote Sensing. 15(8): 1559-1569.

Suh, Y. S., L. H. Jang, N. K. Lee and J. Ishizaka. 2004. Feasibility of red tide detection around Korean waters using satellite remote sensing. J. Fish. Sci. Tech. 7(3): 148−162.

Tomas, C. R. and T. J. Smayda. 2008. Red tide blooms of *Cochlodinium polykrikoides* in a coastal cove. Harmful Algae. 7: 308-317.

Toole, D. A., D. A. Siegel, D. W. Menzies, M. J. Newmann and R. C. Smith. 2000. Remote-sensing reflectance determinations in the coastal ocean environment: impact of instrumental characteristics and environmental variability. Appl. Opt. 39(3): 456-469.

Tosteson, T. R., D. Ballantine and A. Winter. 1997. Sea surface temperature, benthic dinoflagellate toxicity and toxin transmission in the ciguatera food web, p. 48-49. *In* B. Reguera et al. [eds.], Harmful Algae. Proc. 8th Int. Conf. Xunta de Galicia and Interngovernmental Oceanographic Commision of UNESCO.

Trüper, H. G. and C. S. Yentsch. 1967. Use of glass fiber filters for the rapid preparation of *in vivo* absorption spectra of photosynthetic bacteria. J. Bact. 94: 1255-1256.

US Department of Interior. 1968. The bioluminescent bays of Puerto Rico: A plan for their preservation. 48p.

Vaillancourt, R. D., C. W. Brown, R. L. Guillard and W. M. Balch. 2004. Light backscattering properties of marine phytoplankton: relationships to cell size, chemical composition and taxonomy. J. Plankton Res. 26(2): 191-212.

Van Heukelem, L. and C. S. Thomas. 2001. Computer-assisted high-performance liquid chromatography method development with applications to the isolation and analysis of phytoplankton pigments. J. Chromatogr. A. 910: 31-49.

Vasilkov, A. and O. Kopelevich. 1982. The reasons of maximum at about 700 nm on radiance spectra of the sea. Oceanology. 22: 945-950.

Vertucci, F. A. and G. E. Likens. 1989. Spectral reflectance and water quality of Adirondack mountain region lakes. Limnol. Oceanogr. 34(8): 1656-1672.

Walker, L. A. 1997. Population dynamics of dinoflagellates in two bioluminescent bays: Bahía Fosforescente, La Parguera and Puerto Mosquito, Vieques. MS thesis. University of Puerto Rico, Mayagüez. 51p.

Welschmeyer, N. A. 1994. Fluorometric analysis of chlorophyll *a* in the presence of chlorophyll *b* and pheopigments. Limnol. Oceanogr. 39(8): 1985-1992.

WET Labs, Inc. 2008. ac-9 meter. Protocol document. Revision M, 51p.

Whyte, J. N. C., N. Haigh, N. G. Ginther and L. J. Keddy. 2001. First record of blooms of *Cochlodinium sp*. (Gymnodiniales, Dinophyceae) causing mortality to aquacultured salmon on the west coast of Canada. Phycologia. 40: 298-304.

Wright, S. W., S. W. Jeffrey, R. F. C. Mantoura, C. A. Llewellyn, T. Bjørnland, D. Repeta and N. Welschmeyer. 1991. Improved HPLC method for the analysis of chlorophylls and carotenoids from marine phytoplankton. Mar. Ecol. Prog. Ser. 77: 183-196.

Yuki, K. and S. Yoshimatsu. 1989. Two fish-killing species of *Cochlodinium* from Harima-Nada, Seto Inland Sea, Japan, p. 451-454. *In* T. Okaichi, D. Anderson and T. Nemoto [eds.], Red Tides: Biology, Environmental Science, and Toxicology. Elsevier, New York.

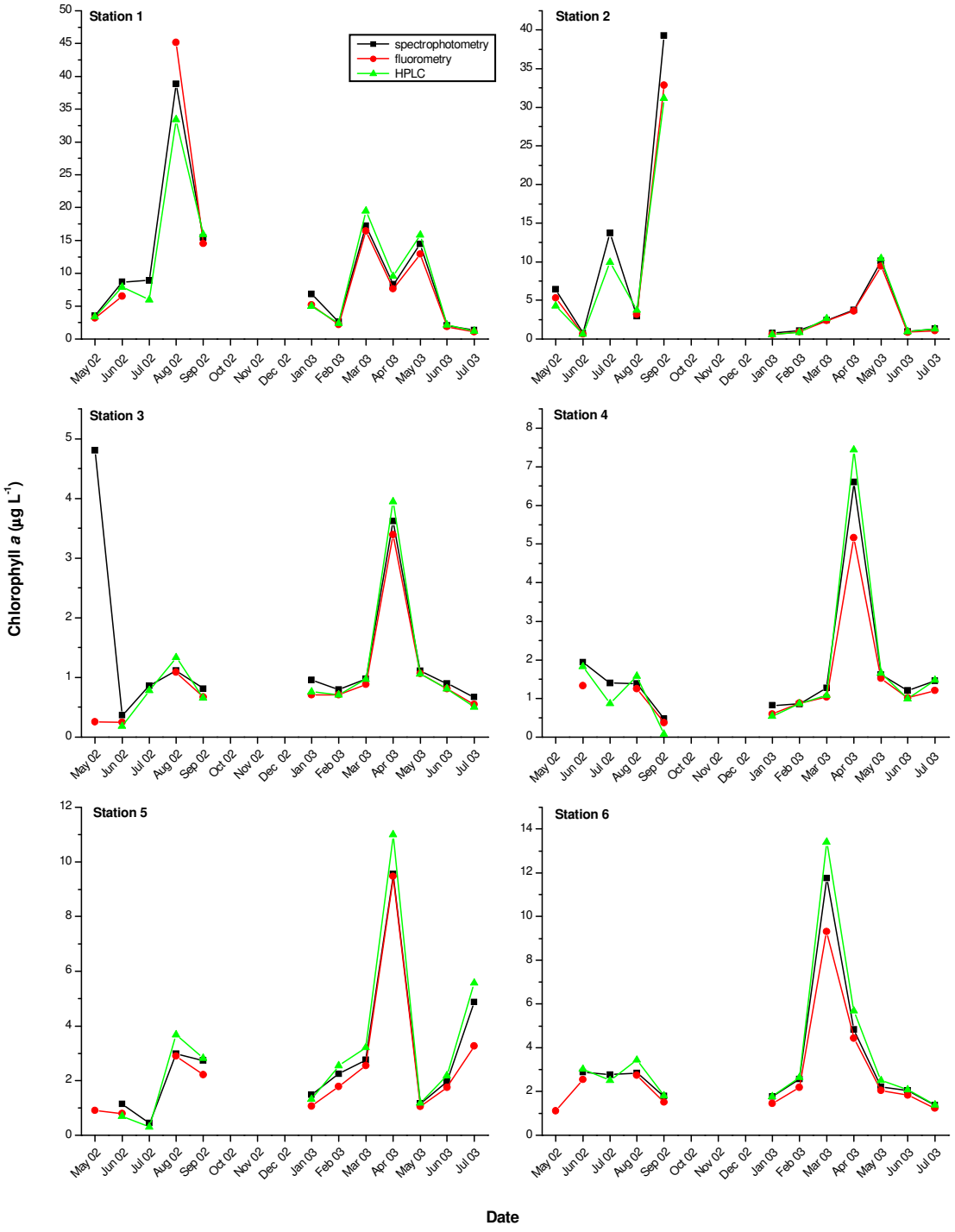

Appendix 1. Chlorophyll *a* concentrations measured at Bahía Fosforescente throughout the study period by spectrophotometric, fluorometric and HPLC methods. Data for October, November and December 2002 was accidentally lost.

Appendix 2. SIMPER analysis of dissimilarities among sampling stations based on physical-chemical properties. Parameters contributing to at least 90 % of the dissimilarity between two particular stations (cumulative %) are listed with their corresponding contribution %. The average squared distance between stations is indicative of their similarity; the greater the distance the greater their dissimilarity and viceversa. The last row indicates the contribution of each parameter to the overall dissimilarity.

Stations	Averaged squared distance	Contribution %							Cumulative %
		PO_4^-	NO_3^-	NO_2^-	NH_4^+	SiO_2	Dissolved oxygen	Salinity	
St 1 & St 2	12.20	35.49		20.00		11.78	10.31	15.55	93.13
St 1 & St 3	18.80	31.39	4.84	17.42		10.99	9.88	17.87	92.39
St 1 & St 4	13.48	36.88		15.58	7.02	11.01	10.22	9.86	90.57
St 1 & St 5	13.65	28.19	11.53	17.19		10.73	11.44	11.64	90.72
St 1 & St 6	20.07	18.27	13.29	19.91	10.72	12.39	12.13	9.89	96.60
St 2 & St 3	5.29	31.04	17.18	16.94	7.88	5.85		15.28	94.17
St 2 & St 4	4.24	32.42	18.83	11.99	8.81		11.13	9.40	92.58
St 2 & St 5	6.81	27.60	24.49	13.49	6.70	9.86		9.08	91.22
St 2 & St 6	10.45	14.98	25.61	11.88	11.48		17.53	9.96	91.44
St 3 & St 4	2.69	10.33		9.04	8.54	6.24	23.19	38.61	95.95
St 3 & St 5	9.53	11.82	26.44	23.73		9.58	10.44	13.96	95.97
St 3 & St 6	5.37		19.85		8.59	5.84	31.86	24.67	90.81
St 4 & St 5	6.57	9.90	34.02	23.14		7.01	12.25	5.80	92.12
St 4 & St 6	4.02		27.73	12.60	15.00	5.44	22.47	9.31	92.55
St 5 & St 6	11.85	8.66	21.00	22.14		7.56	23.56	7.70	90.62
	Overall average contribution %	**22.84**	**20.40**	**16.79**	**9.42**	**8.79**	**15.88**	**13.91**	

Appendix 3. SIMPER analysis of dissimilarities among sampling dates based on physical-chemical properties. Parameters contributing to at least 90 % of the dissimilarity between two particular sampling dates (cumulative %) are listed with their corresponding contribution %. The average squared distance between dates is indicative of their similarity; the greater the distance the greater their dissimilarity and vice versa. The last row indicates the contribution of each parameter to the overall dissimilarity. Physical-chemical data corresponding to the period from May to July 2003 were not included in the analysis since nutrient data were not available for those dates.

Dates	Average squared distance	Contribution %								Cumulative %
		PO_4^-	NO_3^-	NO_2^-	$NH4^+$	SiO_2	Dissolved oxygen	Salinity	Temperature	
Aug 02 & Sep 02	17.79	22.32		12.82		21.34	10.72	9.59	**19.67**	96.46
Aug 02 & Oct 02	16.43	22.97		6.35	27.85			9.12	24.14	90.43
Aug 02 & Nov 02	21.60	16.29	24.47	23.71	11.98		7.02		10.15	93.62
Aug 02 & Dec 02	12.71			34.3	22.04			5.92	29.56	91.82
Aug 02 & Jan 03	29.96	6.12	16.61	10.03	30.35				28.56	91.67
Aug 02 & Feb 03	22.09		20.23	16.31	5.88		5.37	16.42	30.40	94.61
Aug 02 & Mar 03	13.53		9.27	4.50			12.69	23.69	43.27	93.42
Aug 02 & Apr 03	7.78	22.63		10.39		40.44	11.50	12.51		97.47
Aug 02 & May 03	7.81	28.59		6.19		38.98	7.14		14.66	95.56
Aug 02 & Jun 03	6.67	47.56		5.48		9.06	6.43	24.66		93.19
Aug 02 & Jul 03	7.57	56.90				5.60	17.47	9.05	5.73	94.75
Sep 02 & Oct 02	10.11	25.94		5.27	27.43	18.80	16.01			93.45
Sep 02 & Nov 02	13.64	16.62	29.55	9.88	11.67	11.06	11.67			90.45
Sep 02 & Dec 02	13.09	15.06		25.16	13.17	22.67	18.76			94.82
Sep 02 & Jan 03	19.36	9.10	15.24		33.67	10.24	13.02	10.88		92.15
Sep 02 & Feb 03	15.38	10.85	18.09	9.67		17.51	26.07	9.32		91.51
Sep 02 & Mar 03	15.13	13.34	7.14	7.27		20.34	36.80	11.52		96.41
Sep 02 & Apr 03	23.43	8.67				41.70	24.73	4.41	12.84	92.35
Sep 02 & May 03	9.69			11.47		8.21	26.92	35.61	8.36	90.57
Sep 02 & Jun 03	15.94	14.36		5.87		36.41	12.83	9.26	16.30	95.03
Sep 02 & Jul 03	19.64	12.28		7.29		16.3	27.73	22.51	10.96	97.07

Appendix 3. Continued.

Dates	Average squared distance	Contribution %								Cumulative %
		PO_4^-	NO_3^-	NO_2^-	$NH4^+$	SiO_2	Dissolved oxygen	Salinity	Temperature	
Oct 02 & Nov 02	8.88	5.81	41.41	22.29	10.68			10.95		91.14
Oct 02 & Dec 02	6.91	21.45	6.35	43.53	6.93		12.68			90.94
Oct 02 & Jan 03	10.96	7.38	30.54	6.29	21.88		5.77	13.49	9.72	95.07
Oct 02 & Feb 03	9.72	12.92	27.39	12.84	12.68		15.14	8.07	6.76	95.8
Oct 02 & Mar 03	12.82	10.58	14.52		25.71		33.79	7.87		92.47
Oct 02 & Apr 03	14.30				26.45	23.76	16.8	3.84	21.58	92.43
Oct 02 & May 03	12.08	14.84			30.78	14.03		24.43	7.03	91.11
Oct 02 & Jun 03	9.10	9.73			32.06	14.39		6.50	30.36	93.04
Oct 02 & Jul 03	13.90	6.77			21.03		19.55	27.82	15.19	90.36
Nov 02 & Dec 02	10.60	11.66	42.35	18.57		3.72	14.67			90.97
Nov 02 & Jan 03	9.37		20.87	5.57	33.75		6.44		24.33	90.96
Nov 02 & Feb 03	10.36	12.89	16.47	13.61			17.03	18.05	14.35	92.40
Nov 02 & Mar 03	18.42	6.08	28.45	12.51	8.97		28.50	7.75		92.26
Nov 02 & Apr 03	19.24		22.06	9.96	10.42	25.40	17.00		9.38	94.22
Nov 02 & May 03	14.27	8.94	28.09	24.18	13.72	8.50		9.15		92.58
Nov 02 & Jun 03	11.03		26.72	23.57	12.60	13.70		6.12	12.08	94.79
Nov 02 & Jul 03	15.90		21.15	24.01	8.88		21.88	13.46	6.06	95.44
Dec 02 & Jan 03	11.39		26.19	17.73	21.09		11.06	7.53	8.95	92.55
Dec 02 & Feb 03	10.97		29.08	36.10	5.95		7.67	12.34		91.14
Dec 02 & Mar 03	8.12		8.63	24.35	24.2		19.31	16.42		92.91
Dec 02 & Apr 03	12.45		6.20	11.40	18.83	23.40	7.20		26.40	93.43
Dec 02 & May 03	13.97	5.49		31.69	16.37	20.00		12.03	5.53	91.11
Dec 02 & Jun 03	10.39	10.56	7.71	24.38	16.03	6.12			25.33	90.13
Dec 02 & Jul 03	14.1	12.17		28.20	12.15		7.04	17.19	15.49	92.24

Appendix 3. Continued.

Dates	Average squared distance	Contribution %								Cumulative %
		PO_4^-	NO_3^-	NO_2^-	$NH4^+$	SiO_2	Dissolved oxygen	Salinity	Temperature	
Jan 03 & Feb 03	10.34		6.74	9.82	45.00		10.44	19.53		91.53
Jan 03 & Mar 03	16.19		12.24	6.20	44.84		21.54	7.83		92.65
Jan 03 & Apr 03	30.31		15.23		28.47	17.61	7.48		24.88	93.67
Jan 03 & May 03	21.14		18.09	8.99	39.60	7.23			16.60	90.51
Jan 03 & Jun 03	21.43		16.27	5.36	34.67	7.23			31.50	95.03
Jan 03 & Jul 03	23.51		15.51	8.78	31.33		7.44	8.24	24.64	95.94
Feb 03 & Mar 03	9.53		33.58	17.13	9.64			19.44	14.85	94.64
Feb 03 & Apr 03	19.80		18.47	10.98		17.95	5.18	10.26	30.40	93.24
Feb 03 & May 03	17.29		16.59	13.80	5.92	12.42		30.16	14.53	93.42
Feb 03 & Jun 03	14.46	9.07	17.84	14.33		7.45		5.89	35.95	90.53
Feb 03 & Jul 03	19.57	9.4	14.39	14.13				32.65	22.05	92.62
Mar 03 & Apr 03	13.72		20.19			22.63	10.63	5.35	35.35	94.15
Mar 03 & May 03	14.69	5.88	15.85			19.81	16.18	23.47	12.78	93.97
Mar 03 & Jun 03	12.15	8.35	21.34				23.27	4.48	35.36	92.8
Mar 03 & Jul 03	13.80	11.25	17.68				5.30	34.07	24.42	92.72
Apr 03 & May 03	14.85	6.20				60.32	9.40	10.59	6.76	93.27
Apr 03 & Jun 03	5.48	10.44				39.16	27.05	9.98	6.14	92.77
Apr 03 & Jul 03	9.07	9.80		7.53		41.78	7.23	27.52		93.86
May 03 & Jun 03	9.75	12.01				51.6		23.02	6.06	92.69
May 03 & Jul 03	6.05	23.73				44.71	16.22		8.36	93.02
Jun 03 & Jul 03	6.35					16.87	23.02	50.56		90.45
	Overall average contribution %	**14.60**	**19.63**	**15.00**	**20.89**	**21.50**	**15.20**	**15.21**	**18.34**	

Appendix 4. Summary of two-way ANOVA for *C. polykikoides* abundance data. Data was log (sqrt^4) +1 transformed.

	SS	Degrees of freedom	MS	F	p
Intercept	25.33	1	25.33	1618.89	0.000
Dates	6.40	14	0.46	29.24	0.000
Stations	2.77	5	0.55	35.39	0.000
Dates*Stations	1.79	70	0.03	1.64	0.005
Error	2.78	178	0.02		

Appendix 5. Comparison of physical-chemical parameters measured in Bahía Fosforescente in previous studies and during the current study.

Parameter	Range measured
Temperature	26.5-31.1°C (González, 1965)
	27.8-31.1°C (Cintrón, 1969)
	27-31°C (Seixas, 1983)
	27-30°C (Seixas, 1988)
	25.7-31.2°C (Walker, 1997)
	26.3-30°C (Soler, 2006)
	25.9-33.5°C (this study)
Salinity	34.1-36.7 ps (Coker and González, 1960)
	32.96-36.88 ps (Cintrón, 1969)
	34.5-37.0 ps (Smayda, 1970)
	34-38 ps (Seixas, 1983)
	37-39 ps (Seixas, 1988)
	33-37 ps (Walker, 1996)
	33.3-37.8 ps (Soler, 2006)
	33.5-39.5 ps (this study)
Phosphates	0.32 µmol L^{-1} (González, 1965)
	0.06-0.56 µmol L^{-1} (Smayda, 1970)
	0.31-0.53 µmol L^{-1} (Seixas, 1983)
	0.01-0.04 µmol L^{-1} (Soler, 2006)
	0.12-1.08 µmol L^{-1} (this study)
Ammonia (Ammonium)	1.65-6.81 µmol L^{-1} (Soler, 2006)
	0.06-4.97 µmol L^{-1} (this study)
Nitrites	0.25 µmol L^{-1} (González, 1965)
	0.05-0.29 µmol L^{-1} (Soler, 2006)
	0.05-0.63 µmol L^{-1} (this study)
Nitrates	0.12 µmol L^{-1} (González, 1965)
	0.01-0.70 µmol L^{-1} (Smayda, 1970)
	0.14-1.18 µmol L^{-1} (Soler, 2006)
	undetectable -0.91 µmol L^{-1} (this study)
Silicates	4.37 µmol L^{-1} (González, 1965)
	0.34-0.70 µmol L^{-1} (Smayda, 1970)
	0.43-4.19 µmol L^{-1} (Soler, 2006)
	0.37-8.63 µmol L^{-1} (this study)